

Voronoi Tessellation Quality: Applications in Digital Image Analysis

by

Enoch A-iyeh

A Thesis submitted to The Faculty of Graduate Studies of
The University of Manitoba
in partial fulfillment of the requirements for the degree of

Doctor of Philosophy

Department of Electrical and Computer Engineering
University of Manitoba
Winnipeg

January 2017

Copyright © 2017 by Enoch A-iyeh

Abstract

A measure of the quality of Voronoï tessellations resulting from various mesh generators founded on feature-driven models is introduced in this work. A planar tessellation covers an image with polygons of various shapes and sizes. Tessellations have potential utility due to their geometry and the opportunity to derive useful information from them for object recognition, image processing and classification.

Problem domains including images are generally feature-endowed, non-random domains. Generators modeled otherwise may easily guarantee quality of meshes but certainly bear no reference to features of the meshed problem domain. They are therefore unsuitable in point pattern identification, characterization and subsequently the study of meshed regions. We therefore found generators on features of the problem domain. This provides a basis for element quality studies and improvement based on quality criteria. The resulting polygonal meshes tessellating an n-dimensional digital image into convex regions are of varying element qualities. Given several types of mesh generating sets, a measure of overall solution quality is introduced to determine their effectiveness. Given a tessellation of general and mixed shapes, this presents a challenge in quality improvement. The Centroidal Voronoï Tessellation (CVT) technique is developed for quality improvement and guarantees of mixed, general-shaped elements and to preserve the validity of the tessellations.

Mesh quality indicators and entropies introduced are useful for pattern studies, analysis, recognition and assessing information. Computed features of tessellated spaces

are explored for image information content assessment and cell processing to expose detail using information theoretic methods. Tessellated spaces also furnish information on pattern structure and organization through their quality distributions. Mathematical and theoretical results obtained from these spaces help in understanding Voronoï diagrams as well as for their successful applications. Voronoï diagrams expose neighbourhood relations between pattern units. Given this realization, the foundation of near sets is developed for further applications.

Acknowledgements

I acknowledge financial support of The Province of Manitoba through the Manitoba Graduate Scholarship, the University of Manitoba's Graduate Fellowship and that of my supervisor Dr. James F. Peters. The financial aspects of this work were secured by their generous contributions.

I sincerely acknowledge the help and contributions by all my committee members: Dr. James F. Peters, Dr. A.S Alfa, Dr. Dean K. McNeill and Dr. Mark F. Tachie. I am grateful for all your time, efforts and input throughout this journey. Our intellectual discourses shaped this work. I am thankful to Dr. James F. Peters for the opportunity to be part of his research group and for all the research opportunities, directions, leadership and friendship he provided in the course of this work.

Last but not least, I acknowledge the love, care and support of God Almighty, my family and friends.

Table of Contents

| | |
|--|-----------|
| List of Figures | iv |
| List of Tables | vii |
| 1 Topology of Digital Images and Meshes | 1 |
| 1.1 Introduction and Relevant Works | 1 |
| 1.2 Image Fundamentals | 3 |
| 1.3 Image Spaces and Topologies | 4 |
| 1.3.1 Discrete Image Spaces | 4 |
| 1.3.2 Continuous Image Spaces | 5 |
| 1.4 Conclusion | 7 |
| 2 Fundamentals of Voronoï Algorithm and Tessellations | 8 |
| 2.1 Introduction | 8 |
| 2.2 Mathematical Background | 10 |
| 2.3 Definitions and Lemmas | 13 |
| 2.4 Centroidal Voronoï Tessellations | 17 |
| 2.5 Poisson-Voronoï Diagrams | 18 |
| 2.5.1 One-dimensional $\mathbb{P}\mathbb{V}$ Systems | 19 |
| 2.5.2 Two-dimensional $\mathbb{P}\mathbb{V}$ Systems | 21 |
| 2.6 Conclusion | 21 |
| 3 Feature-Based Point Pattern Generator Identification and Representation | 23 |
| 3.1 Introduction | 23 |
| 3.2 Feature-based Tessellation Generators | 25 |
| 3.2.1 Corner Generators | 26 |
| 3.2.2 Edge Generators | 27 |
| 3.2.3 Keypoint Generators | 28 |
| 3.2.4 Modal Pixel and Extrema Generators | 30 |
| 3.2.5 Centroidal Tessellation Generators | 32 |
| 3.3 Conclusion | 34 |

| | | |
|----------|---|------------|
| 4 | Theoretical and Mathematical Results on Voronoï Spaces and Mesh Qualities | 36 |
| 4.1 | Introduction | 36 |
| 4.1.1 | Results on Voronoï Spaces | 36 |
| 4.1.2 | Results on Quality of Cells | 44 |
| 4.2 | Conclusion | 47 |
| 5 | Tessellation Quality, Improvement and Information of Patterns | 49 |
| 5.1 | Introduction | 49 |
| 5.2 | Mesh Quality Computation Algorithm | 50 |
| 5.3 | Application: Digital Image Tessellation Quality | 51 |
| 5.4 | Towards Mesh Cell Solution Quality Guarantees | 68 |
| 5.4.1 | Tessellation Quality Improvement: Centroidal Tessellations . . | 69 |
| 5.5 | Mesh Cell Entropy Assessment | 98 |
| 5.5.1 | Gini Index Mesh Cell Processing | 99 |
| 5.5.2 | Signal Complements | 100 |
| 5.5.3 | Results of Information-Based Complementing of Signals with Applications to Medical Images | 103 |
| 5.6 | Quantifying Information Levels of Voronoï Tessellations | 107 |
| 5.6.1 | Methodology and Datasets | 109 |
| 5.7 | Results and Discussion | 113 |
| 5.8 | Conclusion | 123 |
| 6 | Near Sets | 125 |
| 6.1 | Introduction | 125 |
| 6.2 | Near or Proximal Voronoï Segments | 125 |
| 6.2.1 | Descriptive and Spatially Near Voronoï Sets | 127 |
| 6.3 | Digital Groupoids | 130 |
| 6.3.1 | Neighbourliness in Groupoids | 133 |
| 6.3.2 | Digital Groupoid Set Pattern Generators | 134 |
| 6.4 | General Pattern Generation | 137 |
| 6.4.1 | Descriptive EF-Proximity Pattern Generation Spaces | 141 |
| 6.4.2 | Motif Pattern Generators | 147 |
| 6.4.3 | Spatial Proximity Pattern Generation Method | 151 |
| 6.4.4 | Descriptive Proximity Pattern Generation Method | 153 |
| 6.5 | Assessing Pattern Stability | 154 |
| 6.6 | Descriptive Pattern-Based Approach to Classification | 162 |
| 6.7 | Conclusion | 167 |
| 7 | Summary, Conclusion and Future Work | 169 |
| | References | 173 |

List of Figures

| | | |
|------|--|----|
| 2.1 | Voronoi diagram of a random set of sites | 14 |
| 2.2 | Voronoi polygon | 16 |
| 2.3 | Voronoi diagram of a Poisson process | 18 |
| 3.1 | Corner Generators | 27 |
| 3.2 | Edge Generators | 28 |
| 3.3 | Keypoint Generators | 30 |
| 3.4 | Dominant Generators, $m_d = 0.65$ | 32 |
| 3.5 | Centroid Generators | 33 |
| 5.1 | Corner vs. Edge Tessellations and Quality Distributions | 52 |
| 5.2 | Dominant vs. Keypoint Tessellations and Quality Distributions | 54 |
| 5.3 | Corner vs. Edge Tessellations and Quality Distributions | 56 |
| 5.4 | Dominant vs. Keypoint Tessellations and Quality Distributions | 58 |
| 5.5 | Corner vs. Edge Tessellations and Quality Distributions | 59 |
| 5.6 | Dominant vs. Keypoint Tessellations and Quality Distributions | 61 |
| 5.7 | Corner vs. Edge Tessellations and Quality Distributions | 62 |
| 5.8 | Dominant vs. Keypoint Tessellations and Quality Distributions | 64 |
| 5.9 | Corner vs. Edge Tessellations and Quality Distributions | 65 |
| 5.10 | Dominant vs. Keypoint Tessellations and Quality Distributions | 67 |
| 5.11 | Corner vs. Edge Centroid Tessellations and Quality Distributions | 70 |
| 5.12 | Dominant vs. Keypoint Centroid Tessellations and Quality Distributions | 72 |
| 5.13 | Corner vs. Edge Centroid Tessellations and Quality Distributions | 73 |
| 5.14 | Dominant vs. Keypoint Centroid Tessellations and Quality Distributions | 75 |
| 5.15 | Corner vs. Edge Centroid Tessellations and Quality Distributions | 77 |
| 5.16 | Dominant vs. Keypoint Centroid Tessellations and Quality Distributions | 78 |
| 5.17 | Corner vs. Edge Centroid Tessellations and Quality Distributions | 80 |
| 5.18 | Dominant vs. Keypoint Centroid Tessellations and Quality Distributions | 82 |
| 5.19 | Corner vs. Edge Centroid Tessellations and Quality Distributions | 83 |
| 5.20 | Dominant vs. Keypoint Centroid Tessellations and Quality Distributions | 84 |
| 5.21 | Meshes demonstrating sufficiency of coverings | 90 |
| 5.22 | Symmetry of features | 92 |

| | | |
|------|--|-----|
| 5.23 | An image pair and their meshed domains for SSIM and quality comparisons | 94 |
| 5.24 | An image pair and their meshed domains for SSIM and quality comparisons | 95 |
| 5.25 | Overall quality factors due to categories of images | 96 |
| 5.26 | Linear transformation of an image | 102 |
| 5.27 | a. Original image b. Linear complement c. Feature distributions d. Transformation function | 103 |
| 5.28 | a. Gini image b. Feature distributions c. Transformation function d. Linear complement of Gini image | 104 |
| 5.29 | a. Original image b. Linear complement c. Feature distributions d. Transformation function | 104 |
| 5.30 | a. Gini image b. Feature distributions c. Transformation function d. Linear complement of Gini image | 104 |
| 5.31 | a. Original image b. Linear complement c. Feature distributions d. Transformation function | 105 |
| 5.32 | a. Noisy Gini image b. Feature Distributions c. Transformation Function d. Linear Complement of Gini Image | 106 |
| 5.33 | Perfectly Regular Image Graph Space and Quantities | 112 |
| 5.34 | Datasets | 113 |
| 5.35 | Image Graph Spaces | 114 |
| 5.36 | Image Graph Spaces | 115 |
| 5.37 | Image Graph Spaces | 116 |
| 5.38 | Image Graph Spaces | 117 |
| 5.39 | Image Graph Spaces | 117 |
| 5.40 | Image Graph Spaces | 118 |
| 5.41 | Image Graph Spaces | 118 |
| 5.42 | Image Graph Spaces | 119 |
| 5.43 | Image Graph Spaces | 119 |
| 5.44 | Image Graph Spaces | 120 |
| 5.45 | Image Graph Spaces | 120 |
| 5.46 | Image Graph Spaces | 121 |
| 5.47 | Quantity Relations | 122 |
| 5.48 | Quantity Signatures | 122 |
| 6.2 | Neighbourly mesh cells | 130 |
| 6.3 | Image to groupoid space transformation | 132 |
| 6.4 | Image to groupoid space transformation | 134 |
| 6.5 | Shaded Box Point Set Pattern | 150 |
| 6.6 | Spatial Edge Set Pattern $\mathfrak{P}(M) = \{M, A, B\}$ | 151 |
| 6.7 | Local Spatial Pattern Generation Method | 152 |
| 6.8 | $\mathfrak{P}_\Phi(M) = \{M, A_1, A_2, A_5\}$ | 152 |

| | |
|---|-----|
| 6.9 Local Descriptive Pattern Generation Method | 152 |
|---|-----|

List of Tables

| | | |
|-----|---|----|
| 5.1 | Overall mesh quality based on choice of sites | 87 |
| 5.2 | Overall mesh quality based on centroids of regions due to feature tessellations | 87 |
| 5.3 | SSIM and Quality Indices | 96 |

List of Algorithms

| | | |
|---|--|-----|
| 1 | Mesh Quality Computation Algorithm | 50 |
| 2 | Mesh Quality and Information Computation Algorithm | 111 |
| 3 | Pattern-Based Class Membership Test Method | 165 |
| 4 | Pattern-Based Classification Method | 166 |

Contribution of Work and Authors

Besides seminal works on Voronoï diagram applications in several areas (notable among them is the so-called proximal post office problem. Given a set of post office sites in a topology, Voronoï tessellation shows the nearest one to visit) including the study of the behavior of animals in the habitats/territories, image compression, segmentation *e.t.c* the literature reveals opportunity and need of work focused on:

- Discovering mesh generators based on features of domain that yield high quality solutions,
- Establishing quality guarantees for mixed mesh cells of varying shape and size,
- Cell processing and analysis for pattern understanding, recognition, including extracting domain information from meshed surfaces,
- Identifying and proving useful mathematical results for applications,
- Foundation laying for subsequent near set studies and analysis.

Mesh applications have almost been studied exclusively in all other fields but pattern understanding and analysis. In most of those studies, the chief end is mostly space partition based on structures produced by distances between objects. We adopt the philosophy that mesh tessellations can be a means to an end, as opposed to being an end in themselves. In that regard, the contribution of this work to the application

of mesh tessellations in studying digital image point patterns lie in: (a) identifying suitable forms of generating points for meshing feature-endowed domains [1] in chapter 3 and chapter 5, (b) identifying and proving useful mathematical results including theorems [1, 2] on mesh spaces in chapter 4, (c) formulating a global measure of the quality of meshes as an indicator of pattern structure organization in chapter 5, (d) extracting basic information from an image domain through its point pattern [2] in chapter 5, (d) applications of Voronoï tessellations in mesh quality improvement of general and mixed element shapes based on quality criteria, mesh cell processing, pattern recognition, and information assessment in chapter 5, and (e) pattern studies [3, 4] in chapter 6. Theorems and lemmas form a mathematical background for the study of image mesh quality and applications, solution quality improvement, near segments, pattern generation and stability in chapter 5 and chapter 6.

The best forms of point patterns can be identified by the values of the overall quality index (whether it's high or low). This is noticeable from plots of overall quality factors. Global quality also gives information on basic pattern structure or organization. This is a way of assessing pattern information through the cells in the meshed domain. An indicator such as overall quality is important since cells can be numerous, thus making it impractical to consider qualities individually. Depending on the value of the index in relation to zero and unity, we can assess basic and general information such as whether the summary point pattern of the problem domain is regular or not. Poor element quality is very common in mesh generation schemes. Because of this, several attempts have been made to improve poor quality elements. A general element shape mesh quality improvement technique based on the energy of regions is presented and used to improve cell quality. Results clearly show the

improvement in cell quality even with one iteration. Some important mathematical results based on quality criteria are identified and proved based on cell quality and Voronoï spaces. Point processing of fixed mesh shapes is explored in relation to digital image complementing and processing using a disparity measure related to entropy. General trends on mesh quantity relations of varying element shape and size is also presented. Last but not least, near set fundamentals of mesh domains is presented. This is intended to form the basis for future work.

Applications of mathematical tools [5–7] in signal processing and analysis have increasingly been explored and investigated. This work is of that kind as presented in chapter 1 through chapter 6. Chapter 1 is an introductory chapter which outlines the topology of images and the direction of the work. Chapter 2 outlines the fundamentals of a general partitioning algorithm; the Voronoï algorithm. It also presents several definitions essential in the framework of space partitioning necessary for the theoretical and practical applications and results discussed in the work. Chapter 3 deals with models for point pattern generation in image topologies. Chapter 4 contains mathematical results on mesh spaces, qualities and their proofs. Chapter 5 contains the applications of image tessellation qualities in image analysis, Voronoï cell processing and enhancement, information content assessment. Groupoid element identification, near sets, among others are presented in Chapter 6. Last but not the least, chapter 7 deals with the summary, conclusions and future directions of the work.

I acknowledge the overall contribution and direction of my supervisor Dr. James F. Peters, most especially through provision of images in Fig. 1.1, Fig. 6.5, Fig. 6.6, Algorithm 3 and Algorithm 4.

Chapter 1

Topology of Digital Images and Meshes

1.1 Introduction and Relevant Works

This chapter serves as a brief introduction to points and regions in image spaces in the context of topology. It also serves to give a brief overview of the literature on Voronoi diagrams as a fundamental data structure applied to point sets for various problems. It begins with a literature review in relation to the problem identified for the work. It progresses by examining image spaces, image data organization and norms of image spaces. It concludes by highlighting image spaces as topological spaces.

Domain partitioning algorithms such as Voronoi tessellations and Delaunay triangulations are basic and fundamental data structures indispensable in computational geometry and applications [8–14]. Mesh algorithms have been developed for several problems including segmentation [15–17], clustering [18–20], signal compression,

quantization and behavior of animals in their habitats [?, 21–23], symmetry detection [24, 25], point pattern distribution and statistics calculations [26–34], pattern structure and formation studies [35–43], system modeling and optimization [44–46], set pattern processing, approximation, reconstruction and interpolation [47–55] as well as for general space partitioning [22, 23]. Although the targeted solutions are as varied as the problems themselves and the geometries of the domains, the presence of domain features is a common theme that is hardly given due attention and or exploited for solution quality guarantees. Besides, several mesh solution schemes are iterative in nature in that domain partitioning is done so that initial mesh solutions are adjusted iteratively to approach fulfilling predefined conditions and to terminate on meeting defined stopping criteria up to some limits [22, 23].

Partitioning algorithms such as those developed in [22, 23, 56, 57] vary and adapt generators for better cell qualities. Sites may be moved to attain force equilibrium. A case in point is the example whereby the iteration starts by discretizing the space based on the initial distribution of sites but iterates the initial solution based on preset conditions on the size of elements in fulfillment of equilibrium and termination conditions [23]. This essentially is refining and solving for optimality of meshes [58–61] according to preset conditions. Although this can easily guarantee mesh quality, it has the major limitation that these mesh quality improvements and innovations are founded on generators that are largely determined irrespective of feature point locations or the topology of the surface to be meshed or problem space. Another significant limitation of current solution quality guarantee algorithms is that high solution quality is achieved at the high cost of restricting all mesh cells to the same type of figure. For example all mesh cells may be restricted to triangular shapes for ease of quality guarantees. The technique developed in this work eliminates the

fixed element shape restriction.

Formal expositions on Voronoï diagrams first became available due to works by Ukrainian mathematician G. Voronoï [62–64]. Given prior foundations, the literature has since seen a surge in research on their applications as evidenced by numerous works and success of applications from archeology and astronomy [19, 65] to zoology [21]. Fields of applications in between include geography [66], in musicology [67, 68] for automatic grouping of polyphony, system modeling [44, 69], medical diagnoses [70], in telecommunications for analyzing linear code blocks [71] discretizing regions of code and efficiency of Gaussian channels, just to mention a handful. Following the explosive research and success in applicability, Voronoï diagrams in the context of proximity spaces and pattern analysis have been highlighted recently [1, 72–74].

1.2 Image Fundamentals

The ubiquity of images have been influenced heavily by the wide and available range of technologies for acquiring images. Also studies in many fields for example image processing and understanding, pattern recognition and studies that necessitate the use of images [75] are indirectly responsible for their availability as well as the availability of image-based algorithms. A brief review of pictorial images intended to facilitate the work reported here is provided in the following text.

1.3 Image Spaces and Topologies

There are two types of image spaces, namely digital image spaces and continuous image spaces. The two categories of image spaces are treated next.

1.3.1 Discrete Image Spaces

A two-dimensional digital or discrete image is defined as a function f where the values of f are quantified intensity or gray levels at spatial coordinate pairs (x, y) . The values of $f(x, y)$ are usually quantized intensities or amplitudes at the coordinate pairs (x, y) and expressed as a matrix of entries. The extent of a digital image in space is limited by finite dimensions of the image.

A three-dimensional digital image is represented as a matrix of rows, columns and depth with entries in the matrix as the values of the function $f(x, y, z)$ at the coordinate tuples (x, y, z) . A two-dimensional image function matrix is defined by:

$$I_{m,n} = \begin{bmatrix} f(1,1) & f(1,2) & \cdots & f(1,n) \\ f(2,1) & f(2,2) & \cdots & f(2,n) \\ \vdots & \vdots & \ddots & \vdots \\ f(m,1) & f(m,2) & \cdots & f(m,n) \end{bmatrix}.$$



Figure 1.1: A Bit More, Punch, 1845

A sample two-dimensional digital image is shown in Fig. 1.1. It shows the spatial plane of a signal quantized at coordinate pairs. Two-dimensional digital images are considered in this work.

1.3.2 Continuous Image Spaces

The continuous analogue of a discrete image space results when we assign every point in \mathbb{R}^n of an image a feature value as opposed to assigning values at only some coordinates. It differs from a discrete space in the sense that feature values exist at every coordinate location as opposed to feature values at only some locations within the extent of the signal. To help characterize Euclidean structures in both discrete and continuous image spaces $\mathbb{I}(a, b)$, we introduce the standard norm of \mathbb{I} as follows [76]:

$$\|I(a(x, y), b(x, y))\| = \sqrt{(x_a - x_b)^2 + (y_a - y_b)^2} \quad (1.1)$$

. It is easily verified that \mathbb{I} satisfies the following axioms:

Axiom 1.

$$\|I(a, b)\| \geq 0$$

Axiom 2.

$$\|I(a, b)\| = \|I(b, a)\|$$

Axiom 3.

$$\|I(a, c)\| \leq \|I(a, b)\| + \|I(b, c)\|$$

Notice that Axiom 3 is the so-called triangle inequality.

These axioms, defined on image spaces will be useful in characterizing points and regions/polygons around them in images for the purposes of processing and analyzing image patterns via Voronoï tessellations. A digital image space can be viewed as a Voronoï tessellation as depicted in Fig. 1.2.

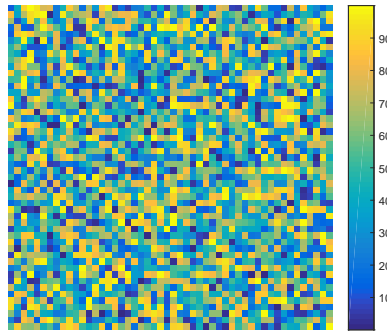


Figure 1.2: A digital image viewed as a Voronoï space

Notice that each region in a digital image can be viewed as a generator with a specific quantized intensity level. A zoomed-in operation reveals the regions as square patches seen in Fig. 1.2. This viewpoint will be instrumental in information theoretic-based digital image processing with the aim of aiding decision making and general image pattern analysis respectively. Meshes may be generated using a summary point pattern or the entire signal space. This can lead to mesh elements of varying shapes and sizes or elements of the same shape or size. This viewpoint

is also essential in pattern processing, recognition, information/entropy assessment and analysis as presented in chapter 5 and chapter 6. In this work, image entropy assessment is conducted given tessellations, whether of varying element shape and size or not. Image enhancement on the other hand is performed given elements of same shape and size. These are presented in chapter 5.

1.4 Conclusion

In this chapter, the fundamental mathematical structure of digital images is laid out. This structure facilitates use/exploration of digital images as feature-endowed topologies. This in turn facilitates tessellation of point sets to obtain Voronoï regions. In addition, tools for examining them have been provided.

Given the structure/organization of image data and their feature-endowed nature, the following chapters explore identification of point sets based on features of the spaces for Voronoï tessellations and further studies/analysis. The fundamentals of space partitioning and the Voronoï partitioning algorithm in computational geometry are presented in chapter 2.

Chapter 2

Fundamentals of Voronoï Algorithm and Tessellations

2.1 Introduction

This chapter serves to introduce fundamental concepts in planar tessellations. It sets out by noting that summary point patterns are to be extracted from sample spaces of the problem in question for the purposes of tessellating and studying the problem domains. The mathematical framework of the Voronoï partitioning algorithm is presented. This framework covers some definitions and lemmas that are necessary in studying tessellations. A special kind of tessellation on which quality improvements are based is presented. The chapter concludes by examining Poisson Voronoï tessellations.

Two-dimensional digital images have bi-directional extensions or dimensions. Assume the row dimension of an image is M and the column dimension is N . This means that we have a total of $M \times N$ features or pixels constituting the image.

Digital images by nature and composition have significant sizes. In some instances it is easily the case that the total number of pixels is extremely large. Large-sized images have implications such as limits of operational speed of utilized algorithms or even the suitability of methods of application. In the following sections, we present the mathematical background necessary for tessellating summary point patterns that will be extracted from image domains. Summary point pattern extraction is advantageous in increasing computational speed of applied algorithms while at the same time sufficiently representing the space with its summary pattern for entire signal analysis.

As previously noted, seeds, generating points or sites of meshes in domains including non-image domains have often been chosen randomly, deterministically on grids [23], using distribution sampling [77] or using centroids of regions based on random tessellations [21]. These ways of choosing generators could easily guarantee quality of meshes that bear no reference to information present in the domain. These choices of generator specification suffices if the major aim and end is general space partitioning. In domain tessellation quality analysis, it is useful to identify the best or most suitable mesh generators (also called sites) based on domain features for mesh generation as opposed to say randomly specifying generators. From this realization, one of the principal aims of this work is to identify generators (based on domain feature information) that produce high quality Voronoï tessellations.

On the one hand, we have ease of quality improvement based on non-feature point pattern generation and single/fixed element shapes. On the other hand, we have the challenge of identifying point patterns based on domain information, mixed element shapes coupled with the difficulty of quality improvement. The latter approach

although hardly explored because of its challenges leads to mesh element generation based on domain information while at the same time produces elements of acceptable quality.

To accomplish this, it is necessary to obtain summary point pattern sets defined by objects and structures and at the same time produce elements in tessellations that tend to maintain high quality factors. This is essential eventually for quality guarantees. This approach is complementary to quality guarantee techniques that bear no information on objects and structures in the problem domain. A principal benefit of models of generators based on feature information is the specification of those generators that produce the highest quality Voronoï tessellations. Examples illustrating the application of quality measures of tessellations are given in terms of comparing digital image Voronoï tessellation covers to detect pattern information derived from features of tessellation covers.

2.2 Mathematical Background

Following several discoveries including the realization that honeycombs are Voronoï tessellations, together with ample successful applications, researchers have pursued to applications of Voronoï tessellations in many other application fields as seen in image processing and compression, data clustering, territorial behaviour of animals [21–23, 78, 79] *e.t.c.* Meshed domains are covered with regular polygons consistent with the partitioning algorithm used. For example, Voronoï partitioning covers a space with polygons of potentially varying side numbers and nonempty interiors whilst Delaunay tessellations cover the space with only triangles with empty interiors. Voronoï partitions are general partitions. Because of this general nature, a

Delaunay tessellation can be extracted from it by triangulation of its generators. Since Delaunay tessellation is embedded in a Voronoï diagram, our focus will be on the latter which is more uniform.

In the following text, the mathematical background on Voronoï diagrams together with definitions essential in the framework of space partitioning is presented. This is necessary for the theoretical and practical applications and results discussed in the work. Some of the theoretical/mathematical results identified in this work are based on important definitions and lemmas provided here.

Given a sampled finite set S of locations called generators, seeds or sites $\{s_i\}$ in \mathbb{R}^n . To compute the Voronoï diagram of S we must partition the space of $S \subset \mathbb{R}^n$ into regions $V(s_i)$ in such a way that region $V(s_i)$ contains points that are nearer to it than to any other region of object

$$s_j, i \neq j \in S.$$

Given the point pattern set

$$S = \{s_1, s_2, \dots, s_k : i \in \mathbb{N}\},$$

where each pattern unit $s_i \in S, i = 1, 2, 3, \dots, \mathbb{N}$ is a mesh generating point, then the Voronoï region $V(s_i)$ is defined by:

$$V(s_i) = \{x \in \mathbb{R}^n : \|x - s_i\| \leq \|x - s_k\|, \forall s_k \in S, i \neq k\}, \quad (2.1)$$

where $\|.,.\|$ is the Euclidean norm (distance between vectors). The set

$$\mathbb{V}(S) = \bigcup_{s_i \in S} V(s_i)$$

is called the n -dimensional Voronoï diagram of S . In \mathbb{R}^2 , this is effectively a covering of the plane with non-overlapping polygons, with exactly one polygon about each generating point $s_i \in S$.

All Voronoï regions share a common property: They are convex polygons. All regions are finite except those on the convex hull. Interior points generate finite polygons whilst a few points on the convex hull generate infinite polygons. Adjacent regions are separated by thin line segments. Although most Voronoï algorithms produce regions separated by thin line segments, some n -dimensional Voronoï diagrams have regions separated by line segments with thick or non-negligible widths [80].

Voronoï regions are cellular growth patterns from a certain viewpoint. This point of view is equivalent to considering the generator of each region as the nucleus of a growing or expanding cell. Cells propagate simultaneously outward from their nuclei at uniform rates until they intersect with others. They then freeze giving the boundaries of the regions defined by line segments separating the regions of the tessellation. Similarly, crystal growth is analogous to Voronoï region formation.

It is interesting to note that since cells are growing at the same rate according to this viewpoint, their first points of contact coincide with the midpoint of pairs of nuclei. These define loci of all equidistant points from their respective nuclei. The locus of points form a perpendicular bisector or line segment from which the pair of nuclei are equidistant. The set of these line segments form edges of the Voronoï regions which may or may not be of negligible widths. The size of each region about a generator is known to be the influence or capture zone of that generator [19, 47].

Voronoï regions with a common edge are said to be *Voronoï neighbours*. The set of triangles formed by connecting the nuclei or generators of Voronoï regions tessellate the area within the convex hull of the set. This partition is known as the Delaunay tessellation dual of the point set.

Voronoï regions are neighbourhood structures induced by the norm $\|\cdot\|$. Such structures allow us to treat regions around dot patterns as continuous, image-like patterns, thus allowing the use of general image processing techniques [81]. This is explored in chapter 5. Another interesting interpretation of a Voronoï tessellation is to view it as a cluster of points partitioned by the regions of the space [18]. In this view, the space is segmented into various Voronoï regions, with the size of the clusters given by the areas of their respective regions. These interpretations of Voronoï tessellations make feature extraction such as boundary extraction possible, with the tessellated space viewed as a mosaic.

2.3 Definitions and Lemmas

To supplement the foregoing mathematical background, some useful formal definitions, properties, lemmas and theorems of Voronoï diagrams are presented in the following text.

Definition Assume a point set $S \subseteq \mathbb{R}^n$ and a distance function $\|\cdot\|$, the set $\{V_i\}_{i=1}^k$ is called a Voronoï tessellation of S provided $V_i \cap V_j \neq \emptyset, \forall i \neq j$.

Definition A planar Voronoï region of a site is a polygon about that site. The set

of all regions partition the plane of the sites S based on a distance function $\|\cdot\|$. This results in covering the plane with polygons about those sites.

Definition Given a set $S = \{s_1, \dots, s_k\}$ of points, any plane (v_i, v_j) is a Voronoï edge of the Voronoï region V if and only if there exists a point x such that a circle centered at x and circumscribing v_i and v_j , which may or may not contain in its interior any point of \mathbb{V} .

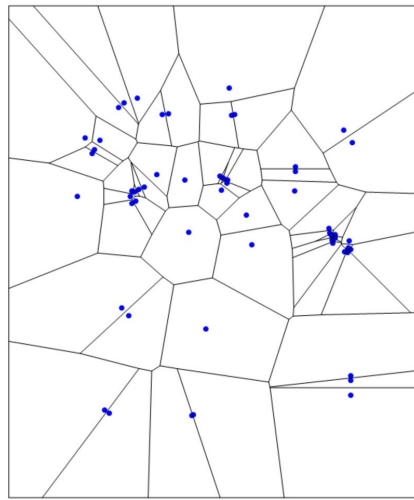


Figure 2.1: Voronoï diagram of a random set of sites

Definition A Voronoï tessellation is a set of polygons with their edges and vertices that partition a given space of sites.

Definition A Voronoï edge is a half plane which is equidistant from two sites and bounds some part of a Voronoï region. Every edge is incident upon two vertices and every vertex upon three or more edges.

Definition A Voronoï vertex is the center of a circle formed by the intersection of three or more edges.

Definition A set of points form a convex set if there is a line connecting each pair of points and lies within the convex hull of the set.

Definition The convex hull of Voronoï regions about a set of sites is the smallest set which contains the Voronoï regions and their union.

Definition A dot or point pattern is a set of points of a signal summarizing its features. For example sets of corners, keypoints *e.t.c* are *point, dot or summary patterns*.

Definition The structural similarity index or quality of a signal is defined as a characteristic of the signal which gives information about perceived signal structure or degradation compared to an ideal.

Definition The quality of a Voronoï cell/region is defined as a factor proportional to the ratio of the area of the region to the sum of squares of the lengths of its sides. This is an indicator of region stability that culminates into perceived pattern structure or organization. Mathematically, the quality factor q is expressed as

$$q \propto \frac{A}{\sum_i l_i^2} \quad (2.2)$$

, where A is the area of the region.

For example the quality of triangular and quadrilateral cells is given by

$$q = \frac{4\sqrt{3}A}{l_1^2 + l_2^2 + l_3^2} \quad (2.3)$$

and

$$q = \frac{4A}{l_1^2 + l_2^2 + l_3^2 + l_4^2} \quad (2.4)$$

respectively. These definitions are adopted following the example of [82, 83]. Assume the polygon in Fig. 2.2 results from a tessellation.

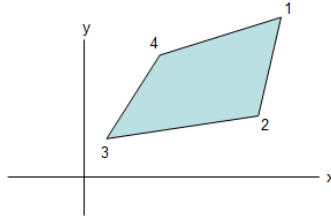


Figure 2.2: Voronoï polygon

Its area, A is given by:

$$A = \frac{1}{2} \left| \sum_{i=1}^n x_i y_{i+1} - x_{i+1} y_i \right| \quad (2.5)$$

, where (x_i, y_i) is the coordinates of the i^{th} vertex. These specifications of quality factors will later allow us to calculate mesh qualities, examine their distributions and develop a mesh quality improvement technique. This is done in chapter 5.

Lemma 2.3.1, Theorem 2.3.1 and Theorem 2.3.2 are very important in studying quality improvement of cells. Their proofs are given in chapter 4.

Lemma 2.3.1. *The energy of a point located in a Voronoï region $V(s_i)$ is minimal with respect to all other regions $V(s_j)$ for $i \neq j$.*

Theorem 2.3.1. *The energy function $E(z, \mathbb{V})$ of a Voronoï tessellation is minimized at the centroid sites of the tessellation.*

Theorem 2.3.2. *For a given set of sites $Z = \{z_i\}$, the energy is minimized when \mathbb{V} is a centroidal Voronoï tessellation.*

Proofs of other theorems and lemmas are given in chapter 4.

In the following section we treat a special kind of Voronoï diagrams with interesting properties: Centroidal Voronoï tessellations.

2.4 Centroidal Voronoï Tessellations

A centroidal Voronoï tessellation is a special case of \mathbb{V} where the sites are centers of mass [21, 79, 84–86]. The centroid of a region is defined by

$$c_i = \frac{\int_{V_i} x \rho(x) dx}{\int_{V_i} \rho(x) dx} \quad (2.6)$$

, where $\rho(x)$ is the density function of $V(s_i)$. A very important mathematical feature of centroidal tessellations is their minimization property of the energy function. This attractive property of theirs is the driving factor behind their great utility [79]. It will be shown later that centroidal tessellations are instrumental in quality improvement and solution quality guarantees especially when the initial tessellation sites are founded on domain feature information.

The energy function of a Voronoï diagram is defined as

$$E(z, \mathbb{V}) = \sum_{i=1}^n \int_{V_i} \rho(x) |x - z_i|^2 dx \quad (2.7)$$

. The energy $E(z, V_i)$ of a Voronoï region V_i depends on the following: Density function $\rho(x)$ of V_i and the squared distances between the generating site z_i and nearby points x in the region. The total energy $E(z, \mathbb{V})$ of a Voronoï diagram is the sum of integrals of the individual energies of the regions V_i comprising the Voronoï diagram \mathbb{V} .

Although centroidal tessellations have these important properties, their usefulness, reliability and applicability is in great doubt if the regions from which centroids are derived are not based on domain information [1]. To obviate this, we choose to construct initial tessellations from which centroids would later be generated on domain feature generators.

2.5 Poisson-Voronoi Diagrams

The literature of Voronoï diagrams is almost exclusively developed for Poisson processes. As a result analytical results and tools abound for Voronoï diagrams of Poisson processes. The progress on analytical results is due to the fact that the processes are assumed to be uniformly random, thus simplifying matters. That is, feature information in those processes are largely ignored.

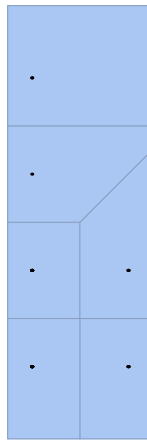


Figure 2.3: Voronoï diagram of a Poisson process

In section 2.2 we introduced the idea of generator sets from which a Voronoï diagram is derived. The only conditions imposed on the generator set S so far is that it be finite. For a Poisson-Voronoi ($\mathbb{P}\mathbb{V}$) diagram we require that elements of S be realizations of a Poisson process and that they be independent.

The probability of observing n events in a given interval of time is a Poisson process with intensity parameter λ . The distribution is a random realization of completely uncorrelated events satisfying

$$P\{N = n\} = \frac{\lambda^n e^{-\lambda}}{n!} \forall n = 0, 1, 2, \dots \quad (2.8)$$

, and the events are disjoint. Notwithstanding the nice properties of Poisson processes and the readily available analytical results due to that, the condition on uniformly and randomly distributed sets could be very restrictive and unsuitable in many practical applications. We therefore choose to found generators on feature-driven models.

2.5.1 One-dimensional $\mathbb{P}\mathbb{V}$ Systems

Assume a ring divided into sections or regions so that the centers of the regions are completely random. Since this follows the Poisson distribution, the probability of finding a gap between X and $X + dX$ is given by

$$\hat{p}^0(X) = \rho e^{-\rho X} \quad (2.9)$$

. The density of their centers is given by ρ . Additionally define a scaled gap function as

$$x = \frac{X}{\langle X \rangle} \quad (2.10)$$

, where $\langle X \rangle = \rho^{-1}$ is the mean gap size. It follows that the distribution of the scaled gap size is

$$\hat{p}^0(s) = e^{-s} \quad (2.11)$$

. By extension

$$p^n(x)$$

is the probability of finding a gap with n additional centers in it [46]. Of course the probability density functions are proper functions. Due to total lack of correlation between the centers, it is possible to express the distribution of the scaled regions for arbitrary values of n in Laplace space as

$$\tilde{p}^n = (\tilde{p}^0(l))^{n+1} \quad (2.12)$$

[46].

One-dimensional $\mathbb{P}\mathbb{V}$ models are found to adequately model the gap size distribution of one-dimensional car-parking problems. The parking behaviour of drivers tend to not favour very small and very large gaps. This means that very small gaps and very large gaps are less probable. On the one hand, small gaps make exit maneuvers very difficult. On the other hand very large gaps are less likely due to multiple reasons: Drivers making parking maneuvers would prefer parking in those gaps for ease of packing and exit and also drivers have a tendency to avoid waste of parking space [46].

2.5.2 Two-dimensional $\mathbb{P}\mathbb{V}$ Systems

Consider the radial probability

$$p^{(n)}(R)$$

that given a generator located at $r = 0$, its $n + 1$ neighbour is located between R and $R + dR$. Given n additional generators inside a circle of radius R , the probability is expressed as

$$\hat{p}^0(R) = c(R)e^{-\int_0^R 2\pi r c(r) dr} \quad (2.13)$$

.

The average number of generators within a disk of radius R is

$$2\pi\rho R,$$

where ρ is the density of the generators.

2.6 Conclusion

Chapter 2 introduced the theoretical background, definitions, theorems and lemmas relevant in the literature of Voronoï diagrams. The mathematical background is necessary and important because it serves as a springboard for connecting quality criteria with mesh element quality improvement, studying pattern organization, connecting derived theorems with behaviour of Human Visual System (HVS) in signal processing etc. A brief review of Poisson Voronoï diagrams is included given their popularity in space partitioning.

Having laid the framework for a general space partitioning algorithm and the mathematical structure of digital images, we proceed to identify the generator sets, S on which the construction of tessellations hinge. This would be done using models that take into consideration important information in the domains. This is presented in chapter 3. Tessellations will later be constructed from feature point sets. The tessellated spaces will also be explored for region processing and associated probabilities with the aim of assessing information content of individual regions and the covered spaces. This could be useful in general signal processing and analysis.

Chapter 3

Feature-Based Point Pattern Generator Identification and Representation

3.1 Introduction

This chapter introduces several feature-based models necessary for point pattern identification and tessellations. Several feature domains are examined and summary point patterns extracted. Extracted point patterns represent shapes, objects and structures formed by domain features. The chapter concludes by presenting the mathematical utility of centroidal tessellations based the definition of energy of cells. The energy minimization property of centroidal tessellations would be useful for cell quality improvement.

Finite dimensional images have finite spatial dimensions. Although spatial dimensions are finite, overall signal sizes can still be significant depending on

application methods considered for signal processing and analysis. Assume the row dimension of an image is M and the column dimension is N . This means that we have in total $M \times N$ feature pixels constituting the image. The nature of digital images is such that although the total number of features is finite, it is usually large and as such limits speed or even the suitability of methods of image processing and analysis. In the following sections, we develop mathematical models to extract subsets of image features as summary pattern representations of the images.

Seeds, generating points or sites of meshes for domains are almost exclusively chosen randomly [21, 23, 87, 88], using Poisson distribution [8], using distribution sampling [77]. They may also be modeled based on uniform distributions. So far, most random generators have been modeled using Poisson (random) processes due to the ease and variety of analytical tools and statistics [8, 89–92] Poisson processes guarantee. Generators so modeled may guarantee quality of meshes but they certainly bear no reference to features of the meshed problem domain. In the search for high quality mesh generating sets, a measure of overall mesh solution quality is introduced. This is useful for identifying the best or most suitable mesh generators (also called sites) based on domain features for mesh generation. The principal benefit of this is the identification of non-random generator sets that produce the highest quality Voronoï tessellations.

Besides, this is necessary to obtain information bearing point pattern sets useful in tessellating feature domains. Another advantage of feature-based models is the identification of initial generators that produce high quality Voronoï tessellations and form initial solution sets for subsequent iterations for solution quality improvement [93–97]

at the same time. Examples illustrating the application of quality measures are given in terms of analyzing and comparing digital image Voronoï tessellation covers. This is presented in chapter 5.

3.2 Feature-based Tessellation Generators

In the open and accessible literature, we do not find works considering the choice of sites for meshing feature-endowed spaces such as images using location of features. We mostly go ahead and tessellate using generators irrespective of locations of features. This approach suffices if the aim and end is general space partitioning. Previously, sites have also been chosen to correspond to center of masses of regions [21, 85] of randomly-inspired tessellations, random locations [9, 98], deterministic or regular locations [9, 22, 23]. In short generators so chosen largely do not take information of the domains into account. The method of centroids has evident advantages [79] but these are questionable if the regions from which we obtain the center of masses do not reflect domain feature locations or information. In this work, various sites based on domain features are first extracted. Subsequently these sites give a tessellation of the space. Given several kinds of sites and their tessellations, quality measures of the meshes are obtained with the view of helping ascertain the best choice of sites for tessellations using an overall quality indicator. This then forms a road map to meshed image studies given sets of sites that yield high quality meshes, as well as for quality improvements based on those initial tessellations.

Important domain features may reside at corners, edges, keypoints, extrema and modal domain feature sites or centers of mass of regions based on feature-inspired Voronoï diagrams. This is different from, but complementary to centroids of regions generated based on random processes. In this approach, domain features and infor-

mation would be used to extract mesh sites. These feature tessellation generators are treated next.

3.2.1 Corner Generators

A very notable thing of a domain such as a digital image imbued with features are corner points. These define points where structures in the image plane intersect. As such they form a solid background for object feature recognition and extraction.

One of the first criteria for corner point identification defines a corner as a point that has low self-similarity [99]. A pixel centered in a patch is compared to nearby pixels in an overlapping patch. This comparison is what produces corner point candidates for further examination. Since inception of the first corner point identification algorithms, improvements in corner point identification through computations of differential corner scores with respect to direction instead of patches have resulted in combined corner and edge detection [100] algorithms. Accuracy of sub-pixel locations in corner identification has been explored [101].

A variety of other corner detection schemes based on different criteria are available: Multiple scales due originally to [100], level curvature [102, 103], difference of Laplacians, Gaussians, and Hessians [104–106], affine-adapted interest point operation [106–108], curvature placement along edges [109], smallest univalue segment assimilating nucleus [110], direct testing of pixel self-similarity and feature accelerated segment [111], non-parametric and adaptive region processing [112], transform [113, 114], adaptive [115] and structure-based [116] techniques. Corner points are identified here as points where lines in an image plane intersect and for which

there are significant changes in intensity of pixels in two or more directions:

$$C(u, v) = \sum w(x, y)[I(x + u, y + v) - I(x, y)]^2 \quad (3.1)$$

The window function $w(x, y)$ may be chosen to be rectangular but could assume other suitable forms. So, a corner point is returned by the corner point function $C(., .)$ if the squared differential intensity between the intensities at locations (x, y) and $(x + u, y + v)$ is large for any given multiple directions. Example of corner points in an image are identified in Fig. 3.1(b). Notice that the point sets identified in Fig. 3.1(b) mostly show and characterize feature points in the image domain where lines intersect.

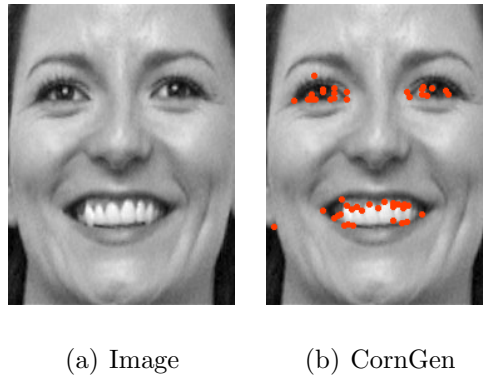


Figure 3.1: Corner Generators

3.2.2 Edge Generators

Edge maps are widely used in pictorial data processing for feature detection and object recognition. Edge information is known to be crucial in detecting jumps in image feature distributions. These have been used due to the fact that edges tend to localize an object of interest for target processing and feature detection.

Edge points are points whose feature values differ sharply from those of neighbouring points [117].

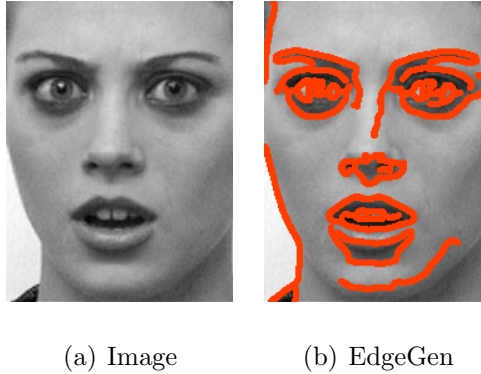


Figure 3.2: Edge Generators

A digital image with edge generators is shown in Fig. 3.2(b). Edge generators can be seen to show borders in the image.

3.2.3 Keypoint Generators

Keypoint criteria are popular for extracting distinct image domain points [118–121]. We shall adopt the scale-space extrema detection process to yield image keypoints [118]. There are potentially numerous keypoint candidates from scale-spaces and so we have to resort to means of identifying the most important ones. For example we could choose to retain the most important ones by eliminating low contrast keypoints. Detecting keypoints invariant to scale changes may be accomplished by obtaining stable features across the scales of an image [118]. In that regard the scale space function $L(x, y, \sigma)$ is obtained by convolving Gaussian functions $G(x, y, \sigma)$ with an image $I(x, y)$ at several scales k . The process is elaborated as follows:

$$L(x, y, \sigma) = G(x, y, \sigma) * I(x, y) \tag{3.2}$$

and

$$G(\vec{x}, \sigma) = \frac{1}{\sqrt{2\pi\sigma^2}} \text{Exp}\left\{-\frac{1}{2}(\vec{x} - \mu)^T \sigma^{-2}(\vec{x} - \mu)\right\}. \quad (3.3)$$

We proceed below to obtain differential functions of the convolved results in the previous step.

$$D(x, y, \sigma) = (G(x, y, k\sigma) - G(x, y, \sigma)) * I(x, y), \quad (3.4)$$

which simplifies to

$$D(x, y, \sigma) = L(x, y, k\sigma) - L(x, y, \sigma) \quad (3.5)$$

In the final step, extrema points are identified by comparing points in the difference functions. Those that attain either minimum or maximum values in their neighbourhoods are selected [118]. Original keypoint locations $D(x, y)$ at scales of $k\sigma$ may be used as estimates in Taylor series expansions about position vectors $\vec{x} = (x, y)$ to obtain more accurate locations of the points [122]. Iterations of locations are illustrated as follows:

$$D_a(\vec{x}) = D + \frac{\partial D^T}{\partial \vec{x}} + \frac{1}{2} \vec{x} \vec{x}^T \frac{\partial^2 D}{\partial \vec{x}^2 \vec{x}} \quad (3.6)$$

, where $D_a(\vec{x})$ is the improved location of a keypoint. A sample space with prominent keypoints is given in Fig. 3.3(b). Notice that keypoints highlight distinct signal points.



(a) Image (b) KeyptGen

Figure 3.3: Keypoint Generators

3.2.4 Modal Pixel and Extrema Generators

Histogram distributions of signals are readily available. They furnish information on the distribution of the features comprising the signal. Pivotal features in an image signal may be sought by considering modal pixel positions in the image. In this way, we get to identify the feature value that dominantly influences the distribution of features in a digital image and use the locations of those as sites for tessellations. However, this approach usually yields too many locations. So a variant to this is to find the modal feature value and displace it by a constant. The resulting feature values and positions form a set of sites for tessellating the image spaces they summararily represent.

The most influential feature m is obtained from the histogram distribution

$$h(k) = \sum_x \sum_y n_k \quad (3.7)$$

as follows:

$$m = \text{Max}_k \left(\sum_x \sum_y n_k \right) = \text{Max}_k (h(k)) \quad (3.8)$$

For a given image function $I(x, y)$, the feature values are in the range $[0, L - 1]$ where L is the number of discrete intensity levels. There exist extrema feature values from this set. Sites corresponding to the extrema can be used for tessellations. However, it would be noted that where any of the extrema is unique, only one site is returned for the tessellation. Extrema sites m_1, m_2, m_d defined below are useful because they can give us geometrical information about shapes and objects that tend to have particular distributions or feature value or range of feature values:

$$m_1 = \text{Min}(f(x, y) \forall x, y) \quad (3.9)$$

$$m_2 = \text{Max}(f(x, y) \forall x, y) \quad (3.10)$$

$$m_d = \text{Max}(\sum \sum n_{ij}) - a \quad (3.11)$$

Extrema sites are discovered using m_1 and m_2 whilst displaced modal sites are discovered using m_d , given the constant a . Due to the numbers of modal and extrema sites and the poor quality of meshes they produce, they are not treated further beyond what is contained herein. Instead, displaced feature sites are extracted and used. The generators returned in Fig. 3.4(c) are of this kind. Observe that dominant points tend to identify points of a particular value where ever they may be.

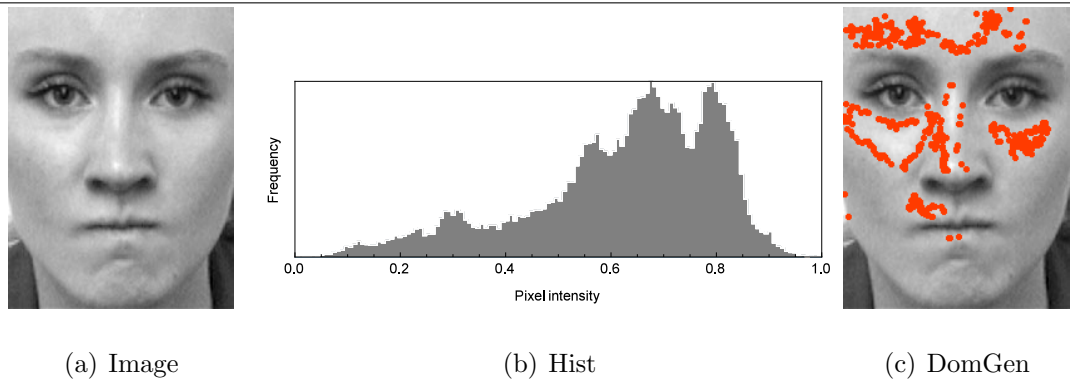


Figure 3.4: Dominant Generators, $m_d = 0.65$

So far, we have identified sites based on corner, edge, keypoint and modal features in digital images. Another important and useful way to model generators is through the centers of mass of regions. Besides, it is necessary to consider the quality of mesh cells based on their feature generators before comparing them with their centroidal tessellations in view of establishing the effects of the choice of sites on mesh quality. This would also prove useful in seeking solution quality improvements and quality guarantees later. In the following subsection, the foundation for centroidal tessellations is presented.

3.2.5 Centroidal Tessellation Generators

To show that the choice of one feature-based generator set or model over another is not arbitrary, we use centroidal tessellations to justify the choice. This will be demonstrated in a later section. For now, we present the underlying theory. Assume a planar tessellation of points. A centroidal Voronoï tessellation resulting from an initial tessellation is a special case of $V(s_i)$ where coordinates of sites are the centroids

of regions computed through

$$c_i = \frac{\int_{V_i} x \rho(x) dx}{\int_{V_i} \rho(x) dx} \quad (3.12)$$

, where $\rho(x)$ is the density function of $V(s_i)$.

Given Voronoï tessellations of image feature generators, we obtain the center of mass of each region from c_i . The centers of mass as defined are used as the generator point sets for further tessellations. The mathematical utility of centroidal tessellations lie in their relationship to the energy function [79] defined by

$$E(z, \mathbb{V}) = \sum_{i=1}^n \int_{V_i} \rho(x) |x - z_i|^2 dx \quad (3.13)$$

. The energy function of a Voronoï region depends on the density function $\rho(x)$ of the region and the squared distances (norms) between the generating sites z_i and nearby points x in the region. The total energy of a Voronoï diagram is the sum of integrals of the individual energies of the regions comprising the Voronoï diagram.

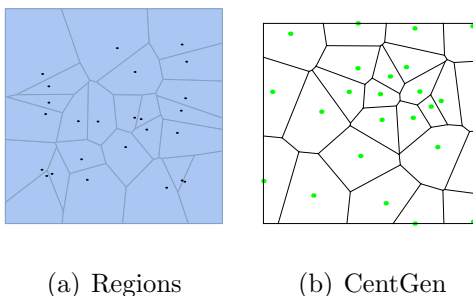


Figure 3.5: Centroid Generators

Centroid generators based on the initial planar tessellation in Fig. 3.5(a) are given in Fig. 3.5(b). Because of the energy minimizing property of centroidal tessellations, they are useful in mesh solution quality improvement. If you overlay the centroidal tessellation Fig. 3.5(b) on the initial tessellation Fig. 3.5(a), it will be noticed that

the centroid generators remain in the capture zones of the initial tessellations. Also, the lengths of the sides of the polygons tend to exhibit less variations compared to those of the initial tessellations. The quasi-perfect polygonal lengths are due to the energy minimization property of the regions and can be exploited for improving quality of cells.

Iterative applications of centroidal tessellations tend to eliminate bad and unstable mesh elements and at the same time guarantee higher qualities in comparison to qualities of previous tessellations. Centroidal Voronoï regions are cells of growth about the centres of mass.

Notice that Voronoï regions are neighbourhoods defined by the norm $\|\cdot\|$. The structure defined by the norm under centroid sites favour uniformity of elements of a structure. More specifically, variations in the lengths of the polygons are usually less than those in the corresponding tessellations from which the centroidal tessellations were generated.

Tessellations and analysis will be based on keypoint, corner, edge, dominant and centroid generators. This is presented in chapter 5.

3.3 Conclusion

Although Poisson Voronoï diagrams are easy to model, they are unsuitable in many instances where the point pattern can not be modeled as a Poisson process. Given this limitation, this chapter presented alternate but complementary models. The models are based on features of the spaces. They identify suitable corners, keypoints, edges and dominant generators or point sets that are later used to tessellate the

spaces in chapter 5. The background is laid for centroidal Voronoï diagrams. They have a special property that is explored for applications in mesh element quality improvement.

In chapter 4, relevant theoretical and mathematical results based on Voronoï diagrams of point set patterns are identified and proved. They are useful in exploring the applications of Voronoï diagrams in signal spaces.

Chapter 4

Theoretical and Mathematical Results on Voronoï Spaces and Mesh Qualities

4.1 Introduction

Several mathematical results including lemmas, properties and theorems relating to Voronoï diagrams are identified and proved here. These are useful observations towards the mathematical foundations of Voronoï diagrams and their applications. Aside from Theorem 4.1.4, Property 1 and the definition of the energy of a Voronoï region, all other mathematical results reported are contributions due to us.

4.1.1 Results on Voronoï Spaces

Lemma 4.1.1. *The energy of a unit pattern located in a particular Voronoï region $V(s_i)$ is minimal with respect to all other regions $V(s_j)$ for $i \neq j$.*

Proof. Consider a point $y \in V(s_i)$. Its energy is evaluated as

$$E(z, V) = \int_{V_i} \rho(y) |y - \hat{z}_i|^2 dy \quad (4.1)$$

. By definition

$$\|y - \hat{z}_i\| = 0 \forall y \in V(s_i) \quad (4.2)$$

, so

$$E(z, V) = \int_{V_i} \rho(y) (0) dy = 0 \quad (4.3)$$

. However $E(z, V)$ of $y \notin V(s_j)$ is

$$E(z, V) = \int_{V_j} \rho(y) |y - \hat{z}_i|^2 dy \neq 0 \quad (4.4)$$

, since neither $\rho(y)$ nor $|y - \hat{z}_i|^2$ is non-zero. □

The energy of a point located within a region is minimum relative to other regions. Knowing this, how does the locations of generators affect the energy of the Voronoï diagram? Theorem 4.1.1 speaks to that.

Theorem 4.1.1. *The energy function $E(z, \mathbb{V})$ is minimized at the centroid sites of the tessellations.*

Proof. Recall that

$$E(z, \mathbb{V}) = \sum_{i=1}^n \int_{V_i} \rho(x) |x - \hat{z}_i|^2 dx$$

. The energy of a Voronoï region V_i is the integral of the product of the density function of that region $\rho(x)$ and the squared distances between the generating site \hat{z}_i and points comprising the region. The total energy $E(z, \mathbb{V})$ is the sum of the energies of all Voronoï regions.

To obtain the minimum value of $E(z, \mathbb{V})$ it is required that the derivative of the function with respect to the sites be equal to zero. The solution of the derivative are the sites \hat{z}_i . That is

$$\frac{dE}{d\hat{z}_i} = 2 \sum_{i=1}^n \int_{V_i} \rho(x)(x - \hat{z}_i)dx = 0 \quad (4.5)$$

and

$$\hat{z}_i = \frac{\int_{V_i} x\rho(x)dx}{\int_{V_i} \rho(x)dx} \quad (4.6)$$

. The solutions \hat{z}_i are the centroids as theorized. □

Theorems 4.1.2 and Theorem 4.1.3 provided in the following texts are direct results of Lemma 4.1.1 and Theorem 4.1.1.

Theorem 4.1.2. *For a given set of sites $Z = \{z_i\}$, the energy is minimized when \mathbb{V} is a centroidal Voronoï tessellation.*

Proof. Immediate from Lemma 4.1.1 and Theorem 4.1.1. □

Theorem 4.1.3. *For a given Voronoï region its energy is minimized if the site of the cell is a centroidal site.*

Proof. Immediate from Lemma 4.1.1 and Theorem 4.1.1. □

Lemma 4.1.1, Theorem 4.1.1, Theorem 4.1.2, Theorem 4.1.3, Theorem 4.1.12, and Theorem 4.1.14 are important and useful because they play a role in cell quality improvement leading to quality guarantees.

Because of the mixed and general shapes of polygons that a Voronoï algorithm produces, the following lemma holds.

Lemma 4.1.2. *Let $A(\mathcal{V}_s)$ be the area of the smallest polygon in a Voronoï mesh and let $A(\mathcal{V}_l)$ be the area of the polygon with the largest area in the same mesh with*

intermediate polygonal areas $A(\mathcal{V}_1) \dots, A(\mathcal{V}_n)$. Then

$$A(\mathcal{V}_s) \subseteq A(\mathcal{V}_l)$$

and

$$A(\mathcal{V}_s) \subseteq A(\mathcal{V}_1) \subseteq A(\mathcal{V}_2) \cdots \subseteq A(\mathcal{V}_n) \subseteq A(\mathcal{V}_l)$$

for a mesh with $n + 2$ polygons.

Lemma 4.1.2 is a general observation. It's not used further.

The following lemma is a result on a sequence of projected mesh cells.

Lemma 4.1.3. *The sequence of all ordered elements of the projections of sets A_1 and B_1 , i.e.*

$$\{a_n\}$$

and

$$\{b_n\}, n = 1, 2, 3, \dots$$

form a metric space.

Consider polygonal elements in \mathbb{R}^n with elements $x = (x_1, x_2, \dots, x_n)$, $y = (y_1, y_2, \dots, y_n)$. Let $\rho(A_1, B_1) = \text{Inf}\{\|x - y\| : x \in A_1, y \in B_1\}$ be the distance between functions of bounded elements A_1 and B_1 of the space. Again let $pr_n(A_1) = \text{Inf}\{x \in A_1 | \exists x_1, x_2, \dots, x_{n-1} \in \mathbb{R} : x = (x_1, x_2, \dots, x_{n-1}) \in A_1\}$ be the projection of set A_1 onto the n^{th} -coordinate space of \mathbb{R}^n and let $\Delta_{l_1 \dots l_{n-1}}$ represent polygons(meshes) of the form $(l_1 h, l_1 h + h] \times \cdots \times (l_{n-1} h, l_{n-1} h + h]$. The parameter h is the edge length and l_1, l_2, \dots, l_{n-1} are integers. The following result pertains [123]:

Theorem 4.1.4. *If A_1 and B_1 are bounded polygons in a Voronoï diagram with a function of the polygons*

$$\rho(A_1, B_1) = \delta_0 > 0,$$

then a family of polygons

$$\{\Delta\}_{k=1}^N, \Delta_k \subseteq \mathbb{R}^{n-1}$$

exists such that

$$pr_{\mathbb{R}^{n-1}}(A \cup B) \subseteq \prod_{i=1}^N \Delta_k$$

for any Δ_k if $x \in A$, $y \in B$, $pr_{\mathbb{R}^{n-1}}x, pr_{\mathbb{R}^{n-1}}y \in \Delta_k$, then $|x_n - y_n| = |pr_n x - pr_n y| \geq \delta = \frac{\delta_0}{2}$.

Proof. Assume $h \in (0, \delta_0(2n)^{-1/2})$. Let $D_{k_1 \dots k_{n-1}} = \Delta_{k_1 \dots k_{n-1}} \mathbb{R}$. Then $D_{k_1 \dots k_{n-1}}$ possesses the following properties:

1. $\bigcup_{k_1, \dots, k_{n-1} \in \mathbb{Z}} D_{k_1, \dots, k_{n-1}} = \mathbb{R}^n$
2. $D_i \cap D_j = \emptyset, i \neq j$
3. $\forall D = D_{k_1, \dots, k_{n-1}}$ and $\forall x, y \in D$ if $\rho(x, y) \geq \delta_0$, then $\rho(pr_n x, pr_n y) \geq \delta_0/2$.

Consider $x, y \in D$ and assume

$$|x_n - y_n| = |pr_n x - pr_n y| < \delta_0/2 \tag{4.7}$$

. Then we have

$$\rho(x, y) = [(x_1 - y_1)^2 + \dots + (x_n - y_n)^2]^{-1/2} \leq (h^2 + \dots + h^2 + \delta_0^2/4)^{-1/2} \tag{4.8}$$

. For

$$h \in (0, \delta_0(2n)^{-1/2}),$$

$$\rho(x, y) = (\delta_0^2(n-1)/(2n) + \delta_0^2/4)^{-1/2} < \delta_0 \quad (4.9)$$

. This is untrue and hence property 3 is proved.

For property 2

$$A \cup B \neq \emptyset$$

and the union of the bounded sets is bounded so

$$\bigcup_{i=1}^N D_i \supseteq A \cup B.$$

Thus the union of all the polygons covers the space

$$\mathbb{R}^n$$

and that proves property 1.

$$pr_{\mathbb{R}^{n-1}}\left(\bigcup_{i=1}^N D_i\right) = pr_{\mathbb{R}^{n-1}}\left(\bigcup_{k=1}^N \Delta_k \mathbb{R}\right) \supseteq pr_{\mathbb{R}^{n-1}}(A \cup B) \quad (4.10)$$

and

$$\bigcup_{k=1}^N \Delta_k \supseteq pr_{\mathbb{R}^{n-1}}(A \cup B) \quad (4.11)$$

.

These statements imply that for

$$x \in A, y \in B$$

we can find

$$\Delta_k$$

such that

$$\rho(x, y) \geq \delta_0$$

by assumption so that

$$\rho(pr_n x, pr_n y) = |x_n - y_n| \geq \delta_0/2 = \delta \quad (4.12)$$

□

Theorem 4.1.4 is a projection theorem. It basically says that if an n-dimensional Voronoï diagram is projected unto one dimension, the result remains a tessellation and generators retain their separation. Theorem 4.1.4 is not used further beyond this point.

Symmetry influences quality of cells. The following is a theorem on the relation of symmetry and cell quality.

Theorem 4.1.5. *Symmetry is a condition for optimality of Voronoï meshes.*

Proof. Note that \mathbb{V} for a set of sites $S = \{s_1, s_2, \dots, s_k\}$ can be expressed as

$$\mathbb{V}(s_i) := \{(s_k - s_i)x \leq \frac{\|s_k\|^2 - \|s_i\|^2}{2}, s_i, s_k \in S, i \neq k, x \in \mathbb{R}^n\} \quad (4.13)$$

[44]. To show optimality we need

$$\frac{\partial \mathbb{V}(s_i)}{\partial s_i}.$$

Taking the derivative gives

$$\frac{\partial \mathbb{V}(s_i)}{\partial s_i} = -x = -\frac{2\|s_i\|}{2} \quad (4.14)$$

. The immediate expression is equivalent to

$$x = \begin{cases} \|s_i\|, & \text{if } x \geq 0 \\ \|s_i\|, & \text{if } x < 0 \end{cases} \quad (4.15)$$

. This is seen to be the mathematical expression for symmetry. \square

Theorem 4.1.5 is important because symmetry perception is influenced by relational structure revealed by Voronoï diagrams [24].

In terms of the relation of numbers of generators, vertices and edges of a Voronoï diagram the following property holds.

Property 1. [8] *The Voronoï diagram of a set S consisting of $n \geq 3$ non-collinear objects with a measure q for the polygons has at most $2n - 5$ vertices and $3n - 6$ edges respectively.*

In the context of near sets, the following theorems have been identified.

Theorem 4.1.6. [124] *The closure of any Voronoï region A in the proximity space X is the set of points $x \in X$ that are close to A .*

Theorem 4.1.7. [125] *The descriptive closure of any Voronoï cell A in a descriptive proximity space X is the set of points $x \in X$ that are descriptively close to A .*

Theorem 4.1.8. [126] *Let $(X, \delta_\Phi), (Y, \delta_\Phi)$ be descriptive proximity Voronoï spaces, $A \subset X, B \subset Y$. If groupoids $A(\circ_\Phi), B(\bullet_\Phi)$ are neighbourly, then $A \delta_\Phi B$ and implies $X \delta_\Phi Y$.*

Theorem 4.1.9. *In a descriptive Voronoï proximity space, a proximal groupoid containing regular elements generates a proximal groupoid pattern in the Voronoï diagram.*

Proof. If A is a Voronoï region in a descriptive proximity space X and is the only proximal groupoid containing neighbourly elements, then $\mathfrak{P}(A) = \{A\}$ is a proximal groupoid pattern containing only the groupoid A . If A, B are a pair of neighbourly proximal groupoids in X , then, from Theorem 6.3.1, $A \delta_{\Phi} B$ and either A or B is a generator of a proximal groupoid pattern. \square

Theorem 4.1.10. *In a descriptive proximity space, a proximal groupoid pattern is a collection of neighbourly groupoids.*

Proof. Immediate from Theorem 4.1.9 and the definition of a proximal algebraic pattern. \square

Theorem 4.1.11. *Let $(X, \delta_{\Phi}), (Y, \delta_{\Phi})$ be descriptive proximity spaces and let $A \subset X, B \subset Y$ generate neighbourly patterns $\mathfrak{P}_{\Phi}(clA), \mathfrak{P}_{\Phi}(clB)$. If every $b \in B$ is neighbourly with some $a \in A$, then $\mathfrak{P}_{\Phi}(clB)$ is a salient proximal algebraic pattern.*

Proof. Immediate from the definition of a salient proximal algebraic pattern. \square

Theorem 4.1.6, Theorem 4.1.7, Theorem 4.1.8, Theorem 4.1.9, Theorem 4.1.10 and Theorem 4.1.11 are important and useful in near set studies explored in chapter 6.

4.1.2 Results on Quality of Cells

We will now consider how using quality factor definitions adopted from [82, 83], maximum cell quality can be attained. In terms of placement of generators and resulting mesh quality, the following results have been identified.

Theorem 4.1.12. *For any plane, an arbitrary a set of sites exists for which the quality of their mesh cell is maximum.*

Proof. Consider an arbitrary n-sided mesh cell. Assume a quad cell without loss of generality. For maximum q , the partial derivatives of q with respect to the l_i should be equal. Assume a cell with $n = 4$ sides. The quality of the cell is given by

$$q = \frac{4A}{l_1^2 + l_2^2 + l_3^2 + l_4^2} \quad (4.16)$$

. The partial derivatives

$$\frac{\partial q}{\partial l_1} = \frac{\partial q}{\partial l_2} = \dots = \frac{\partial q}{\partial l_n} \quad (4.17)$$

with respect to the lengths of the sides evaluate to

$$\frac{-8Al_1}{(l_1^2 + l_2^2 + \dots + l_n^2)^2} = \frac{-8Al_2}{(l_1^2 + l_2^2 + \dots + l_n^2)^2} \dots = \frac{-8Al_n}{(l_1^2 + l_2^2 + \dots + l_n^2)^2} \quad (4.18)$$

. For this condition to be satisfied we must have $l_1 = l_2 = \dots = l_n$. So generators that are such that the side lengths of their polygons are equal satisfy the condition. This also means that their half planes of the cell are equidistant from the generator. \square

Theorem 4.1.12 is important and useful in studying quality improvement of mesh cells.

Let $\{q_i\}, i = 1, 2, \dots, n < \infty$ be the set of qualities of cells resulting from a Voronoï tessellation \mathbb{V} . We have the following result.

Theorem 4.1.13. *Qualities of Voronoï cells, $\{q_i\}$ satisfy the inequality*

$$(q_1 + q_2 + q_3 + \dots + q_n)^2 \leq n^2 \quad (4.19)$$

Proof. Without loss of generality assume a tessellation comprising 4 cells. Notice that

$$q_i \in [0, 1]$$

and

$$(q_1 + q_2 + q_3 + q_4)^2 = q_1^2 + 2q_1q_2 + q_2^2 + q_1q_3 + q_1q_4 + q_2q_3 + q_2q_4 + q_3^2 + 2q_3q_4 + q_4^2 \quad (4.20)$$

. Each individual term

$$q_i^2, q_iq_j$$

is potentially less than its maximum value since all cells may not have $q_i = 1$. This means that the squared sum of the qualities is equal to n^2 if and only if $q_i = 1$ for all cells. The quality inequality must be as it is to take care of qualities other than the extremes of zero and unity. Thus we must have

$$(q_1 + q_2 + q_3 + \dots + q_n)^2 \leq n^2 \forall n < \infty \quad (4.21)$$

□

. Theorem 4.1.13 is useful in examining pattern structure or organization.

Given a cell of unit quality, the following results pertain.

Theorem 4.1.14. [1] *A Voronoï cell of quality $q_i = 1$ has a point inside the cell to which all vertices are equidistant.*

From the result on the maximum cell quality, the following pertain:

Theorem 4.1.15. [1] *For a Voronoï diagram \mathbb{V} with a cell of quality $q_i = 1$, there exists a polygon of \mathbb{V} whose edge lengths are not unequal.*

It is some times of interest to find out how some transformations may affect the quality of a cell. The following is a theorem on scaling transformation of cells.

Theorem 4.1.16. *The quality of a scaled Voronoï cell is scale invariant.*

Proof. Consider an arbitrary triangular cell with quality $q = 1$ before scaling. Now assume the edge lengths of the cell have been scaled with a multiplier $m > 0$. The quality before scaling is given by

$$q = 4\sqrt{3} \frac{\frac{\sqrt{3}l^2}{4}}{l^2 + l^2 + l^2} = 1 \quad (4.22)$$

. The quality after scaling is expressed by

$$q = 4\sqrt{3} \frac{\frac{\sqrt{3}(ml)^2}{4}}{(ml)^2 + (ml)^2 + (ml)^2} = 1 \quad (4.23)$$

. The quality of a cell is therefore unchanged by scaling transformations. □

The following property is a result on the correspondence between the number of quality factors and the number of cells.

Property 2. *Given a measure function $q(\cdot)$ for a Voronoï diagram of an $n \geq 3$ point pattern, the Voronoï tessellation has a total number of qualities equal in number to the number of Voronoï cells.*

4.2 Conclusion

This chapter presented our contributions to the mathematical theory of Voronoï diagrams. Contributions are founded on existing Voronoï diagram literature. The

applicability of theorems and lemmas in connecting element quality to quality criteria, quality improvement, symmetry detection, pattern organization etc. are pointed out.

The utility results and the foregoing foundations, centroidal Voronoï diagrams, mathematical results and theorems on Voronoï spaces in applications of pattern tessellation quality, quality improvement, assessing information levels of Voronoï tessellations, groupoid and proximal element identification among others are presented in chapter 5 and chapter 6.

Chapter 5

Tessellation Quality, Improvement and Information of Patterns

5.1 Introduction

In the following sections, mesh tessellations of digital image patterns based on feature generators are studied. The nature of meshes are characteristic of their generator sets especially when generators reflect domain features. The nature of the resulting meshes is studied via examining distributions of mesh cell qualities and a technique for quality improvement presented. The applications of Voronoï regions in cell processing is explored. This could be useful in terms of exposing information to aid decision making, for example in medical imagery. Estimated quantities such as entropy may also be useful in pattern nature identification, general image understanding and further processing. The Voronoï partitioning algorithm has different time complexities depending on the method of implementation. Given the finite nature of the point sets, the computation times are usually fast and could be linear.

To synthesize and crystallize preceding deliberations on mesh quality analysis, a mesh quality computation algorithm is provided in the following subsection. Subsequently, this sets the tone for mesh space analysis.

5.2 Mesh Quality Computation Algorithm

Observe from the results presented in Fig. 5.1-Fig. 5.20 that a Voronoï diagram is a collection of several polygons, possibly of varying dimensions in accord with the mathematical criteria already laid out. Of course a pattern influences the nature of the polygonal meshes and their quality distributions generated by its point set. Quality factors of polygons in a tessellation were computed using Algorithm 1 in Wolfram Mathematica 10 environment. All quality factors are computed following the definitions from [82,83] as shown by the examples given in chapter 2.

Algorithm 1: Mesh Quality Computation Algorithm

Input : Number of sides, vertex coordinates, area

Output: Quality

for each Voronoï region $V_i \in \mathbb{V}$ **do**

 Access the number of sides and coordinates of the vertices of the polygon

 Using the coordinates, compute the lengths l_i and Area A of the polygon

 Use l_i and A in the appropriate expression to compute its quality q_i

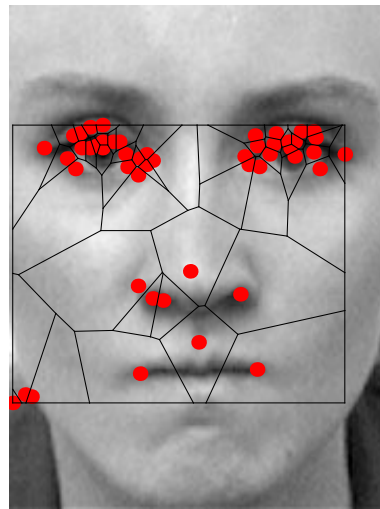
$Q = \{q_i\}$

The results presented in the following sections show tessellated image spaces side by side with the distribution of quality factors depicting the nature of the cells. These are shown for image data of several human faces. From the distributions of quality factors, we obtain the mean quality measure as an indicator of overall quality of meshes due to each type of generating pattern set.

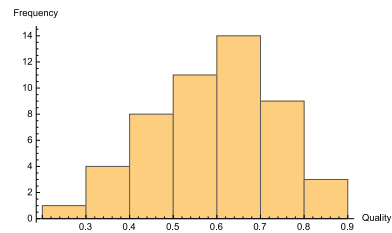
5.3 Application: Digital Image Tessellation Quality

Mesh sites are obtained from 2- D face images [127]. All images are monochrome with dimension 181×241 showing human subjects portraying different facial expressions and orientations. The sites obtained from digital image features are used to tessellate their corresponding image planes. Subsequently, quality factors of cells are computed. Quality factors are shown in histogram distributions next to the tessellated images in Fig. 5.1-Fig. 5.10. The horizontal and vertical axes of histogram plots in Fig. 5.1-Fig. 5.10 represent quality factors and their frequencies respectively. Tessellations and their quality histograms are laid side by side for ease of comparison and economy of space.

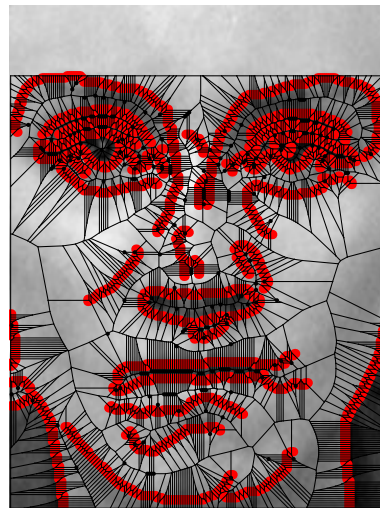
Notice that the cells of the tessellations are mixed. They include triangles, quadrilaterals, pentagons, hexagons etc. in Fig. 5.1-Fig. 5.20. This is opposed to restricting all elements to the same shape such as triangles in the case of Delaunay triangulation [22, 23, 128].



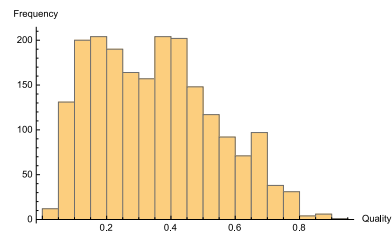
(a) Corners



(b) CorHist



(c) Edges



(d) EdHist

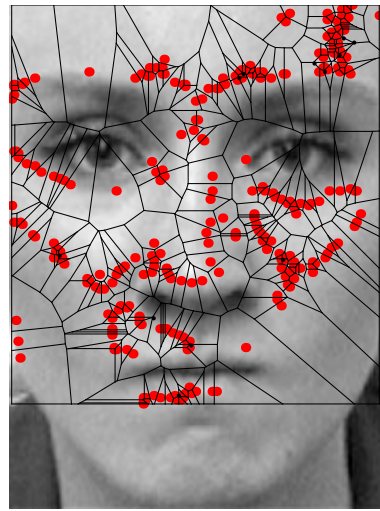
Figure 5.1: Corner vs. Edge Tessellations and Quality Distributions

Remark Corner-based vs. Edge-based Voronoi Tessellations.

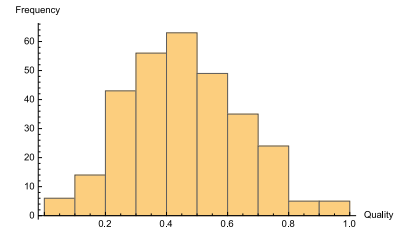
A Voronoi tessellation of a digital image constructed from a corner point pattern set is shown in Fig. 5.1(a). The distribution of their mesh quality is shown in Fig. 5.1(b). The horizontal axis of the histogram represents mesh cell qualities and vertical axis represents the frequencies of the qualities. Because the number of image corners

found are both sparse and clustered in some facial regions exhibiting high gradient changes in multiple directions, the corresponding corner-based mesh consists of fairly large polygons in most regions except around the eyes. Observe that the corner-based mesh histogram has a quasi-normal distribution somewhat skewed to the right. Edge-based cells are skewed in the opposite direction. This shows that in comparison to corner-based cells, edge-based cells tend to produce lower quality cells.

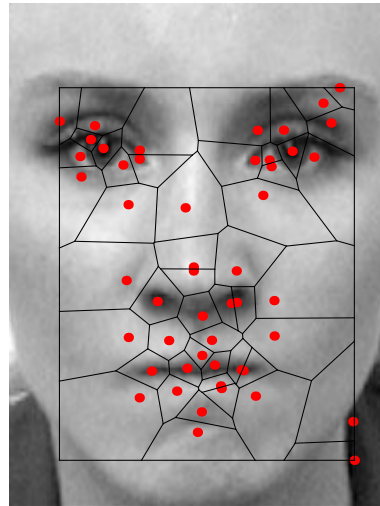
An edge-based Voronoï tessellation of the image in Fig. 5.1(a) is shown in Fig. 5.1(c). The corresponding edge-quality mesh histogram is given in Fig. 5.1(d). By comparison, the number of edge generators is larger than corner generating points. However, edge generator sets are more closely grouped together than corner sets. Hence the corresponding edge-based mesh contains many small Voronoï regions grouped closely together. Consequently, the distribution of qualities due to edge generator sets show a significant population of cells on the lower half of the quality scale. The resulting edge-based mesh histogram exhibits several peaks, which may be an indicator that edge-based meshes generally have poor quality. \square



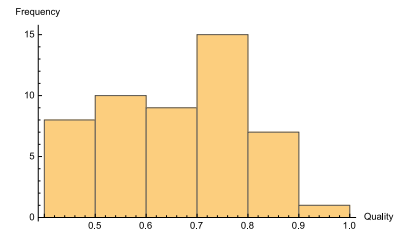
(a) Dominants



(b) DomHist



(c) Keypts



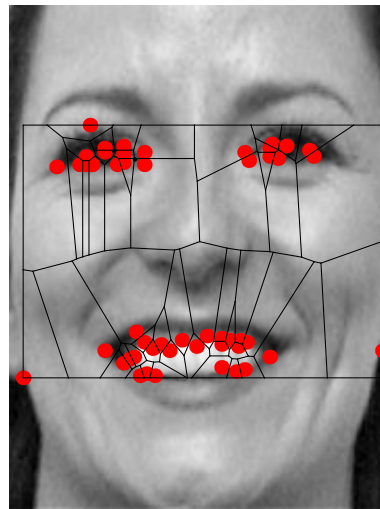
(d) KeyHist

Figure 5.2: Dominant vs. Keypoint Tessellations and Quality Distributions

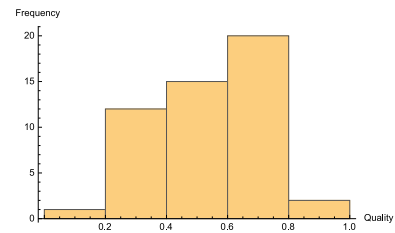
Remark Dominant-based vs. Keypoint-based Voronoï Tessellations.

Fig. 5.2(a) shows tessellations based on a dominant generator point pattern. The distribution of quality of their cells is depicted in Fig. 5.2(b). Keypoint-based tessellations and their qualities are shown in Fig. 5.2(c) and Fig. 5.2(d) respectively. Observe that the dominant-based cells tend to have quality values that fall within

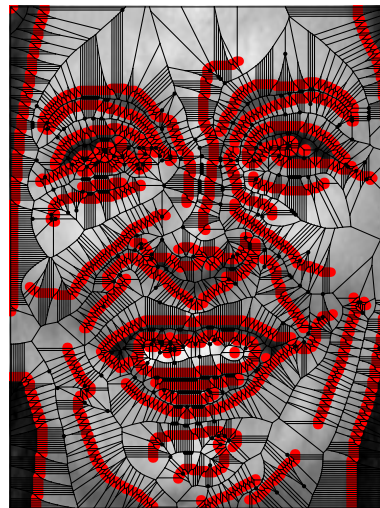
several ranges of the quality scale (global distribution) compared to those of keypoint-based cells. Generally, keypoint-based cells show higher quality factors. Although dominant generators tend to have higher numbers like edge generators, they generally give higher qualities compared to edge-based cells. Keypoint-based cells like dominant-based cells tend to have their qualities distributed in several ranges of quality except the number of fragmented ranges is usually smaller compared to those of dominant-based cells. Keypoint generators tend to be smaller in number compared to dominant generators and their locations and distribution tend to favor creation of more perfect mesh cells as evident by the less fragmented quality scale and the shift of the qualities more to the upper half of the scale. Qualities of dominant-based cells peak around mid scale whilst those of keypoints tend to favour a more flat distribution. The histogram of keypoint-based cells is skewed more to the right compared to dominant-based cells. \square



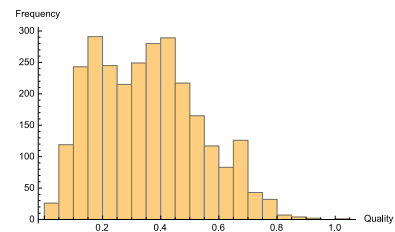
(a) Corners



(b) CorHist



(c) Edges



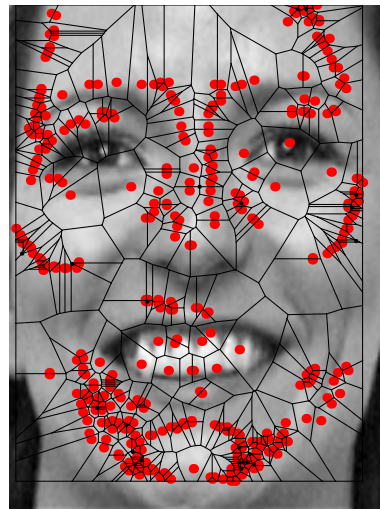
(d) EdHist

Figure 5.3: Corner vs. Edge Tessellations and Quality Distributions

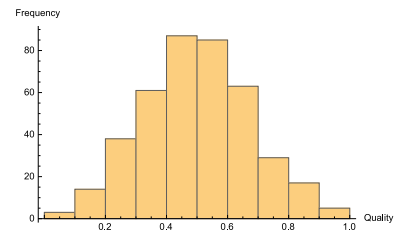
Remark Corner-based vs. edge-based Voronoi Tessellations.

Observe that the corner generators of Fig. 5.3(a) are concentrated in the mouth and eye regions of the subject. The clustering of generators in those regions led to unequal distribution of cell qualities in Fig. 5.3(b). Edge-based generators on the other hand are distributed around the borders of the entire image and separation between

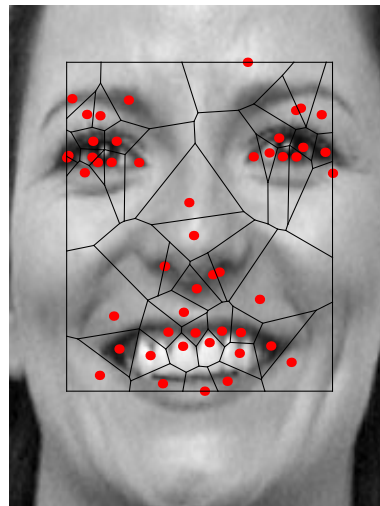
generators is less than in corner-based generators. Distribution of qualities in both instances show clear peaks (see Fig. 5.3(b), Fig. 5.3(d)). The most prominent differences between the two tessellations is that there is greater fragmentation of qualities in Fig. 5.3(d) compared to those in Fig. 5.3(b) and the distribution of qualities in the former is bi-modal compared to the uni-modal nature of the latter. The histograms in both scenarios have comparable skews except quality of majority of corner-based cells lie in the middle and upper portions of the quality scale. \square



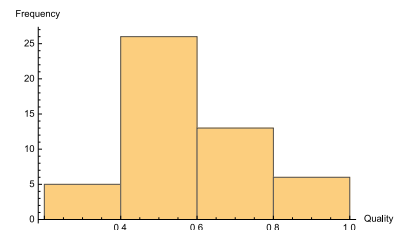
(a) Dominants



(b) DomHist



(c) Keypts



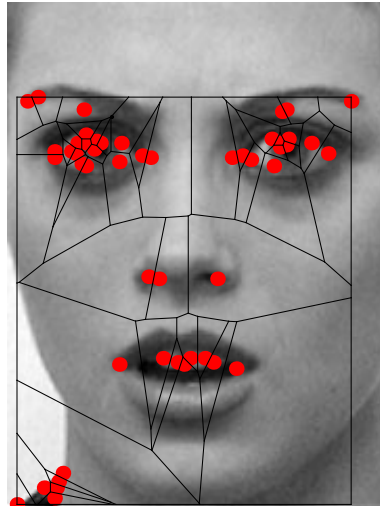
(d) KeyptHist

Figure 5.4: Dominant vs. Keypoint Tessellations and Quality Distributions

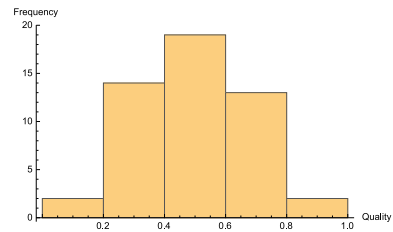
Remark Dominant-based vs. Keypoint-based Voronoi Tessellations.

Dominant generators outweigh keypoints in number (see Fig. 5.4(a), Fig. 5.4(c)). Dominant generators are distinguished by the concentration of extra points around the chin region. Both generator patterns show clustering in the mouth and eye regions. Due to the nature of the distributions of these generators, their cells have compar-

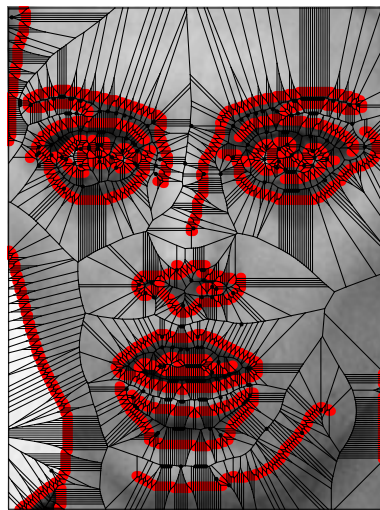
atively high qualities with peculiar uni-modal quality factor distributions shown in Fig. 5.4(b) and Fig. 5.4(d). Quality of keypoint-based cells are skewed more towards the right of the histogram in comparison to dominant-based cells. \square



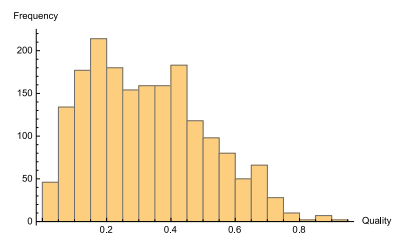
(a) Corners



(b) CorHist



(c) Edges

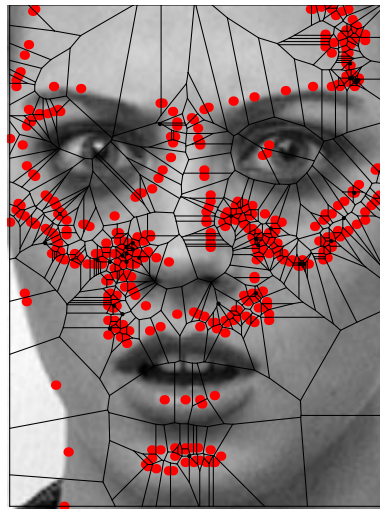


(d) EdHist

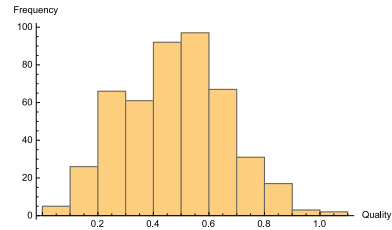
Figure 5.5: Corner vs. Edge Tessellations and Quality Distributions

Remark Corner-based vs. Edge-based Voronoï Tessellations.

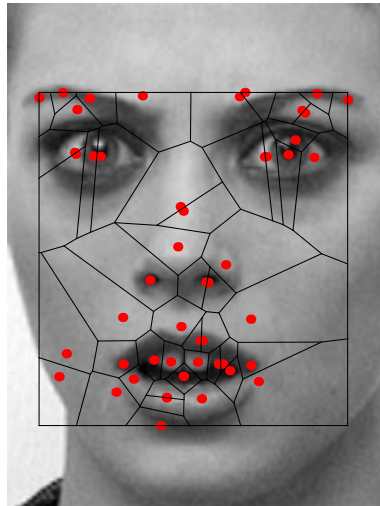
Corner and edge generator sets of a subject are shown in Fig. 5.5(a) and Fig. 5.5(c) respectively. Besides generators around the eye and mouth regions, generators around the nose and lower neck areas are returned for corner sites. Edge generators on the other hand are returned for regions of feature discontinuities and show closer spacing between units of the set. Quality distributions in Fig. 5.5(b) and Fig. 5.5(d) represent cells of more well laid out features on one hand and clustered generators on the other. A marked skewed is not apparent but the concentration of cell qualities is mostly in the middle to upper range of the scale in the case of corner-based cells. \square



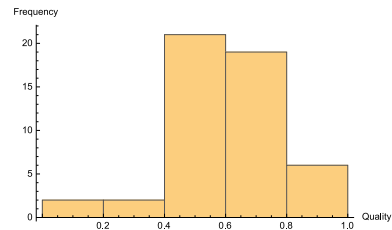
(a) Dominants



(b) DomHist



(c) Keypts



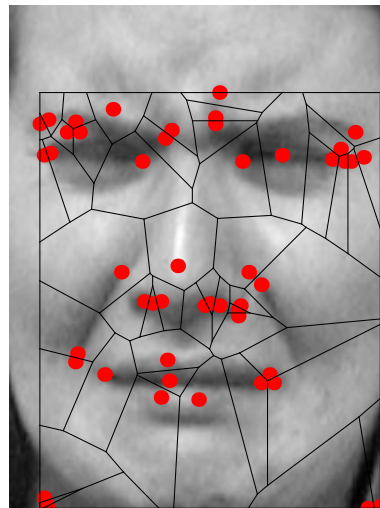
(d) KeyptHist

Figure 5.6: Dominant vs. Keypoint Tessellations and Quality Distributions

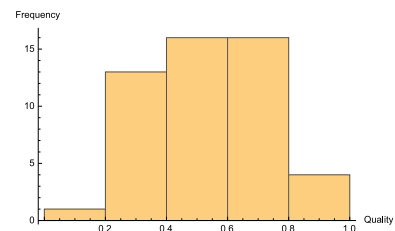
Remark Dominant-based vs. Keypoint-based Voronoi Tessellations.

Dominant generators are distinct from those of the keypoints (Fig. 5.6(a), Fig. 5.6(c)). Keypoint generators are better localized as opposed to the more or less global nature of dominant generators. These fundamentally different generators and their distributions produce a somewhat flat distribution of cell qualities (taken in two halves) and

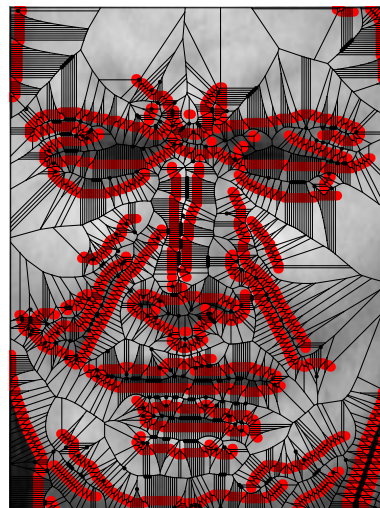
an alternating distribution of qualities seen in Fig. 5.6(d) and Fig. 5.6(b) respectively. A marked skew is not apparent although the histogram of keypoint-based tessellations shows majority of quality factors concentrated in the middle and upper portion of the scale in comparison to dominant-based tessellation. \square



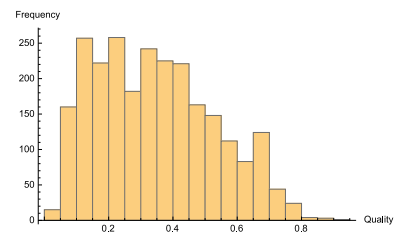
(a) Corners



(b) CorHist



(c) Edges



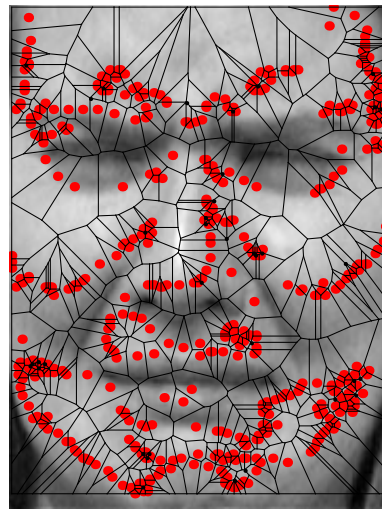
(d) EdHist

Figure 5.7: Corner vs. Edge Tessellations and Quality Distributions

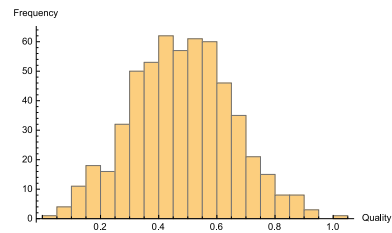
Remark Corner-based vs. Edge-based Voronoï Tessellations.

Distinct and better separated generators are returned in the case of Fig. 5.7(a) as opposed to less distinct and clustered ones in Fig. 5.7(c). Although corner generators are smaller in number, they include a lot of distinct and important features in the image. Edge generators however are localized to boundary regions. Given the layout of generators, corner generators favor creating meshes approaching perfect lengths compared to edge generators in Fig. 5.7(b) and Fig. 5.7(d) respectively. The histogram of the corner-based tessellation shows fewer quality factor concentration in the lower portion of the scale. This appears to be the opposite for the edge-based tessellation.

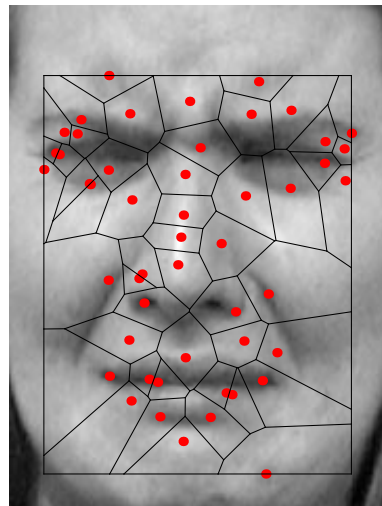
□



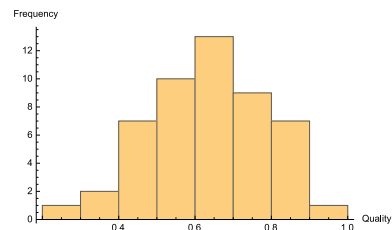
(a) Dominants



(b) DomHist



(c) Keypts



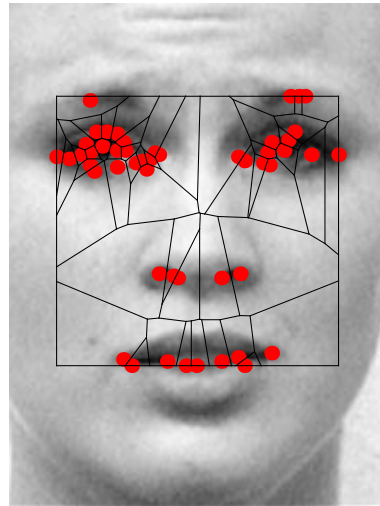
(d) KeyptHist

Figure 5.8: Dominant vs. Keypoint Tessellations and Quality Distributions

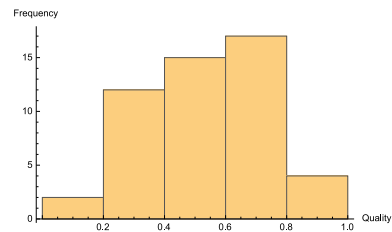
Remark Dominant-based vs. Keypoint-based Voronoi Tessellations.

In Fig. 5.8(a) the layout of the generators largely did not favour polygons with equal lengths. This is evident in the fragmented nature of the quality factors in Fig. 5.8(b). Generators in Fig. 5.8(c) performed better in their quality distributions in Fig. 5.8(d) due to a better layout hence favouring more quasi-equal polygon lengths. The natures

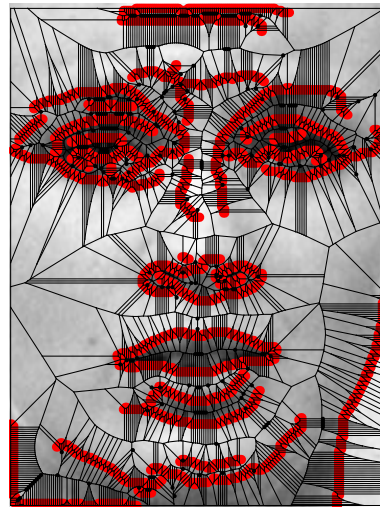
of the histograms appear similar. The difference lies in the numbers of cells and the concentration of the quality of cells in the lower, middle and upper portions of the scale. □



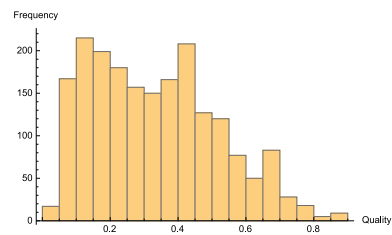
(a) Corners



(b) CorHist



(c) Edges



(d) EdHist

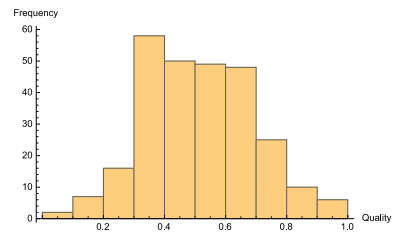
Figure 5.9: Corner vs. Edge Tessellations and Quality Distributions

Remark Corner-based vs. Edge-based Voronoï Tessellations.

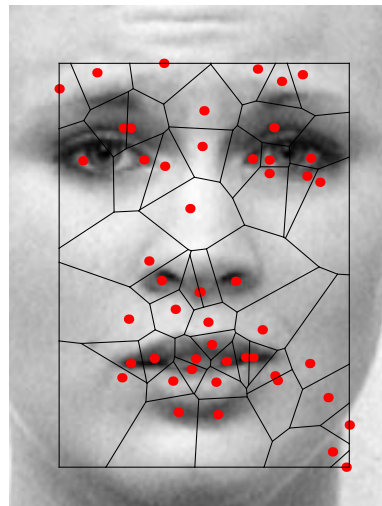
Examine briefly the corner and edge generators and their tessellations in Fig. 5.9(a) and Fig. 5.9(c) respectively. The mesh quality factor distributions are in Fig. 5.9(b) and Fig. 5.9(d) respectively. Observe that there is significant clustering of generators around the eye, nose and mouth regions. Despite significant clustering of corner generators, their cells are generally of superior quality compared to those of edge generators. This is because the clustering of corner generators is less intense compared to edge generators. The histogram for the corner-based tessellation shows concentration of qualities in the middle and upper portions of the scale. The histogram of the edge-based tessellation however shows significant concentration of qualities in the lower portion of the scale. □



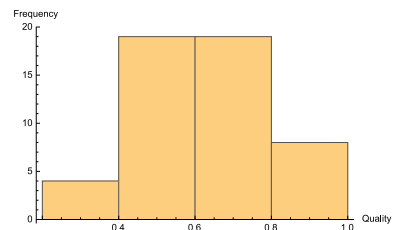
(a) Dominants



(b) DomHist



(c) Keypoints



(d) KeypHist

Figure 5.10: Dominant vs. Keypoint Tessellations and Quality Distributions

Remark Dominant-based vs. Keypoint-based Voronoi Tessellations.

Dominant generators and their tessellations in Fig. 5.10(a) occupy a larger pictorial area compared to keypoints and their tessellations in Fig. 5.10(c). There are numerous cells in Fig. 5.10(b) and most of their quality factors are concentrated in the first half of the scale. Keypoints on the other hand are better laid out. Although they are less

in number compared to dominant generators, they tessellate and cover a comparable space. This distribution results in better overall solution quality in Fig. 5.10(d). The histograms show similarity in that qualities are concentrated in the middle portion of the scale. The difference lies in concentration of qualities in their lower and upper portions. \square

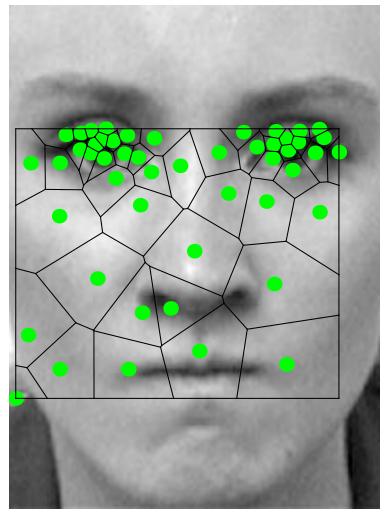
5.4 Towards Mesh Cell Solution Quality Guarantees

Quality guarantees have been established in the literature for mostly mesh triangulations. However, this is not so for mesh cells with four or more sides [129]. Currently, mesh cell qualities are improved by Laplacian smoothing [22, 23, 128, 130], adding extra points known as *Steiner points*, relocating vertices, splitting and merging cells or replacement of elements, also known as face swapping [131]. Aside from the fixed element shape restriction, these quality improvements largely lack motivation because they are not directly connected to any specific quality criteria [132]. Also, smoothing does not guarantee improved element quality. The smoothed mesh may not also remain a valid tessellation as observed in the literature [128]. In the following section, a mesh quality improvement technique is explored towards guaranteeing mesh solution qualities for given initial tessellations. In the case of fixed shape tessellations such as triangles, it's known that the Delaunay triangulation of a random set of sites maximizes the smallest angle, thereby producing cells of good qualities [128]. In this section, we base mesh smoothing on feature point patterns, not random patterns. The motivation lies in connecting quality improvement with side lengths of the cells. Tessellation quality discussed next relies on the energy minimization property of the energy function. This is applicable in quality improvement of cells with $n \geq 3$ sides. Lemma 4.1.1, Theorem 4.1.1, Theorem 4.1.2, Theorem 4.1.3 are important and use-

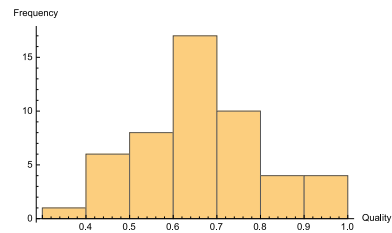
ful because they play a role in cell quality improvement through minimization of quantities such as varying side lengths of polygons. This is so because elements with quasi perfect lengths approach maximum cell quality as shown by Theorem 4.1.12, Theorem 4.1.14, and Theorem 4.1.15.

5.4.1 Tessellation Quality Improvement: Centroidal Tessellations

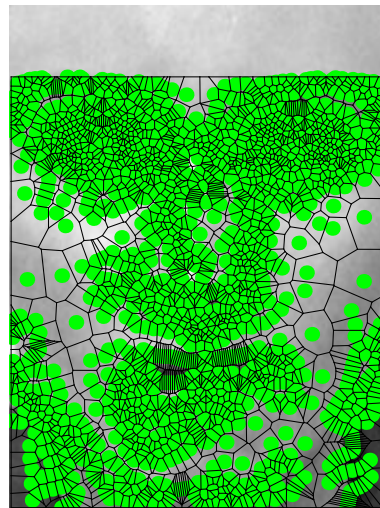
In this section, the utility of centroidal tessellations in cell quality improvement is demonstrated. Prior to this, the applications of centroidal tessellations focused primarily on signal compression, segmentation, territorial behaviour of animals etc. [21]. A complete set of results based on centroids of Voronoï regions specified by corner, edge, dominant and keypoint tessellations in Fig. 5.1-Fig. 5.10 is presented in Fig. 5.11-Fig. 5.20. For the results presented, generators have been obtained corresponding to Voronoï regions of corner, edge, dominant and keypoint-based tessellations. These are the centroids of Voronoï regions in Fig. 5.1-Fig. 5.10. In the following text, remarks are included pertaining to the regions and their qualities. Observe that the minimum quality of cells in centroidal tessellations is generally higher than the minimum quality of cells in the initial feature-based tessellations, courtesy of Lemma 4.1.1, Theorem 4.1.1, Theorem 4.1.2, Theorem 4.1.3. Notice that histogram distributions of centroid-based tessellations tend to be skewed towards the right in comparison to histogram distributions of the initial tessellations. Quality factors are shown in histogram distributions next to the tessellated images in Fig. 5.11-Fig. 5.20. The horizontal and vertical axes of histogram plots in Fig. 5.11-Fig. 5.20 represent quality factors and their frequencies, respectively.



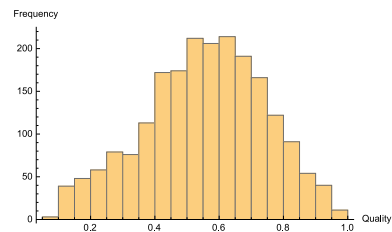
(a) Cornercentroids



(b) CorcentHist



(c) Edcentroids



(d) EdcentHist

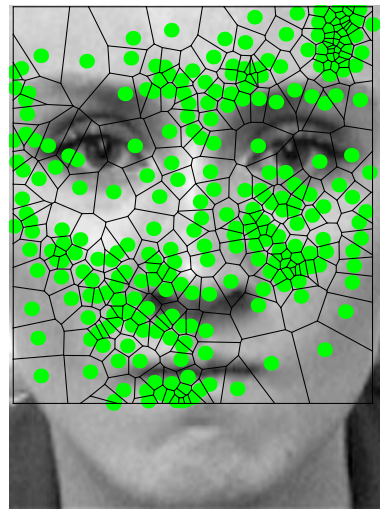
Figure 5.11: Corner vs. Edge Centroid Tessellations and Quality Distributions

Remark Corner centroid-based vs. Edge centroid-based Voronöi Tessellations.

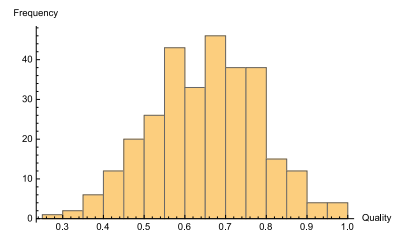
The number of generators in Fig. 5.1(a) is the same as those in Fig. 5.11(a). However, an interesting situation arises. The polygons in the latter demonstrate visible reduced variability in their lengths. This means that we have better or higher quality

of cells giving the quality distribution in Fig. 5.11(b). In a similar vein the number of generators are the same for edge generators and edge-centroid generators. The overall quality has been improved from the neighbourhood of 0.3 to above 0.5 (Fig. 5.11(c), Fig. 5.11(d)). As seen previously, edge generators generally result in poor mesh solution quality so the centroidal tessellation is responsible for the improvement.

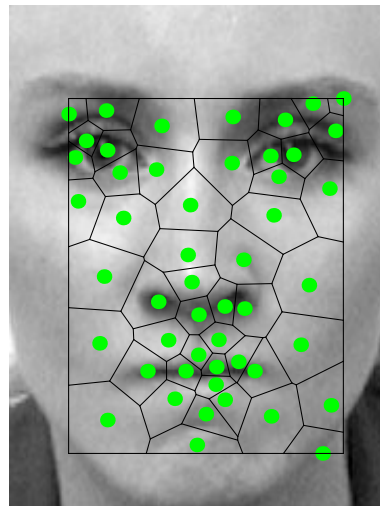
□



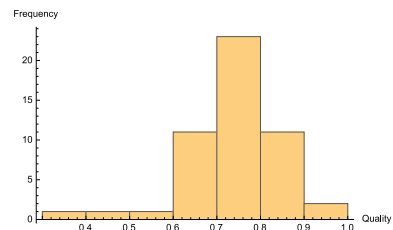
(a) Dominantcentroids



(b) DomcentHist



(c) Keyptcentroids



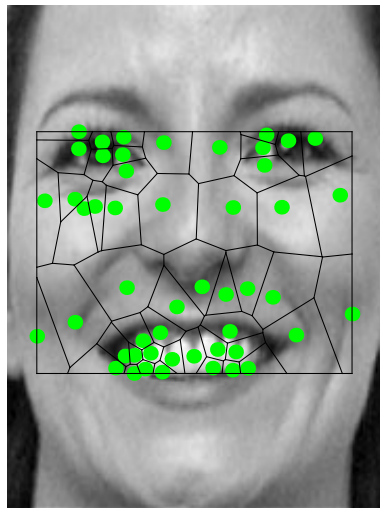
(d) KeyptcentHist

Figure 5.12: Dominant vs. Keypoint Centroid Tessellations and Quality Distributions

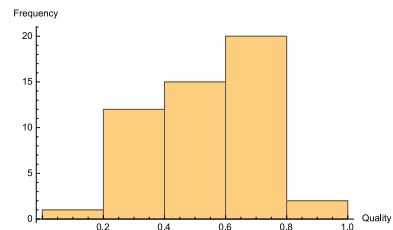
Remark Dominant centroid-based vs. Keypoint centroid-based Voronoi Tessellations.

Observe that the locations of dominant-centroid generators are different from those of dominant generators. The distribution of generators led to a mesh covering of about three quarters of the pictorial surface area in Fig. 5.12(a). Centroid genera-

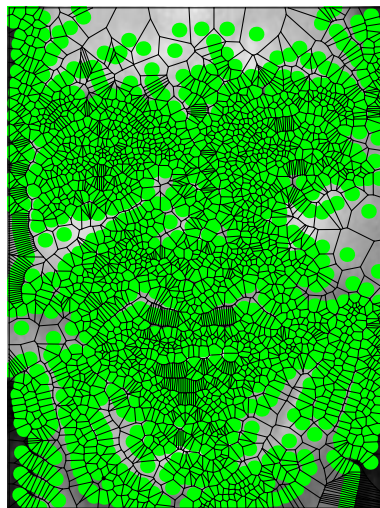
tors favoured better mesh qualities with the distribution in Fig. 5.12(b). Keypoint centroids of Fig. 5.12(c) and their tessellations cover comparable area compared to keypoint generators. The use of centroid generators improved the somewhat high mesh qualities from the previous tessellation. The resulting distribution is given in Fig. 5.12(d). □



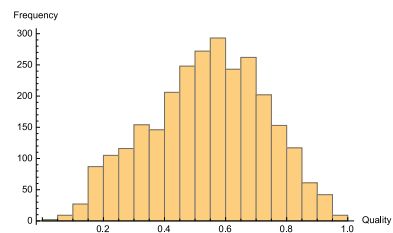
(a) Corcentroids



(b) CorcentHist



(c) Edgecentroids

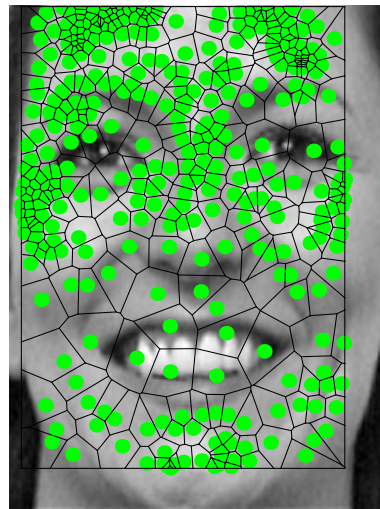


(d) EdcentHist

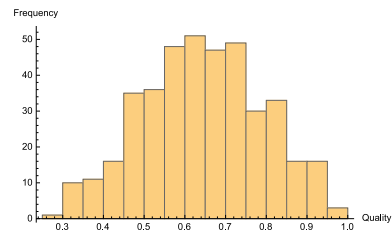
Figure 5.13: Corner vs. Edge Centroid Tessellations and Quality Distributions

Remark Corner centroid-based vs. Edge centroid-based Voronoï Tessellations.

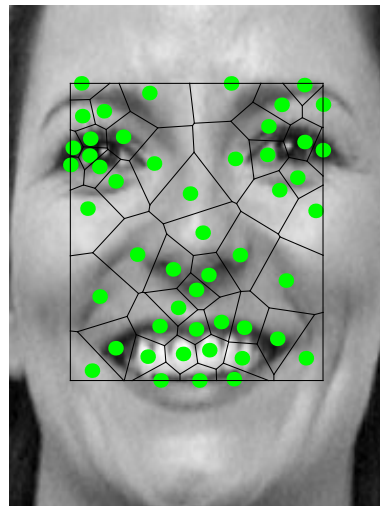
Centroid sites of corner regions in Fig. 5.13(a) barely cover the eyes, nose and part of the mouth region. As expected, edge centroids cover and tessellate the entire pictorial surface area in Fig. 5.13(c). Although the mesh qualities are improved compared to qualities of the initial edge tessellation, the fractional nature of the quality scale is persistent. The distribution of cell qualities in Fig. 5.13(b) and Fig. 5.13(c) is uni-modal. \square



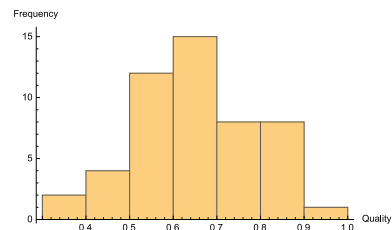
(a) Dominantcentroids



(b) DomcentHist



(c) Keypointcentroids



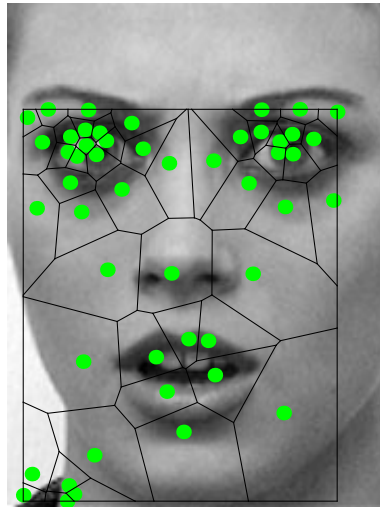
(d) KeypcentHist

Figure 5.14: Dominant vs. Keypoint Centroid Tessellations and Quality Distributions

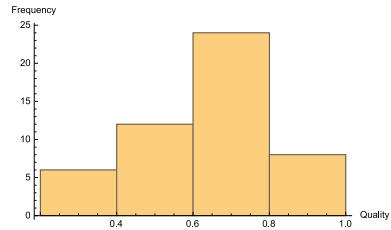
Remark Dominant centroid-based vs. Keypoint centroid-based Voronoi Tessellations.

Observe in the tessellated image spaces that dominant centroid generators are mostly clustered in all areas except in the central eyes and the mouth regions (see Fig. 5.14(a)). Keypoint centroids are distributed primarily in the mouth, nose and eye

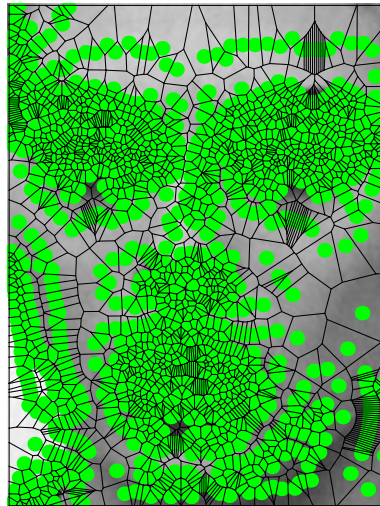
regions observed in Fig. 5.14(c). These generators are less clustered and better laid out compared to their counterparts for dominant and keypoint generator tessellations. It is expected that this distribution would favour improved cell qualities compared to those of centroid dominant generators. Qualities of centroid-based cells are generally distributed across the entire quality scale and are shifted more to the upper half of the scale as shown in Fig. 5.14(b) and Fig. 5.14(d). In most of the cases, the minimum cell quality for keypoint centroid-based generators is in the neighbourhood of 0.4 – 0.5. □



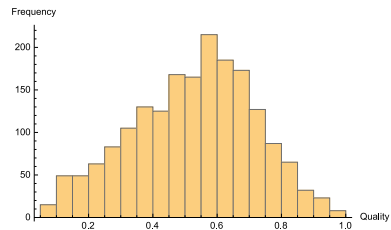
(a) Cornercentroids



(b) CorcentHist



(c) Edgecentroids



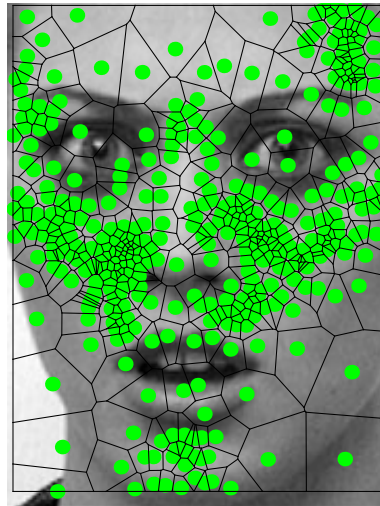
(d) EdcentHist

Figure 5.15: Corner vs. Edge Centroid Tessellations and Quality Distributions

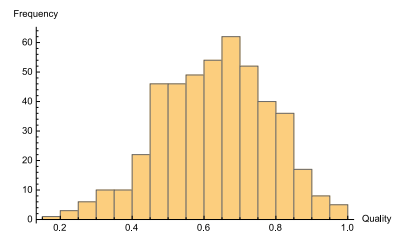
Remark Corner centroid-based vs. Edge centroid-based Voronoi Tessellations.

Notice that there is a significant concentration of generators in the eye ball regions in Fig. 5.15(a). The tessellated regions cover up to the chin. Less variability in polygonal lengths led to distribution of mesh qualities in Fig. 5.15(b). On the other hand the

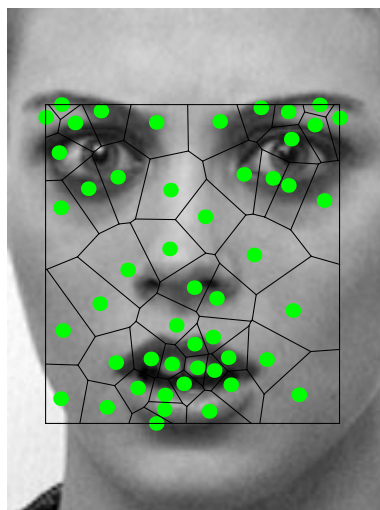
entire image plane is covered by edge centroid generators (Fig. 5.15(c)). Although the qualities remain fragmented, they cover the entire range with the distribution shown in Fig. 5.15(d). The minimum quality value in this case is close to 0.2. \square



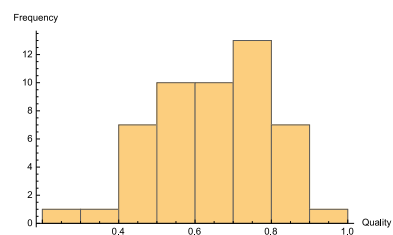
(a) Dominantcentroids



(b) DomcenHist



(c) Keypointcentroids

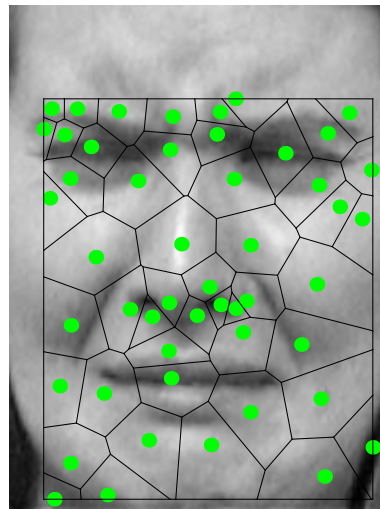


(d) KeyptHist

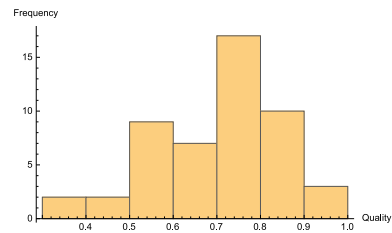
Figure 5.16: Dominant vs. Keypoint Centroid Tessellations and Quality Distributions

Remark Dominant centroid-based vs. Keypoint centroid-based Voronoi Tessellations.

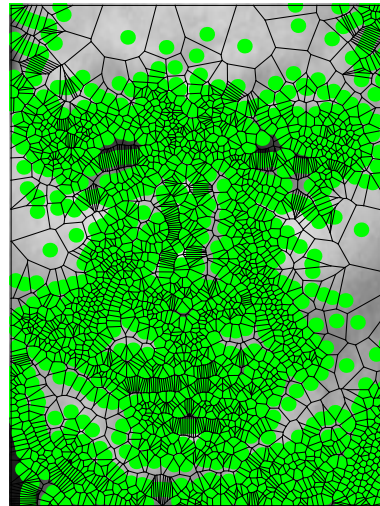
Dominant centroid generators cover most of the pictorial plane. However, most of the generators tend to be concentrated just below the eyes and nose regions. Generators in the forehead, central eye positions and regions to both sides of the mouth are not clustered. As a result cells in these areas exhibit polygons whose length distributions tend to produce cell qualities in the mid and upper portions of the scale. These distributions of the generators afford cells and qualities in Fig. 5.16(a) and Fig. 5.16(b) respectively. Keypoint centroid generators in the eye, nose and mouth regions of Fig. 5.16(c) are not as clustered compared to those in Fig. 5.16(a). They are better spaced out giving the qualities in Fig. 5.16(d). □



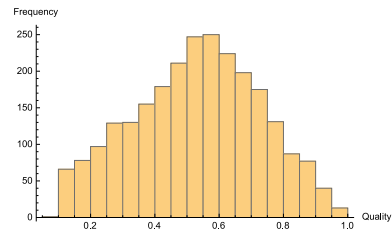
(a) Cornercentroids



(b) CorcentHist



(c) Edgecentroids



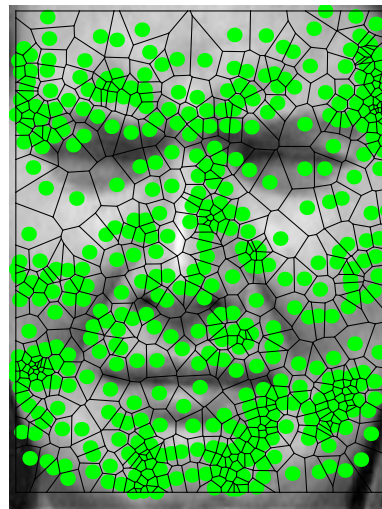
(d) EdcentHist

Figure 5.17: Corner vs. Edge Centroid Tessellations and Quality Distributions

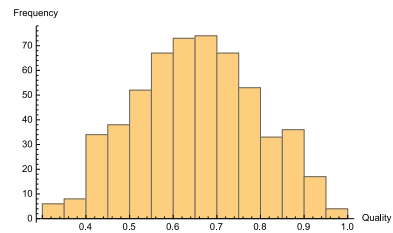
Remark Corner centroid-based vs. Edge centroid-based Voronoi Tessellations.

Centroid corner generators tessellate the image plane captured by the eye, nose and mouth facial features to the exclusion of the forehead and the cheeks. This placement of the generators yielded cells with flat distribution of qualities across segments of

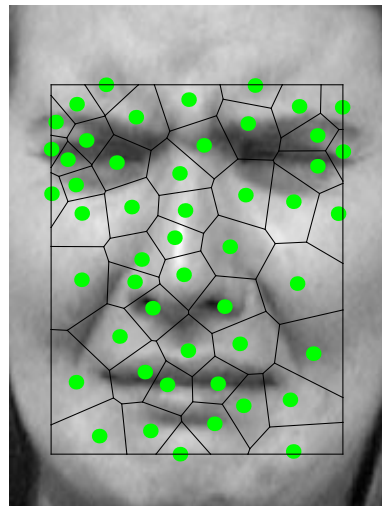
the scale (see Fig. 5.17(a), Fig. 5.17(b)). Edge centroid generators on the other hand tessellate the entire image with heavy clustering in most areas. Clustering is characteristic of both edge generators and edge centroid generators. They tessellate the entire pictorial plane, but cells in the latter case fair better in their solution qualities. As expected, cells in Fig. 5.17(a) have a minimum quality in the neighbourhood of 0.4 in Fig. 5.17(b) compared to cells of Fig. 5.17(c) with minimum quality in the neighbourhood of half of the minimum for cells in Fig. 5.17(a). This is depicted in Fig. 5.17(c) and Fig. 5.17(d). \square



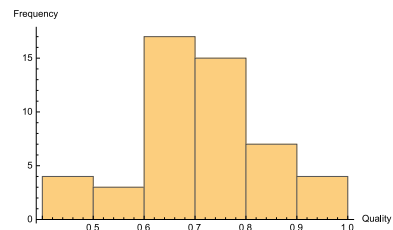
(a) Dominantcentroids



(b) DomcentHist



(c) Keypointcentroids



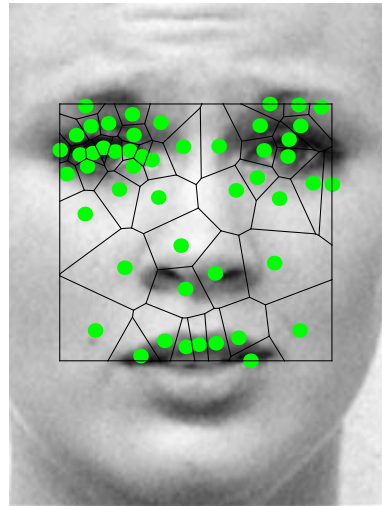
(d) KeypcentHist

Figure 5.18: Dominant vs. Keypoint Centroid Tessellations and Quality Distributions

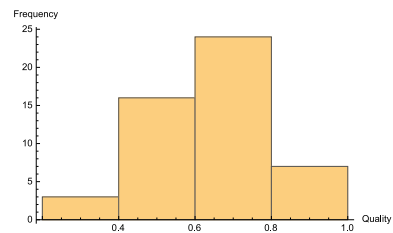
Remark Dominant centroid-based vs. Keypoint centroid-based Voronoi Tessellations.

Dominant centroid generators tessellate most of the image with cells of improved qualities compared to previous dominant generators. The mesh cells and their qualities are given in Fig. 5.18(a) and Fig. 5.18(b) respectively. The qualities of the cells

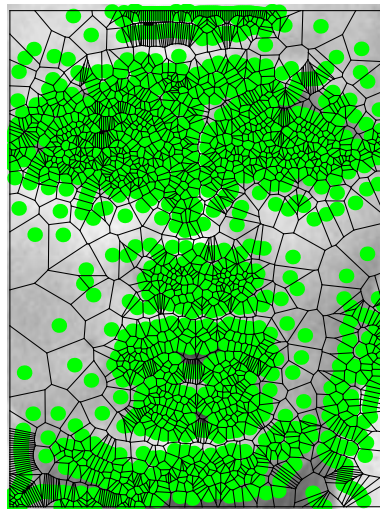
cover the entire scale in both scenarios. However it is noticeable that the cells of Fig. 5.18(c) are of superior quality as shown Fig. 5.18(d). \square



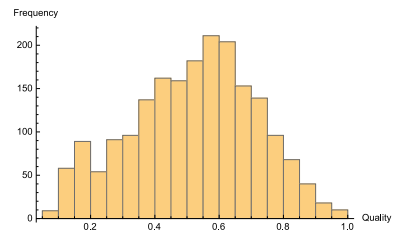
(a) Cornercentroids



(b) CorcentHist



(c) Edgecentroids

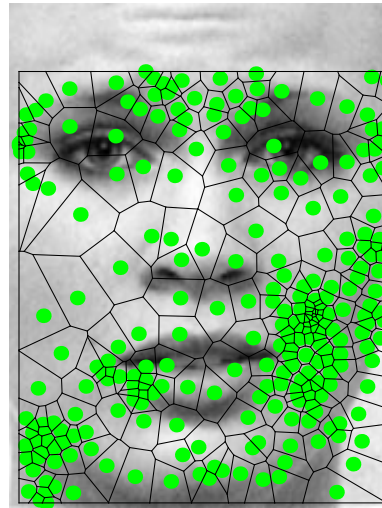


(d) EdcentHist

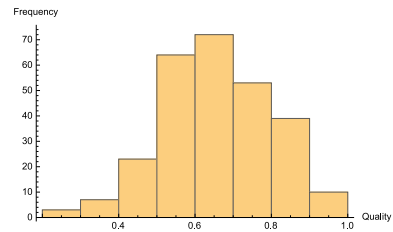
Figure 5.19: Corner vs. Edge Centroid Tessellations and Quality Distributions

Remark Corner centroid-based vs. Edge centroid-based Voronoi Tessellations.

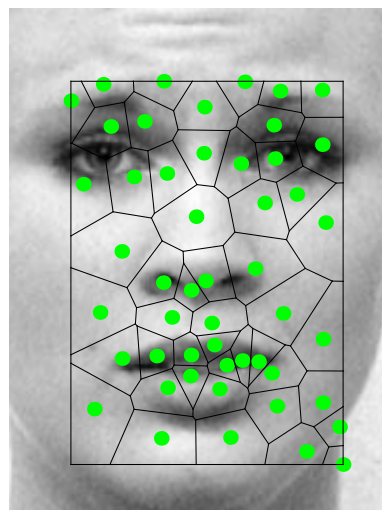
Cell qualities cover the entire scale in Fig. 5.19(b) and Fig. 5.19(d). The difference however lies in the numbers of the generators and locations of generators as seen in Fig. 5.19(a) and Fig. 5.19(c). \square



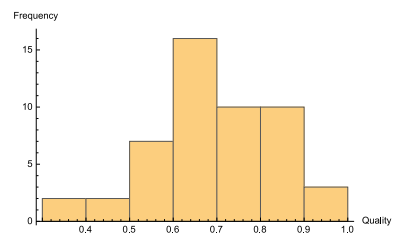
(a) Dominantcentroids



(b) DomcentHist



(c) Keypointcentroids



(d) KeypcentHist

Figure 5.20: Dominant vs. Keypoint Centroid Tessellations and Quality Distributions

Remark Dominant centroid-based vs. Keypoint centroid-based Voronoï Tessellations.

The locations of some generators in Fig. 5.20(a) and Fig. 5.20(c) are approximately the same. However, there is a significant concentration of generators in the left cheek and chin regions of the subject in Fig. 5.20(a). The clustering is not as heavy compared to that in edge generators and their centroids, so they favour better mesh quality generation as seen in comparing Fig. 5.20(b). As expected from the pattern layout, the cells of Fig. 5.20(c) have a minimum cell quality in the neighbourhood of 0.4 which is higher than the minimum cell quality of Fig. 5.20(a) in Fig. 5.20(d). \square

The overall or global mesh quality of a planar tessellation is an indicator of the solution fidelity and stability as well as the nature of the point pattern . It is defined as

$$q_{all} = \frac{1}{n} \sum_{i=1}^n q_i \quad (5.1)$$

, where q_i is the quality of the i^{th} Voronoï cell and n is the total number of cells. Overall quality measures of meshes based on corner, edge, dominant and keypoint generators are presented in Table. 5.1. Images of the various subjects form categories, so in this case we have 5 categories as shown in Table. 5.1 and Table. 5.2. Given any particular image, q_{all} is computed for each set of generators. The plot presented therefore shows the relationships between generator sets and the overall quality of their meshes. Table. 5.1 shows that among all sets of generators and their tessellations, keypoints produce meshes with the best qualities. This is due to the distribution of the sites in such a way that they tend to produce quasi-perfect polygons. Edge generators consistently produced low quality tessellations. This is the case because edge sites tend to be heavily clustered and lie on curve points that are not separated very well. This is characteristic of them and is responsible for

qualities mostly on the lower half of the scale. Qualities of corner and dominant generators assume a place in between those of edge and keypoint tessellations. The overall quality of the cells due to different sets of generators is in proportion to the extent to which they are well laid out or distributed. These distributions influence their tendencies to produce perfect polygons.

Quality analysis of centroidal tessellations based on initial feature-based tessellations show how mesh qualities of initial tessellations are improved (Table. 5.2). In this figure, the qualities of the cells have been improved irrespective of the generator sets. In addition, the order of mesh qualities has been preserved. This improvement is attributed to the energy minimization property of centroids and the quasi-perfect polygons centroids tend to produce, courtesy of Lemma 4.1.1, Theorem 4.1.1, Theorem 4.1.2, Theorem 4.1.3, Theorem 4.1.12, Theorem 4.1.14, and Theorem 4.1.15. In comparing feature-point tessellations and centroidal tessellations derived from them, it can be seen that cells in the latter scenario tend to have reduced variations in their side lengths. This is so because a mesh cell with equal side lengths attains the maximum quality value of unity. That this is so can be corroborated from comparing Table. 5.1, Table. 5.2 and the applicable lemmas and theorems. Notice that overall indices for cells is higher in Table. 5.2 for all point sets. Since the number of cells is the same for corresponding situations, the average cell in Table. 5.2 has higher quality in comparison to the average cell in Table. 5.1. The improvement is due to the non-random centroidal tessellations.

Notice that the tessellations resulting from the quality improvement technique in Fig. 5.11-Fig. 5.20 remain valid tessellations. Also, the qualities are improved as seen in Table. 5.2 and by comparing it to Table. 5.1. This holds for all image data and

Table 5.1: Overall mesh quality based on choice of sites

| Image category | Corners | Edges | Dominants | Keypoints |
|----------------|----------|----------|-----------|-----------|
| 1 | 0.574136 | 0.350751 | 0.487133 | 0.634695 |
| 2 | 0.541544 | 0.361521 | 0.523992 | 0.639031 |
| 3 | 0.505775 | 0.352158 | 0.535527 | 0.604138 |
| 4 | 0.492676 | 0.373659 | 0.461309 | 0.570689 |
| 5 | 0.503550 | 0.347021 | 0.490117 | 0.617198 |

Table 5.2: Overall mesh quality based on centroids of regions due to feature tessellations

| Image category | Corners | Edges | Dominants | Keypoints |
|----------------|----------|----------|-----------|-----------|
| 1 | 0.659837 | 0.541074 | 0.649045 | 0.717758 |
| 2 | 0.615935 | 0.535919 | 0.676633 | 0.704141 |
| 3 | 0.681983 | 0.541327 | 0.655376 | 0.684982 |
| 4 | 0.623852 | 0.540730 | 0.633316 | 0.675515 |
| 5 | 0.649826 | 0.531006 | 0.641290 | 0.692912 |

tessellations represented as categories in Table. 5.1 and Table. 5.2. This is opposed to some algorithms such as the popular Laplacian smoothing algorithm which does not guarantee a valid tessellation and quality improvement [128]. The fixed element requirement, and the lack of connection between the improvement techniques and quality criteria that was previously pointed out are very restrictive. The quality improvement technique presented here is motivated by quality criteria and eliminates the fixed element requirement.

Remark What Quality of Meshes Reveal About Point Patterns in Tessellated Images.

Point pattern sets generate Voronoï diagrams or meshes on planar pictorial image spaces. The geometric region about each element of the point pattern is a convex set represented by a polygon.

Associated with each convex polygon is a quality factor. An aggregate of qualities give the overall quality measure. The value of the quality factor of each cell indicates

if the cell is a good or bad element and hence whether it is stable or not. Given sets of generators and overall tessellation qualities, the tessellation quality characterizes the underlying local structure of a collection of Voronoï regions. Quality of Voronoï polygons give us shape information about the region they cover. For the tessellated spaces, notice that the numbers of interior Voronoï polygons is greater than the number of open border polygons. For example $q = 1$ for a cell would indicate the presence of a perfect polygon and hence a distribution of points that makes it possible. Consider quality expressions for triangles and quads below:

$$q = \frac{4\sqrt{3}A}{l_1^2 + l_2^2 + l_3^2}$$

and

$$q = \frac{4A}{l_1^2 + l_2^2 + l_3^2 + l_4^2},$$

respectively. Now assume two tessellations from the Delaunay triangulation and Voronoï algorithms respectively. If

$$q_i = 1 \forall i$$

in both tessellations, it indicates completely regular and simple underlying patterns in both situations. It's also indicative of the geometrical nature of the cells to fit together on a planar surface without leaving gaps. This is the economy of form and formation employed by honey bees in building their combs. Each bee 'knows' exactly what to do so that one bee does not have to wait for another to complete a cell before it decides what to build next to fit the overall design. Each cell perfectly fits with adjacent ones, producing a tight design.

For small quality measurements as seen for edge point patterns sets, the measures are indicative that the generators could be on a curve and are closely spaced as characteristic of tessellations from edge generators.

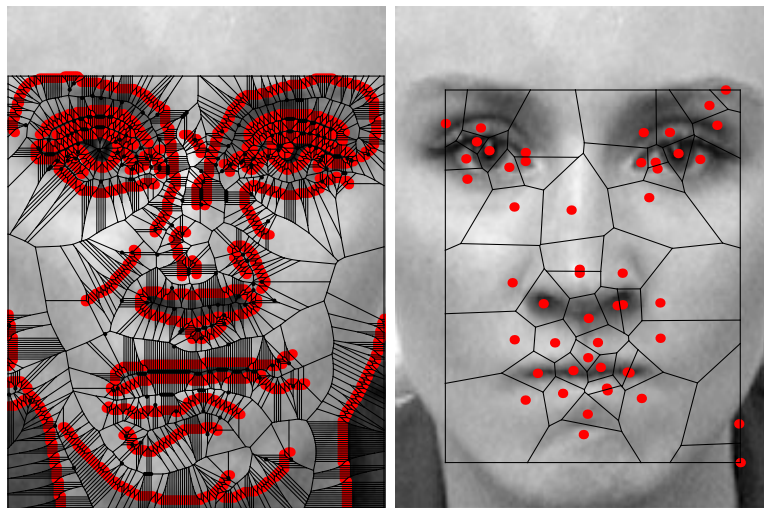
The qualities of cells and the overall quality of a tessellation characterizes the regularity and repeatability of a pattern set. If the space is covered with individual cells of equal quality, that indicates that the pattern points produce perfect polygons in the space. Associated with this is the simplicity of the design of the underlying pattern. Higher qualities indicate simple and predictable distributions while the converse holds for low qualities. This reveals the regularity and predictability of distributions of units of a pattern set.

The quality of mesh cells and their associated image spaces give information on the separability of units of dot patterns. Generally, the higher the quality the greater the separation and regularity of separation between points in the set. For example, the quality of edge generators is small compared to those of corners, keypoints and dominant generators and hence the separation of edge point pattern sets is poor and less regular compared to corner, keypoint and dominant pattern sets.

An extension of the separability of dot patterns and their associated factors is the notion of how adequately the point pattern represents the image space. The quality of a tessellation tells us about the nature or shape of the object depicted by the pattern set. For example, if keypoints are used as mesh generators, then the generated mesh contains a distribution of polygons that surround well spaced out object points in an image where an image object is a structure with distinct and identifiable features. Keypoints tend to surround image objects because they tend to characterize the most important and recognizable features of the object. Edge generators on the other hand tell us about objects localized to image boundaries.

In other words, the high quality of a keypoint-based mesh yields more distinct or precise information about image objects. To illustrate, notice that edge tessellations give meshes with overall quality of 0.352 versus 0.665 for keypoint tessellations in Fig. 5.21(a) and Fig. 5.21(b) respectively.

Although high level insights are not readily evident in terms of image understanding, general image understanding cues are however apparent. For example high individual mesh cell qualities are indicative of object shape points distribution and their interaction as noted above. Relative to each other, overall quality indices show how sufficiently uniform point patterns model the physical image space. Clearly keypoint patterns model the same space more adequately than edge, corner or dominant point sets. In terms of detecting basic information, it can be seen from Theorem 4.1.13 that completely regular patterns would satisfy the inequality exactly. All other patterns would satisfy it to the extent to which they approach regularity.

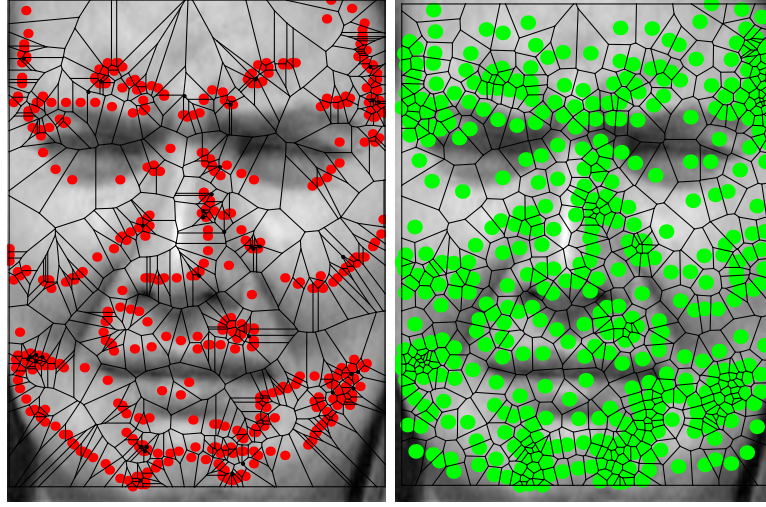


(a) Sufficient1

(b) Sufficient2

Figure 5.21: Meshes demonstrating sufficiency of coverings

Important information may be furnished by point patterns and their resulting tessellations as relates to symmetry. Symmetry of image objects stems from the presence of points that mirror one another. A sense of symmetry is created if given a set of points on one side of the image there is another set of objects on an opposite side with corresponding approximate mirror locations. The higher the quality, the greater the symmetry of image objects. High quality meshes tend to have connected sets of highly symmetrical polygons. That this is so is proven by Theorem 4.1.5. This is important because symmetry perception is influenced by relational structure revealed by Voronoï diagrams [24]. To demonstrate symmetry, consider two generators $S_1(x_1, y_1)$ and $S_2(x_2, y_2)$ on either side of a vertical line $x = k$ through a nose point. The generators S_1 and S_2 are symmetrical if and only if $\|(x_1, y_1), k(x, y)\| = \|(x_2, y_2), k(x, y)\|$ where $k(x, y)$ is a point on $x = k$. Consider the mesh coverings in Fig. 5.22 due to dominant generators and their centroids. A vertical line through the center of the nose region reveals that the generators in Fig. 5.22(b) demonstrate a better reflection of features than in Fig. 5.22(a). Symmetry thus furnishes us with a tool for location of matching features given a feature subset on one half of the space.



(a) Symmetry1

(b) symmetry2

Figure 5.22: Symmetry of features

The quality of an image mesh covering can be used as an estimate of visual image quality. Two image quality assessment methods will be compared here: Image structural similarity index (SSIM) and image quality through Voronoi tessellations. SSIM compares normalized local pixel patterns [133]. For a signal pair X, Y it is defined by [133]:

$$SSIM(X, Y) = \frac{(2\mu_X\mu_Y + C_1)(2\sigma_{XY} + C_2)}{(\mu_X^2 + \mu_Y^2 + C_1)(\sigma_Y^2 + \sigma_X^2 + C_2)} \quad (5.2)$$

. In the definition above, the SSIM between X and Y uses signal statistics; the mean values of the signals μ_X, μ_Y , their variances σ_X^2, σ_Y^2 , cross correlation between signals σ_{XY} and default constants $C_1 = 0.01$ and $C_2 = 0.03$ [133].

Voronoi mesh image quality on the other hand is defined by geometrical attributes of the polygons enclosing image object points and regions in a tessellated space. Given $\{q_i\}$ of a tessellated image space, the visual mesh image quality is defined by q_{all} .

Notice that $SSIM(X, Y)$ uses entire image spaces for image quality assessment and

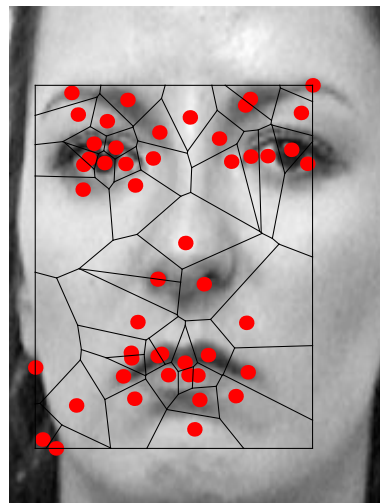
the images must be of the same size. Besides the size constraint, huge signal sizes can make it a computationally burdensome and intensive task. Voronoï analysis of image quality on the other hand uses a small set of the features used in SSIM. To demonstrate, four image signals and their mesh coverings are given in Fig. 5.23 and Fig. 5.24 respectively.



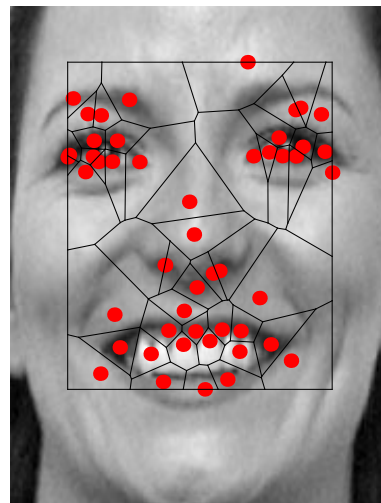
(a) Image 1



(b) Image 2



(c) MeshCover 1



(d) MeshCover 2

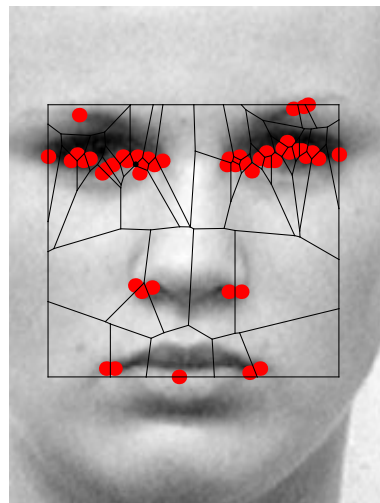
Figure 5.23: An image pair and their meshed domains for SSIM and quality comparisons



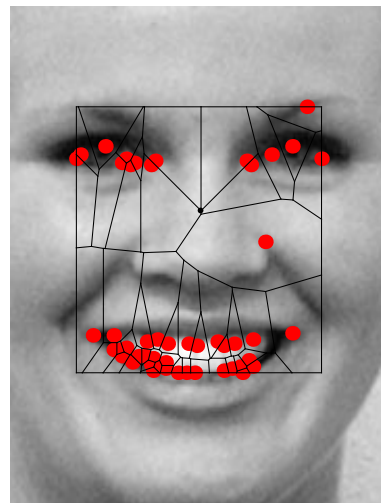
(a) Image 3



(b) Image 4



(c) MeshCover 3

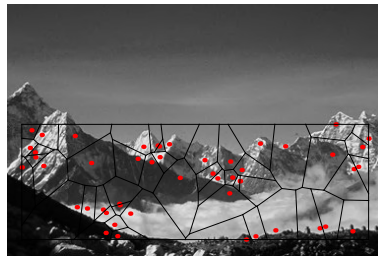


(d) MeshCover 4

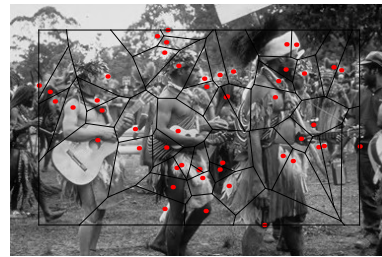
Figure 5.24: An image pair and their meshed domains for SSIM and quality comparisons

Table 5.3: SSIM and Quality Indices

| Image | SSIM | q_{all} |
|-------|--------|-----------|
| 1 | 0.5569 | 0.562207 |
| 2 | - | 0.581664 |
| 3 | 0.5969 | 0.538463 |
| 4 | - | 0.538030 |



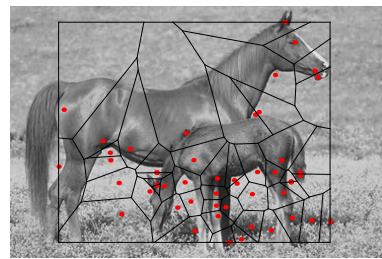
(a) Mountain



(b) Humans



(c) Building



(d) Horses

Figure 5.25: Overall quality factors due to categories of images

Image quality indicators of the signals in Fig. 5.23 and Fig. 5.24 are reported in Table. 5.3. Although the entire feature space is utilized in the calculation of the SSIM, their values are comparable with those obtained with Voronoi tessellations. Notwithstanding, the Voronoi image quality method provides a quality indicator for each image whereas two signals of equal size are needed to output their SSIM. The ideal index possible is unity. An image Voronoi index of 1 means that the point

pattern spatial geometry or arrangement is perfectly regular while an SSIM of 1 would mean a perfect match between the two images.

□

Observe that there are differences between the SSIM and q_{all} indices in Table. 5.3, albeit small. Differences arise because the mesh approach uses polygonal regions of uniform density functions and the shape information they capture based on a subset of image features whilst the SSIM index utilizes the entire feature space. The SSIM index is influenced by constants C_1, C_2 as such their values affect the indicators. The mesh approach however depends on image features only.

Note that mesh qualities show that low overall quality generators are not sufficient descriptors of image features. On the other hand high mesh qualities indicate important and influential image features useful for image and mesh analysis. Also, note that the numbers of generator sites are different for corner, edge, dominant and keypoint sites. Even though edges tend to have the highest numbers, their qualities are very poor in comparison to the other generators. This shows that high quality meshes such as those generated by keypoints identify better the most influential, more well laid out and important features in image characterization and representation.

In terms of what overall quality factors could tell us about images, observe that as the lengths of sides of polygons approach equality, the shape defined by the contour of the polygons more accurately approximates the shape of an underlying image object. To illustrate, consider the meshed image facial image topologies in Fig. 5.23 as well as topologies from mountain, human, building and horse categories in Fig. 5.25. Notice that Fig. 5.23(a) and Fig. 5.23(b) are images of the same subject.

The q_{all} of Fig. 5.23(a) and Fig. 5.23(b) although they are of the same subject are 0.562207 and 0.581664 respectively as given in Table. 5.3. The indices correspond to different facial expressions of images in the same class, so they could therefore be used for facial expression detection and classification. Likewise indices 0.538463 and 0.538030 in Table. 5.3 correspond to different facial expressions of the same subject in Fig. 5.24(a) and Fig. 5.24(b) respectively.

In terms of potential ability of q_{all} in discriminating between different classes of images, the overall quality factors of mountain, human, building and horse image categories in Fig. 5.25 are 0.614676, 0.576321, 0.59573 and 0.563512 respectively. Although differences between the values are not large, no two are equal. So, given an overall quality index of a test categorical image, it could be classified based on the closeness of its index to that of a given class.

5.5 Mesh Cell Entropy Assessment

Informative and interesting Voronoï region processing and measures utilizing probability density functions and qualities of Voronoï cells resulting from tessellations of digital image point patterns are introduced. This is done using the entire signal space and regions of interest respectively.

We may expose more detail in a signal if we use the entire signal space as shown by the results in the section on image complementing and processing. On the other hand, we can learn general and basic information about a signal from processing of regions of summary point patterns. The approach of using the entire signal space can be useful when seeking to expose more detail to aid decision making. The latter approach suffices when the aim is discerning general information and trends of quantity

relations.

5.5.1 Gini Index Mesh Cell Processing

Distribution of image features can be exploited for image analysis to reveal imbedded information content. Mathematical models utilizing Gini indices [3, 134–138] have been adopted in a number of areas for pattern recognition and classification, signal comparison, measuring sparseness, signal reconstruction, enhancement and denoising [139–145]. Gini's coefficient or index is defined as a disparity measure expressed by the difference between unity and sums of squares of probabilities of variables. The following subsection on signal complementing is directly related to recent work on the topology of digital images [146] and visual pattern processing [147]. In this subsection, the utility of Gini indices as information measures is extended to pixel patches viewed as Voronoï regions. Mesh cell processing can be applied in image processing in two ways: Restricting element shapes to a fixed shape or allowing general and mixed element shapes. Given the fixed square patch nature of image pixels, the former approach is consistent with signal complementing. In Section 5.6, the latter approach is adopted since it's consistent with general and mixed element shapes of the Voronoï algorithm. Fixed element shapes defined by square patches are explored for the purposes of image complementing and enhancement of an entire signal space. Gini index-based techniques have seen several applications in signal analysis because of readily available distributions of signal features [3]. This disparity measure is used here for region complementing and processing. A signal is mapped to another when a transformation function based on signal information is applied. In this image processing application, a transformation function maps an input image to a processed image to reveal several features not readily apparent in the input image depending on

the nature of the transformation function. In this application, transformation functions to accomplish mappings based on feature information is usually not a simple linear function as assumed and observed in traditional signal complementing. A linear transformation function lacks flexibility besides the fact that the distribution and interaction of features may not be linear. Transformation functions developed here are therefore based on nonlinear point-wise formulations via Gini indices introduced by C. Gini (1884-1965). This formulation uses discrete probability values of signal features in the transformation function that yields the signal complement given fixed region shapes. The formulation is also seen to be the Tsallis entropy of the feature values given the appropriate choice of parameters.

5.5.2 Signal Complements

Generally a gray level transformation is a point-wise operation defined by

$$g(m, n) = \mathcal{T}[I(m, n)] \quad (5.3)$$

, where

$$I = \begin{bmatrix} f(1, 1) & f(1, 2) & \cdots & f(1, n) \\ f(2, 1) & f(2, 2) & \cdots & f(2, n) \\ \vdots & \vdots & \ddots & \vdots \\ f(m, 1) & f(m, 2) & \cdots & f(m, n) \end{bmatrix}.$$

Here, $g(m, n)$ is the value of the pixel $I(m, n)$ produced by the operation of the transformation $\mathcal{T}[\cdot]$. Each square patch of the image is a Voronoï region about generating point $p(x, y)$ at the center of the patch. An image complement or negative

is defined by the following point-wise operation

$$g(m, n) = L - 1 - r \quad (5.4)$$

, where $L - 1$ is the maximum gray value in I and r is the input gray value from I .

The traditional complement of an image with intensity values in the range $[0, L-1]$ is obtained via the immediate transformation given.

In the set theoretic approach, the images I and G are typically ordered pairs of numbers and so we can write:

$$f(m, n) \in I$$

and

$$g(m, n) \in G.$$

Notice that I and G are generally non-empty sets and so by this analogy the complement of the set I is the set of elements that are not in I . This is expressed as

$$G = I^c = \{t | t \notin I\} \quad (5.5)$$

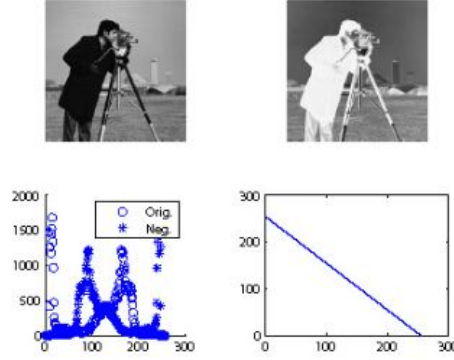


Figure 5.26: Linear transformation of an image

Notice that when an image complement is obtained via a linear transformation function, it is based on only the pixel values in the image (see Fig. 5.26). This formulation makes use of only the pixel values. Alternatively, it would be advantageous to have an approach that makes use of the pixels and information by incorporating their probability distributions. In the explored technique, the pixel values in the complement image are obtained through the pixel values of the original image and their probability distributions through an entropy criterion. This formulation is implemented by first obtaining the Gini complement of an image. The result can further be enhanced by subsequent processing.

This technique of image complementing is effectively an information theoretic approach utilizing pixel values and their probabilities. Given pixel values are in $[0, L - 1]$, Gini transformed pixels or Voronoï regions are defined by

$$\text{Gini}(k) = 1 - \sum_k p^2(r_k) = 1 - \frac{1}{(MN)^2} \sum_k n_k^2 = 1 - \left(\sum_k p(r_k)\right)^2 - \text{const} \quad (5.6)$$

, where $k \in [0, L - 1]$, MN is the total number of features comprising the signal and const is a constant.

5.5.3 Results of Information-Based Complementing of Signals with Applications to Medical Images

Negatives of medical images [148] based on Gini index transformation functions are presented [3]. The medical images shown here include a Computed Tomography (CT) scan of a lymph node of a patient shown in Fig. 5.27, CT scan of abdomen (pancreas area) capturing the lungs and mediastinum of a patient (Fig. 5.28 and Fig. 5.29) and a Magnetic Resonance Image (MRI) of axial slices of the abdomen of a patient through the liver and kidneys (Fig. 5.30 and Fig. 5.31). Gini images obtained are comparable with image negatives obtained through the traditional linear complementing approach. However, processed images demonstrate visual acuity not apparent in original signals. This could be useful in detail medical image analysis and decision making. These signal complementing and enhancement techniques were implemented in MATLAB R2014b.

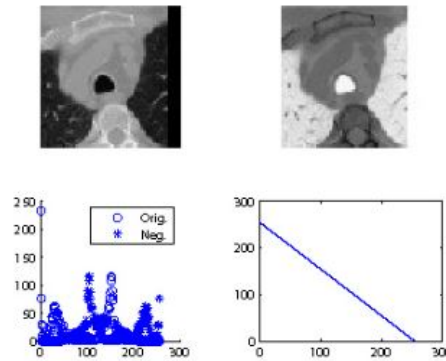


Figure 5.27: a. Original image b. Linear complement c. Feature distributions d. Transformation function

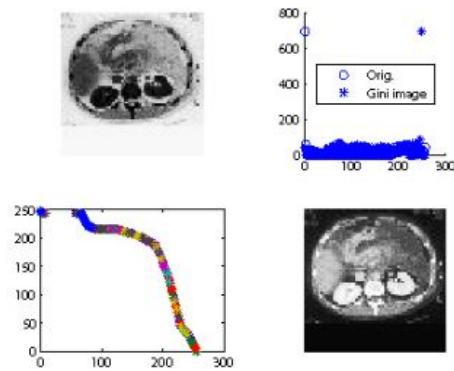


Figure 5.28: a. Gini image b. Feature distributions c. Transformation function d. Linear complement of Gini image

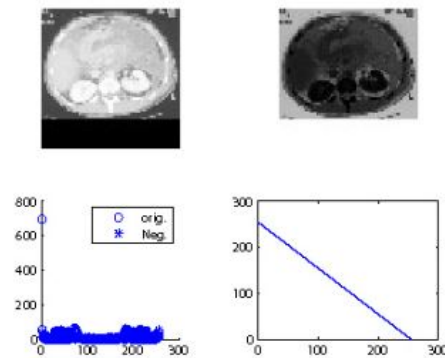


Figure 5.29: a. Original image b. Linear complement c. Feature distributions d. Transformation function

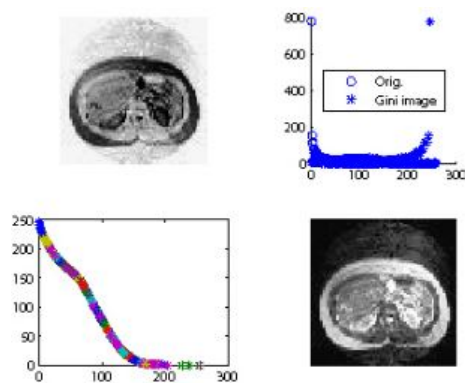


Figure 5.30: a. Gini image b. Feature distributions c. Transformation function d. Linear complement of Gini image

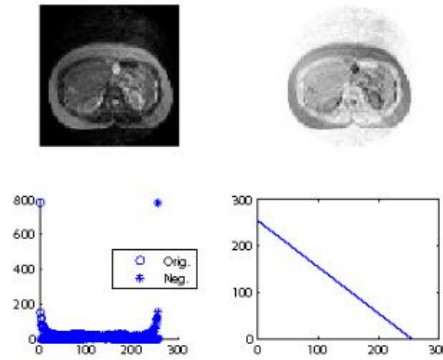


Figure 5.31: a. Original image b. Linear complement c. Feature distributions d. Transformation function

Structural similarity of reference images and their transformed versions is of interest in image similarity analysis [1,133,139]. In that regard it is of interest to see how Gini processed images compare with the original versions. The SSIM indices for Gini processed images and their corresponding reference pairs in Fig. 5.28 and Fig. 5.29 and Fig. 5.30 and Fig. 5.31 are 0.5395 and 0.6658 respectively. The processed results of this information theoretic approach are comparable with those resulting from histogram equalization [3].

The technique has also been applied to a noisy image and the result is shown in Fig. 5.32. Note that noise affects the transformation function (see Fig. 5.32). As with most approaches, the performance of the method is noise-dependent but preprocessing could enhance the result.

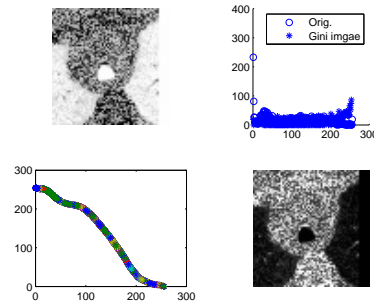


Figure 5.32: a. Noisy Gini image b. Feature Distributions c. Transformation Function d. Linear Complement of Gini Image

The flexibility of the transformation functions for Gini images is clearly demonstrated by the results. Even in the case of a somewhat linear transformation function for the complemented Gini image a lot more detail is visible (see Fig. 5.28-Fig. 5.31).

In comparing linear complements of Gini index images with corresponding reference signals it is observable that backgrounds are more visible and quite well differentiated from the foregrounds in the processed Gini images. Besides, the pixel value transitions in the backgrounds are clearer and apparent in Gini index images compared to more or less uniform pixel distributions in the backgrounds of traditional complement images.

Notice that in the processed Gini images more detail is apparent as seen in the sample processed non-linearly complemented medical images. The processed results are influenced by each unit of the pattern, probability of intensity of the unit and the area of the polygon surrounding the generator. The exposed detail in processed Gini images is attributable to the flexibility of the transformation functions and utility of information of signal features. This could be advantageous for decision making.

Linear complements of Gini index images bear semblance with their histogram equalized reference images [3]. Similarity in results is due to the fact that both

techniques utilize cumulative distribution functions of the pixel values.

In conclusion, it is observed that the Gini index transformation is generally a non-linear and flexible transformation function for obtaining signal complements. This is advantageous in that it utilizes the probability distributions of the pixels in an entropic formulation. As a result Gini index transformation enhances local contrast and exposes details thanks to Tsallis entropy. In addition, the linear complement of a Gini image is an image enhancement technique useful for image processing and contrast enhancement to aid decision making. Its results are comparable to image enhancement through histogram equalization and adaptive histogram equalization.

5.6 Quantifying Information Levels of Voronoï Tessellations

This section introduces measurement of information levels of Voronoï cells via Rényi entropy. The focus is on the Rényi entropy of Voronoï meshes with varying quality. Let $p(x_1), \dots, p(x_i), \dots, p(x_n)$ be the probabilities of a sequence of events $x_1, \dots, x_i, \dots, x_n$ and let $\beta > 1$. The Rényi entropy [149] $H_\beta(X)$ of a set of events X is defined by

$$H_\beta(X) = \frac{1}{1-\beta} \ln \sum_{i=1}^n p^\beta(x_i) \quad (\text{Rényi entropy}) \quad (5.7)$$

. Rényi's entropy is based on the work by R.V.L. Hartley [150] and H. Nyquist [151] on the transmission of information. A proof that $H_\beta(X)$ approaches Shannon entropy as $\beta \rightarrow 1$ is given in [152], *i.e.*,

$$\lim_{\beta \rightarrow 1} \frac{1}{1-\beta} \ln \sum_{i=1}^n p^\beta(x_i) = - \sum_i p_i \ln p_i \quad (5.8)$$

The information of order β contained in the observation of the event x_i with

respect to the random variable X is defined by $H(X)$. In our case, $H_\beta(X)$ is the information level of the observation of the quality of a Voronoï mesh cell (proportional to its area) viewed as a random event. The principal application of the proposed approach to measuring information levels of mesh cells is in the tessellation of digital images.

A main result reported in this study is the correspondence between image quality and Rényi entropy for different types of tessellated digital images. In other words, the correspondence between the Rényi entropy of mesh cells relative to the quality of the cells varies for different classes of images. For example, with Voronoï tessellations of images of humans, Rényi entropy tends to be higher for higher quality mesh cells (see, *e.g.*, the plot in Fig. 5.47 for different Rényi entropy levels, ranging from $\beta = 1.5$ to 2.5 in 0.5 increments). Global mesh cell quality exhibits a fairly linear behaviour in its range of convergence across categories of digital images. Also, estimated quantities such as entropy could be useful in pattern nature identification and even further processing. Simulation results unambiguously demonstrate that information discrimination is apparent in Voronoï meshes and is mostly revealed when the general information parameter β is in the range $1 < \beta \leq 2.5$. For the given range of the information parameter, maximum information discrimination is apparent. Mesh information is seen to be generally a non-linear, non-decreasing function of point patterns.

Voronoï tessellation makes it possible to understand fundamental properties of elements of regions of space by exploiting properties and geometry of the resulting meshes. Image geometry tends to be revealed, whenever the choice of generating

points accurately reflects the image visual content and the structure of the objects in an image scene. For example, keypoints or corners would be the logical choice for image scenes containing buildings or objects with sharply varying contours such as hands or facial profiles. Identifying appropriate sets for generating meshes is a fundamental and necessary step in several domains, including engineering, computing, geometric and scientific applications [1, 10, 153, 154].

5.6.1 Methodology and Datasets

Applications of Voronoï tessellations have often been limited to space partitioning as opposed to fundamental pattern analysis and understanding of the partitions. This is evidenced by numerous articles in the literature in which the chief aim of algorithms is directed at space partitioning. Due to this, an abysmal number of works explore the potential of Voronoï diagrams beyond space partitioning. Even fewer works examine properties of Voronoï cells with the viewpoint of understanding the underlying nature of patterns from which the partitions result.

We explore a way of representing part of a signal space from a point set sample distribution that summarizes the pattern by its equivalent Voronoï signature. The units of a point pattern form generators for Voronoï diagrams. Keypoint image patterns of buildings, animals, humans and mountains as previously utilized in [1] were sampled from images of dimensions $M \times N$ to summarize the signals. These point patterns consist of 50 units corresponding to the most prominent keypoints in the images. To establish a fair basis for cross analysis, the same number of point sets is sampled for all images. In addition all images are gray scale of their respective categories from the dataset of [155] as shown in Fig. 5.34.

All quality factors are computed following the definitions from [82, 83] as shown by

the examples given in chapter 2.

With the preamble above in place, we tessellate and cover the pattern spaces with Voronoï polygons of varying shapes. Since point patterns are significantly distinct, it is expected that their Voronoï diagrams would exhibit discriminatory properties. This could be key in pattern discrimination using computed quantities.

Upon identifying a set of points summarizing an image space, we apply the Voronoï partition algorithm to the generators in the signal space. The result is a tessellated space of Voronoï polygons. Open polygons are typical of Voronoï partitions, as such in the mathematical formulation of derived quantities of the tessellated spaces we adopt techniques that allow the infinite polygons as well as the finite ones to be well behaved.

To help examine the nature and behaviour of patterns, plots of various quantities are given. There are as many qualities as cells, so we define a global quality index or fidelity to capture the geometry of the pattern. Using all cell qualities in a tessellation, it is defined by

$$q_{all} = \frac{1}{n} \sum_{i=1}^n q_i.$$

This enables a one-to-one correspondence between quantities.

Due to the finite nature of digital images, we limit the geometrical extent of point patterns to their convex sets. The information content of images are assessed using the general entropy criterion $H_\beta(X)$. A special case of the general entropy criterion $H_\beta(X)$ occurs when $\beta = 2$. This is the so called Rényi entropy denoted here H_R .

Simulation results are included for $\beta = 1.5, 2, 2.5$. This range of β captures a range of entropies with Shannon entropy recoverable when $\beta \rightarrow 1$.

The choice of β in the neighbourhood of 2 is not arbitrary. The reasons are two fold; on one hand we are not far off from Shannon entropy. This enables us to obtain information on the distribution of elements. On the other hand it gives us insight on how units of a point pattern influence its distribution or organization. Just as l_0 and l_∞ norms represent extremes of the smallest and largest elements of a set, H_0 and H_∞ are the extremes of information measures of which $H_{0 < p < \infty}$ gives a tradeoff. The simulation process is summarized in Algorithm 2. The steps in the algorithm were implemented in Wolfram Mathematica 10.

Algorithm 2: Mesh Quality and Information Computation Algorithm

Input : Number of sides, vertex coordinates, area, probability

Output: Quality, Entropy

Qualities, Q for each Voronoï region $\mathbb{V}_i \in \mathbb{V}$ of S **do**

 | Access the number of sides and coordinates of the vertices of the polygon
 | Using the coordinates, compute the lengths l_i and Area A of the polygon
 | Use l_i and A_i in the appropriate expression to compute its quality q_i

$Q = \{q_i\}$

Mesh Entropy, H

for each Voronoï region $\mathbb{V}_i \in \mathbb{V}$ **do**

 | Compute Pr_i
 | Use Pr_i to compute H_i

$H = \{H_i\}$

Example Consider a completely regular, tessellated pattern as shown in Fig. 5.33.

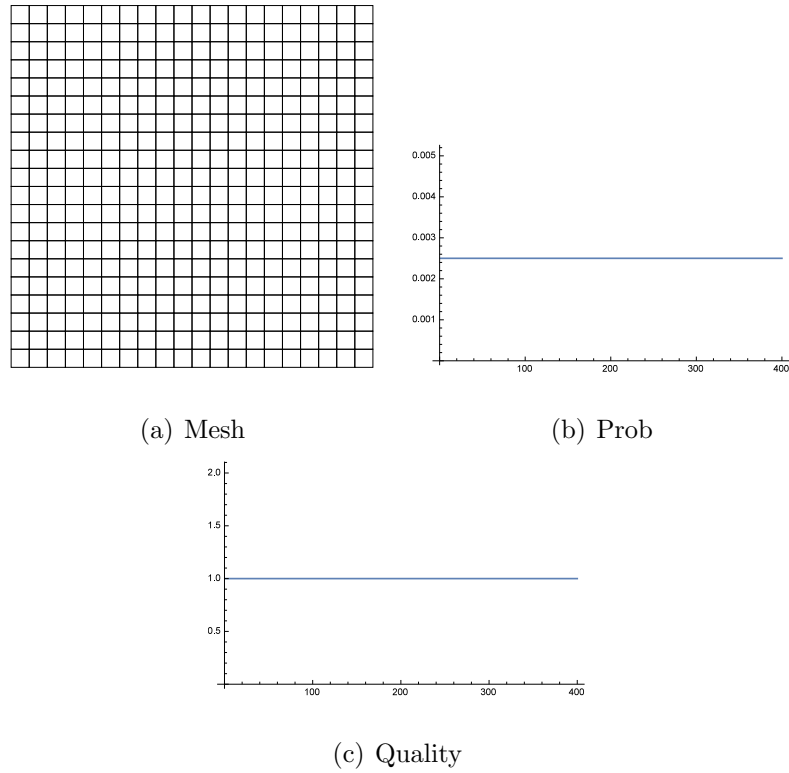


Figure 5.33: Perfectly Regular Image Graph Space and Quantities

In Fig. 5.33 all Voronoï cells have the same area resulting in a uniform distribution of their probabilities. Also all cells have the same quality. Now there are 400 cells in the tessellation and so H attains its maximum value of 5.99146. The global quality index also attains its maximum value of unity. From the distribution of the probability of cells and their qualities it's straight forward to see that a plot of general entropy against global quality indices would be a simple linear function (straight horizontal line).

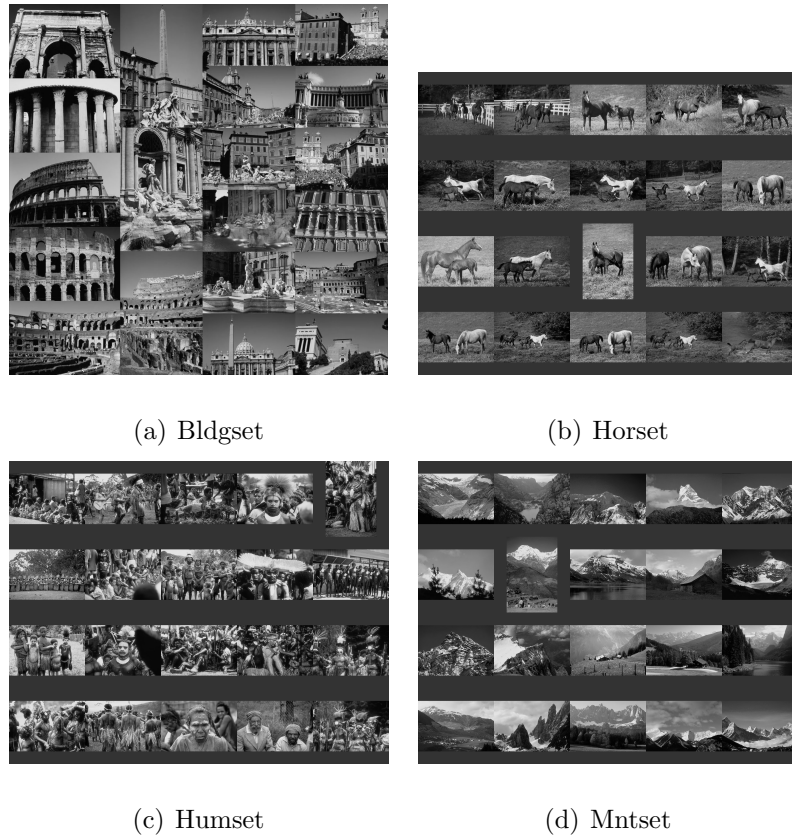


Figure 5.34: Datasets

5.7 Results and Discussion

Polygons typically have non-zero area so their probabilities Pr_i are defined for all regions in the plane. In the following image Voronoï graphs, plots of probability functions, entropy and quality of cells are given. Quality of cells and information are studied by examining the nature of their plots. The results of our simulations are shown for only three images per category of the data set given in Fig. 5.34 for space reasons although the plots are for the entire data set of 20 images per category amounting to 80 images in total. Corresponding cell area probabilities and distribution of cell qualities are shown next to tessellated spaces in Fig. 5.35-Fig. 5.46 in that

order. The horizontal and vertical axes of the histogram plots represent quality of cells and their frequencies respectively.

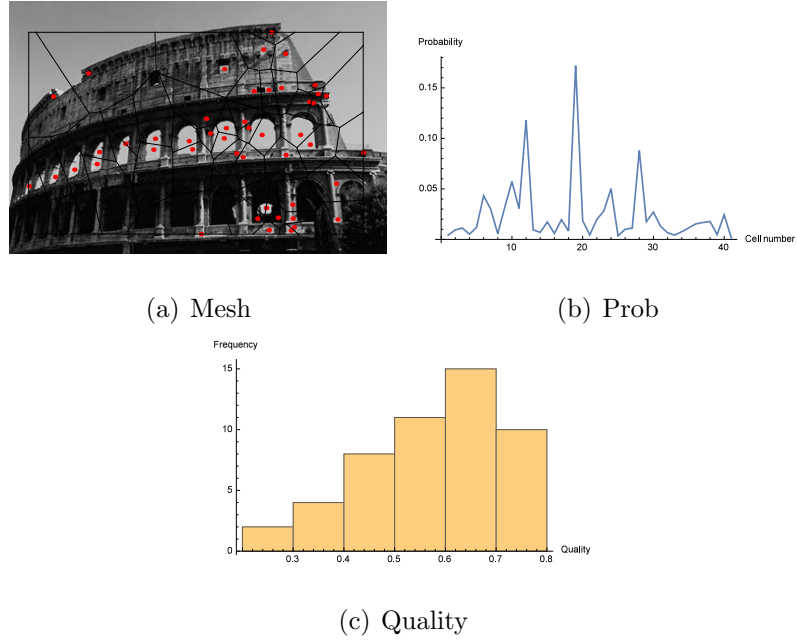
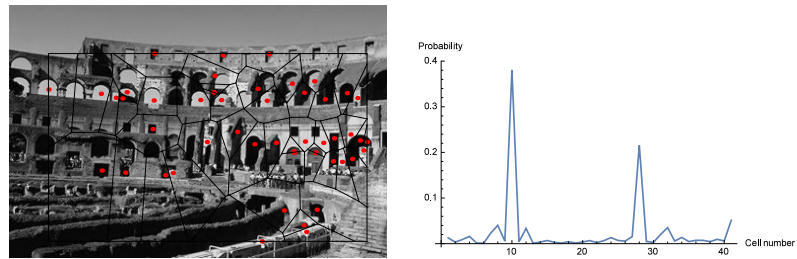


Figure 5.35: Image Graph Spaces



(a) Mesh

(b) Prob

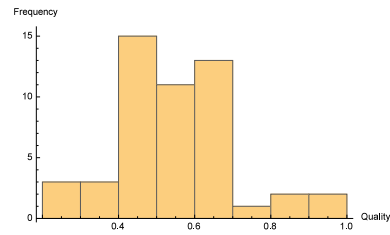
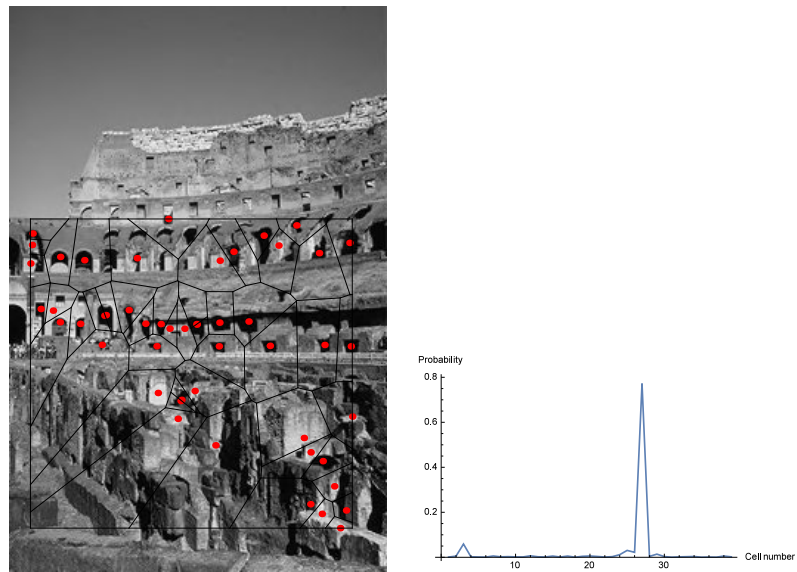
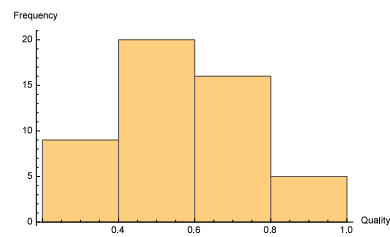


Figure 5.36: Image Graph Spaces



(a) Mesh

(b) Prob



(c) Quality

Figure 5.37: Image Graph Spaces

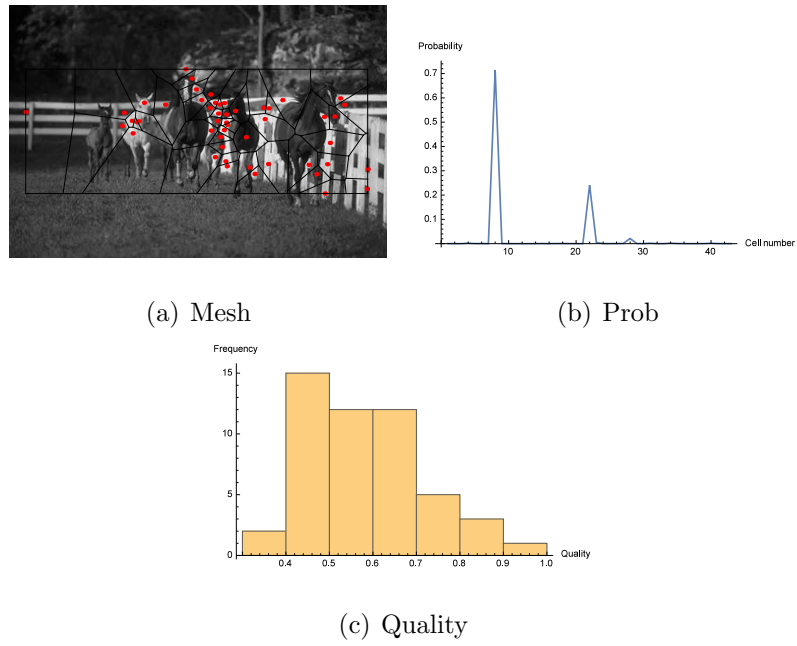


Figure 5.38: Image Graph Spaces

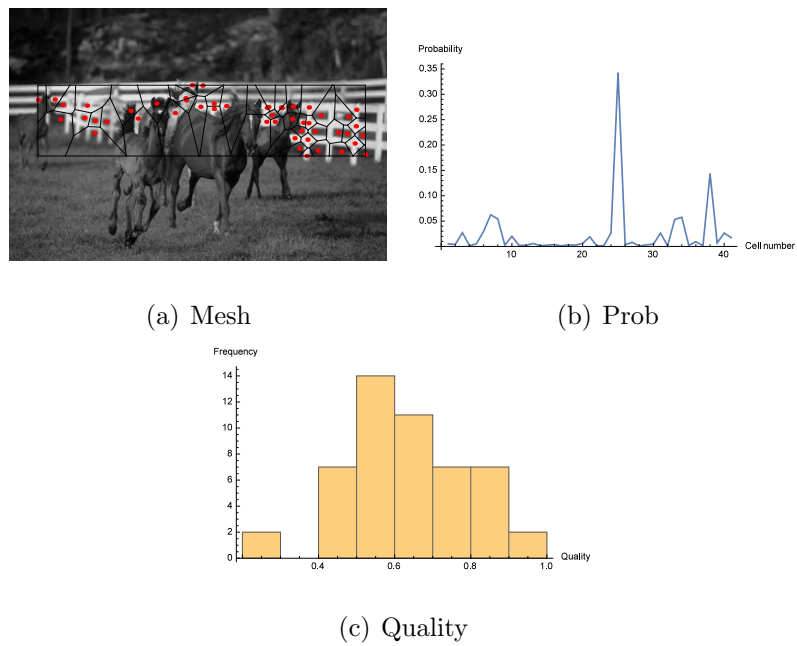
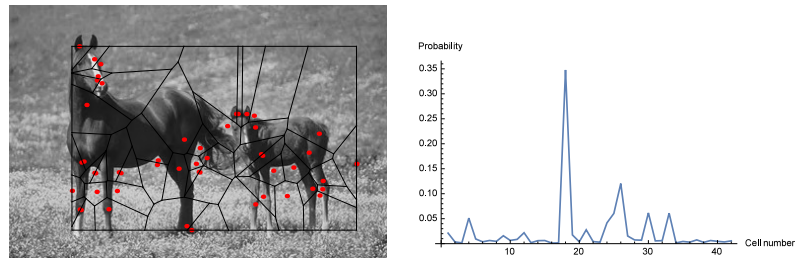
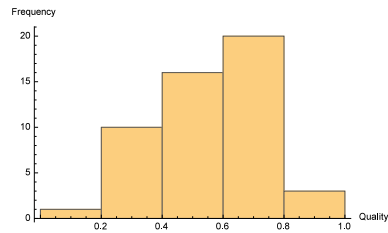


Figure 5.39: Image Graph Spaces



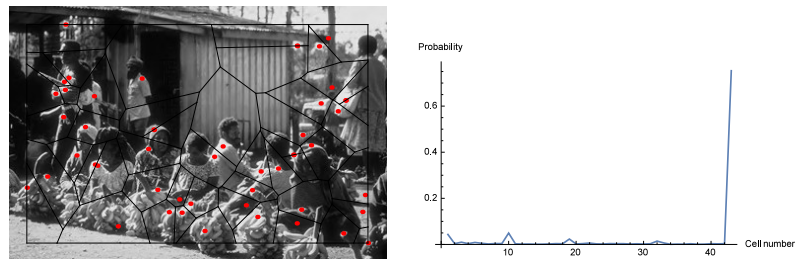
(a) Mesh

(b) Prob



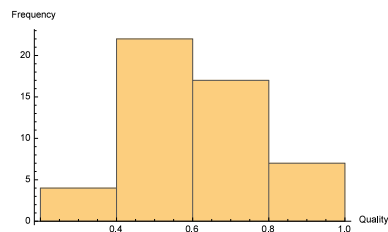
(c) Quality

Figure 5.40: Image Graph Spaces



(a) Mesh

(b) Prob



(c) Quality

Figure 5.41: Image Graph Spaces

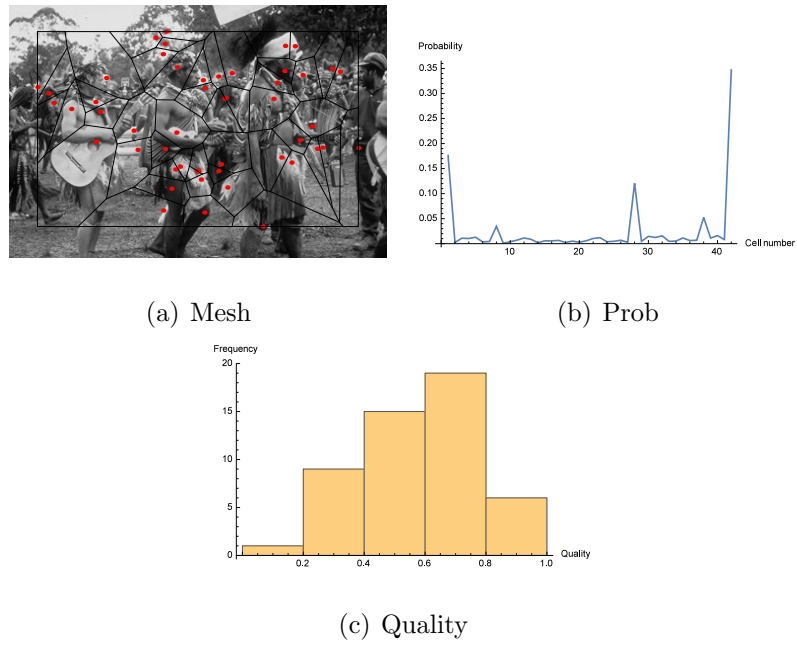


Figure 5.42: Image Graph Spaces

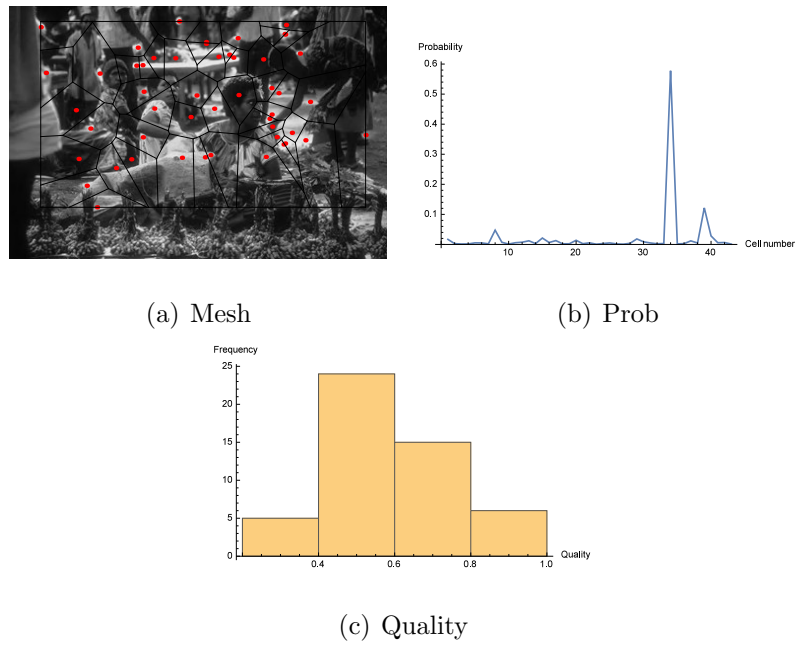


Figure 5.43: Image Graph Spaces

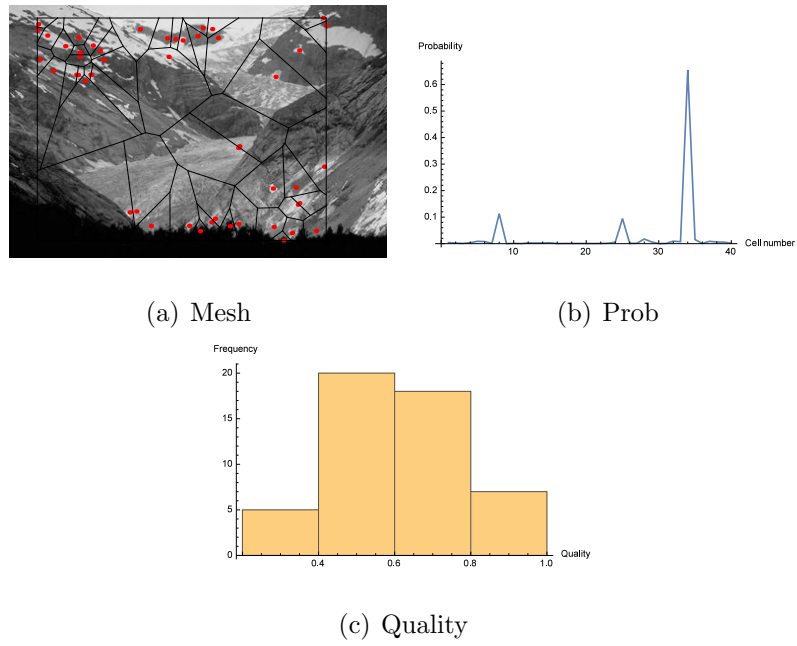


Figure 5.44: Image Graph Spaces

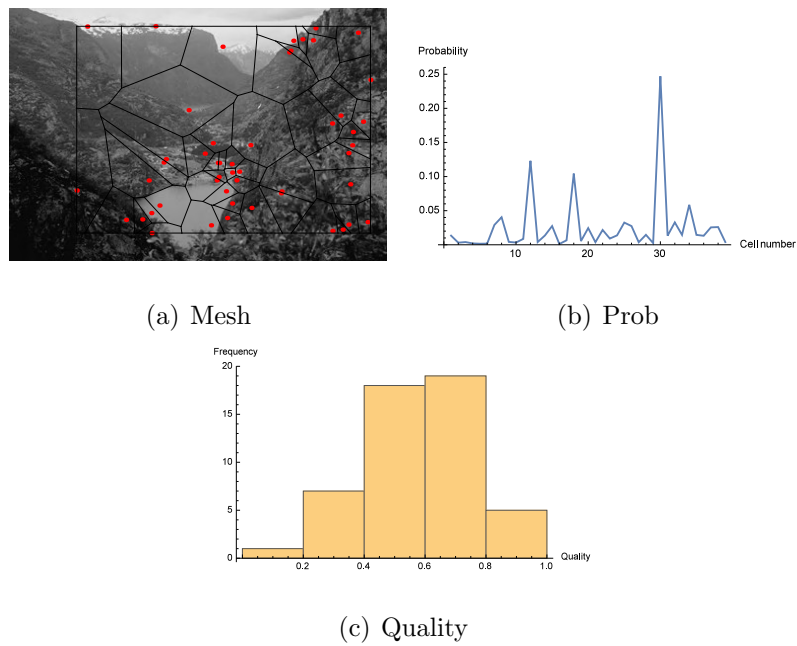


Figure 5.45: Image Graph Spaces

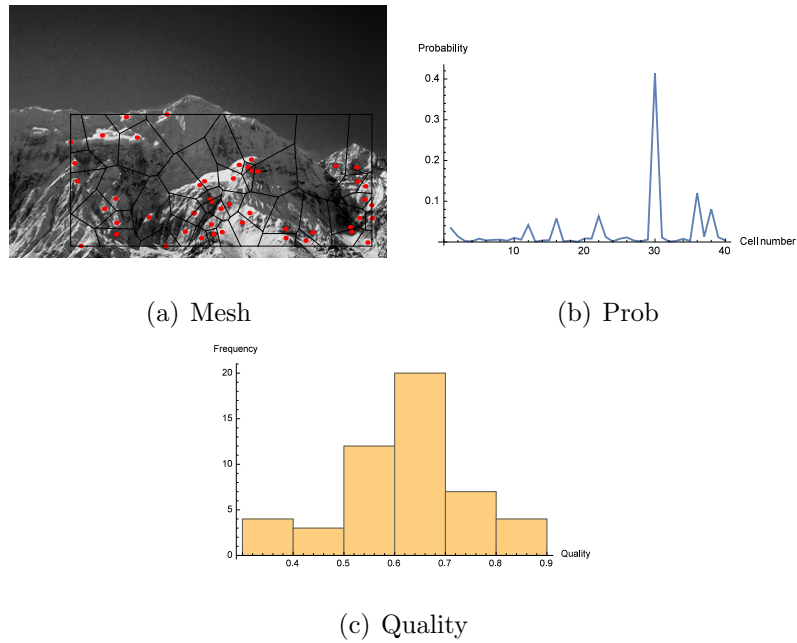


Figure 5.46: Image Graph Spaces

Entropy of tessellations and global quality indices are condensed into quantity relation plots. For 50 Voronoi cells exhibiting a uniform probability distribution, the maximum possible entropy is 3.912. All entropy values fall short of this value. Plots of entropy and global qualities are shown for building, horse, human and mountain scenery categories in Fig. 5.47. Notice the flat nature of the global qualities for the images. Rényi entropy as a function of the images is non-decreasing.

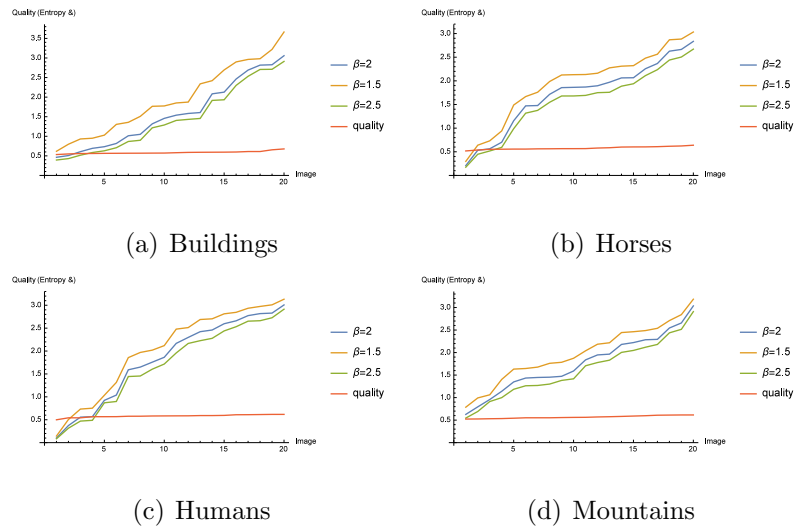


Figure 5.47: Quantity Relations

In Fig. 5.48 quantity signatures showing plots of Rényi entropy versus global qualities are given.

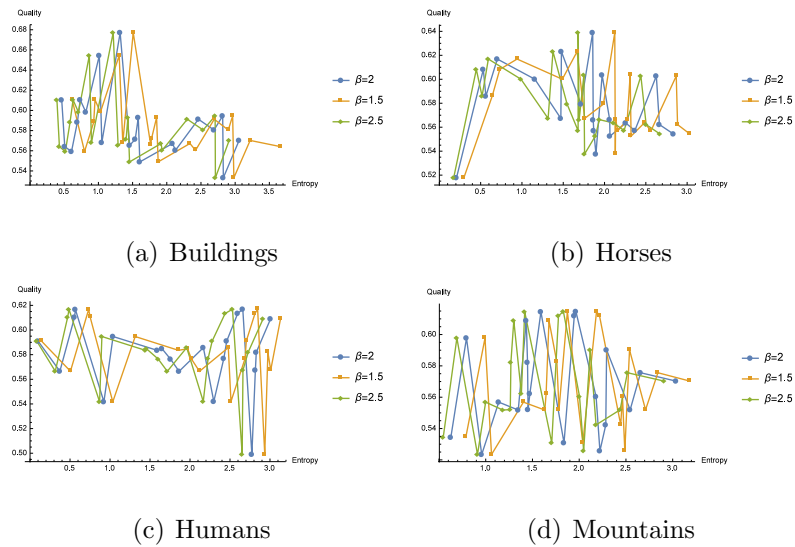


Figure 5.48: Quantity Signatures

Notice the monotonically non-decreasing entropy and global qualities in Fig. 5.47.

Also observe that the quantities are distinct across categories. Most importantly entropic information is decreasing for $\beta = 1.5, 2.0, 2.5$ in that order. Recall that $\beta \rightarrow 1$ yields Shannon entropy from the general entropy criterion H . Note the interesting oscillatory nature of the quantity relations in Fig. 5.48. This is opposed to a simple straight line relationship that would result between entropy and global quality of perfectly regular patterns having the same quality factors. This confirms the departure of the images from the less interesting case of completely regular patterns in Fig. 5.33. Observe that no two signature pairs are the same. So, they could therefore be used for categorical discrimination of images.

5.8 Conclusion

Chapter 5 crystallizes the theory and background of Voronoï diagrams into practical and tangible applications. Definitions, theorems and lemmas have found their practical realization in construction of Voronoï diagrams with mixed element shapes, improved element quality using quality criteria and energy of regions in the construction of centroidal tessellations. Observe that in some tessellations in the literature, mixed element shapes pose a restrictive challenge in quality improvement. That has been eliminated here. Also, quality improvement has been proven without restricting the point pattern generation process to Poisson processes or to any random process. Our results clearly show that keypoint patterns generate the best quality meshes. Mesh element region processing and information content assessment has also been studied and presented. It's found that processing general and fixed element shapes can yield general domain information and detail respectively. Quantity computation procedures are provided in algorithms. The potential utility of the average mesh

quality indicator in revealing information about a pattern, facial expression detection and image classification is hinted.

An important limitation of the algorithms is that slight perturbation of generators would mean changing locations leading to possibly different interactions between pattern units, polygonal lengths and areas, hence the need to readjust or compute measures. Choosing a subset of the entire signal space for generators does not seem to be a significant limitation since their tessellations usually cover a significant portion of the space. However, we can always increase the numbers of generators to cover larger spaces and to encompass more features, although at higher computational costs.

Notice that Voronoï diagrams are structures that expose neighbourhood relations. With this in mind, chapter 6 treats the foundations of near sets with applications in groupoid and proximal set identification. This is intended to form background for near set studies and analysis with the end goal of pattern recognition in mind.

Chapter 6

Near Sets

6.1 Introduction

This chapter introduces near sets as a foundation for studying point set meshes and patterns. It begins by defining element relations in terms of proximity. The types of near sets are discussed. Groupoids are discussed as a special kind of near set application. Mathematical results including theorems and lemmas are provided. Pattern stability and stable pattern generation is discussed. General observations are made and algorithms provided towards further studies in pattern understanding. The chapter concludes by looking at the near set applications in meshed topologies with a focus directed on future image classification. Most of the mathematical foundation provided here is due to initial works by James F. Peters, now elucidated in the context of descriptive proximity and groupoids.

6.2 Near or Proximal Voronoï Segments

Set patterns fall into two broad classes: Spatial set patterns and descriptive set patterns. A *spatial set pattern* contains sets that are spatially near each other. A

point cluster \mathcal{C}_x in an EF-proximity space is an example, *i.e.*, $A \in \mathcal{C}_x$, provided $x \in \text{cl}A$. A *descriptive set pattern* contains sets that are descriptively near a given set and possibly near each other. A descriptive point cluster \mathcal{C}_x in an EF-proximity space is an example, *i.e.*, $A \in \mathcal{C}_{\Phi(x)}$, provided the description of at least one $a \in A$ matches the description of x .

A pair of nonempty sets are near given that the intersection of the sets is nonempty. In other words discrete proximity or near sets have elements in common. A more general form of proximity considers *metric proximity* based on the distance between sets (see, *e.g.*, [156, 157]). In that context, a pair of nonempty sets are near if the distance between the sets is zero. Discrete proximity as a foundation for introducing near sets is perhaps the simplest form of proximity to implement and provides a straightforward basis for applications in pattern generation, pattern stability analysis among others. For more general forms of proximity, there are many sources including [156–159].

The study of near sets has a rich history that spans more than 100 years, starting with the address by F. Riesz at the International Congress of Mathematicians in Rome in 1908 [160] and more recently commented on by S.A. Naimpally [161] and A. Di Concillio [157, 162, 163]. One of the earliest forms of nearness (proximity) relations was introduced by E. Čech during a 1936-1939 Brno seminar and available in 1966 [164, §25.A.1]. Čech used the symbol p to denote a proximity relation defined on a nonempty set X , which Čech axiomatized. Čech's work on proximity spaces started two years after V.A. Efremovič's work (in 1933), who introduced a widely considered axiomatization of proximity, which was published in 1951 [165]. For a

detailed presentation of Efremovič's proximity axioms, see, *e.g.*, [156, 157] and for applications, see, *e.g.*, [159, 166, 167].

6.2.1 Descriptive and Spatially Near Voronoï Sets

This section gives a brief overview of near sets in relation to Voronoï meshes. The foundation of near sets is closeness (proximity) of objects referred to as *discrete proximity*. When we endow a nonempty set with a nearness or proximity (see, *e.g.*, [156, 157, 159] and [168, Ch. 21]) relation, we obtain a structured set called a *proximity space*. Let $\mathcal{P}(X)$ denote the power set of a nonempty tessellation X . A form of nearness relation p (later denoted by δ) that was introduced by E. Čech in the mid-1930s led to the discovery of spatially near sets *i.e.*, those sets that have elements in common. That is, given a proximity space (X, δ) , for any subset $A \in \mathcal{P}(X)$, we can discover nonempty nearness collections

$$xi(A) = \{B \in \mathcal{P}(X) : A \delta B\} \quad (6.1)$$

. Recently, descriptively near sets were introduced for solving classification and pattern recognition problems arising from disjoint sets (*i.e.*, sets with empty spatial intersections) that resemble each other.

Descriptively near sets are discovered by choosing probe functions Φ that represent features of points in a set and endowing the set of points with a descriptive proximity relation δ_Φ and obtaining descriptively structured sets (called descriptive proximity space). Given a descriptive proximity space (X, δ_Φ) , one can discover collections of subsets that resemble each other. This leads to the discovery of descriptive nearness collections

$$xi_{\Phi}(A) = \{B \in \mathcal{P}(X) : A \delta_{\Phi} B\} \quad (6.2)$$

. That is, if $B \in \xi_{\Phi}(A)$, then $A \delta_{\Phi} B$ (relative to the chosen features of points in X , A resembles B).

Let $\mathcal{P}(X)$ denote the collection of all Voronoï regions of X . Voronoï regions $A, B \in \mathcal{P}(X)$ are spatially near (denoted by $A p B$) provided the intersection of $A \cap B \neq \emptyset$. This implies $A p B$. Čech was one of the first to axiomatize a proximity relation. A spatial nearness relation denoted by δ was later introduced instead of the Čech symbol p (see, *e.g.*, [156]). The proximity relation δ is a spatial relation, since $A \delta B$ means that A and B have points in common. This means that any two Voronoï regions that are spatially near must have at least one point in common. This common intersection could be as simple as a point on their common edge or the entire edge itself. To understand what it means to say that a pair of finite sets are spatially near each other, consider the *closure* of a subset $A \in \mathcal{P}(X)$ (denoted by $\text{cl}A$), defined by

$$\text{cl}A = \{x \in X : x \delta A\} \quad (6.3)$$

, *i.e.*, $\text{cl}A$ is the set of all points x in X that are near A . In effect, this means $\text{cl}A$ contains all of the boundary points of A as well as all of the interior points of A .

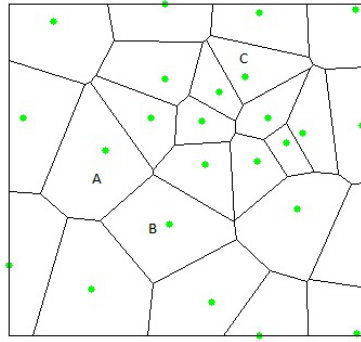


Figure 6.1: Near and far Voronoi sets

Example Spatially Near Sets.

Let X be the Voronoi tessellation in Fig. 6.1 and let the closures of sets $A, B, C \in \mathcal{P}(X)$ be represented by $\text{cl}A = A, \text{cl}B = B, \text{cl}C = C$ in Fig. 6.1. Observe that $\text{cl}A \cap \text{cl}B \neq \emptyset$. Hence, $A \delta B$. ■

A spatial nearness relation δ (called a *discrete proximity*) is defined by

$$\delta = \{(A, B) \in \mathcal{P}(X) \times \mathcal{P}(X) : \text{cl}A \cap \text{cl}B \neq \emptyset\} \tag{6.4}$$

. Whenever sets A and B have no points in common, the sets are *far* from each other (denoted by $A \underline{\delta} B$), where

$$\underline{\delta} = \mathcal{P}(X) \times \mathcal{P}(X) \setminus \delta. \tag{6.5}$$

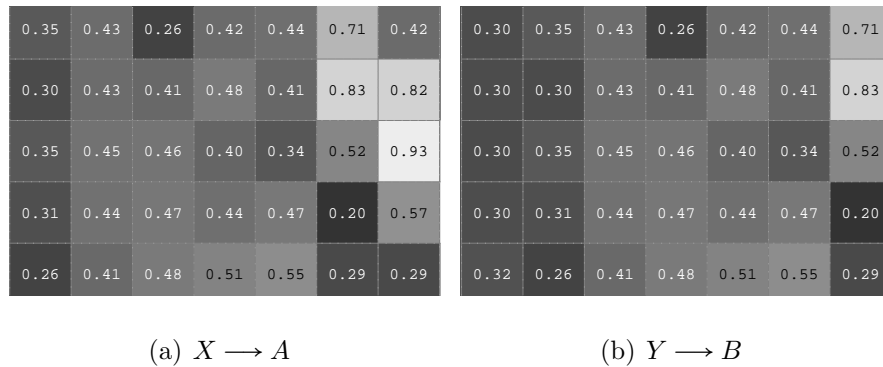


Figure 6.2: Neighbourly mesh cells

Example Spatially Non-Near Sets.

Let X, Y represent the pictures in Fig. 1.1 and Fig. 6.1. Let $A, B \in \mathcal{P}$ be the set of points in the knight’s horse and set of points in the suspended knight respectively. $A \not\delta B$, since there are no points in A that are touching points in B . That is, the closure of A (denoted $\text{cl}A$) has no points in common with the closure of B . A point $x \in B$ lies in the closure of A , provided x is near A . In effect, $A \delta B$. Likewise let A, B, C denote the mesh cells in Fig. 6.1. It is clear that A and B are near cells but they are both far from C .

Observe that although two sets may be spatially far, they can be descriptively near. For example any two spatially far cells in Fig. 5.33 are descriptively near because the intersection of their descriptive sets is non-empty. ■

6.3 Digital Groupoids

This section introduces digital groupoid patterns in descriptive proximity spaces. The basic approach uses the descriptive proximity of points to introduce neighbourly groupoid elements. This leads to a study of proximal groupoids; neighbourly proximal groupoids that serve as generators of proximal algebraic patterns. A practical

application of the approach is the use of neighbourly proximal groupoid patterns in classifying digital images. Digital proximal groupoid patterns is an outgrowth of recent research [169]. A *groupoid* is a system $S(\circ)$ consisting of a nonempty set S together with a binary operation \circ on S . The binary operation $\circ : S \times S \rightarrow S$ maps $S \times S$ into S , where $S \times S$ is the set of all ordered pairs of elements of S . A *digital proximal groupoid* is a groupoid in a digital image endowed with a proximity relation.

Proximal groupoids can either be spatially near in a traditional Efremovič proximity space [170] or descriptively near in a descriptive proximity space. A descriptive proximity space [126, 171] is an extension of an Efremovič proximity space [170]. This extension is made possible by the introduction of feature vectors that describe each point in the proximity space. Sets A, B in an EF-proximity space X are near provided $A \cap B \neq \emptyset$. Sets A, B in a descriptive proximity space X are near, provided there is at least a pair of points $a \in A, b \in B$ with matching descriptions.

In proximity spaces, groupoids provide a natural structuring of sets of points. Operations often lead to descriptions of sets endowed with structures for potential applications in proximity spaces for pattern description, recognition and identification. In this section, the applications of descriptive proximity-based groupoids in digital image analysis is presented. A practical application of the proposed approach is in terms of the analysis of stability of image patterns for identification and classification.



Figure 6.3: Image to groupoid space transformation

The following is an example on groupoid patterns of digital image spaces of an image in [148] based on feature vector Φ .

Example Let X be a grayscale digital image and let A be a subimage in X . Let x, y be pixels in the subimage A in Fig. 6.3 and let $\phi : X \rightarrow \mathbb{R}$ be defined by $\phi(x) =$ grayscale intensity of $x \in X$. Further, define the set $\Phi = \{\phi\}$. Hence, $\mathcal{Q}(A)$ is the set of feature vectors $\Phi(x)$, where each feature vector contains a single number $\phi(x)$, which is the intensity of $x \in A$. Then define the binary operation $\circ : \mathcal{Q}(A) \times \mathcal{Q}(A) \rightarrow \mathcal{Q}(A)$ by

$$\Phi(x) \circ \Phi(y) = \min \{ \Phi(x), \Phi(y) \} = 0.21, \text{ where } \Phi(x), \Phi(y) \text{ are pixel intensities} \quad (6.6)$$

. From this, we obtain a digital groupoid $\mathcal{Q}(A)(\circ)$. ■

Recall that a partial binary operation on a set X is a mapping of a nonempty subset of $X \times X$ into X . A partial groupoid is a system $S(\ast)$ consisting of a nonempty set S together with a partial binary operation “ \ast ” on S . Let

$$\mathcal{Q}(A) = \{ \Phi(a) : a \in A \}, \text{ set of descriptions of members of } A \quad (6.7)$$

. Next, to arrive at a partial descriptive groupoid, let “ \ast_Φ ” be a partial descriptive

binary operation defined by

$$*_\Phi : \mathcal{Q}(S) \times \mathcal{Q}(S) \longrightarrow \mathcal{Q}(S).$$

6.3.1 Neighbourliness in Groupoids

In general, given a finite groupoid $A(\circ)$ represented by an undirected graph, for $x, y \in A$ let $x \sim y$ denote the fact that x, y are neighbours. In particular, given a finite descriptive proximal groupoid $A(\circ_\Phi)$, for $\Phi(x), \Phi(y) \in \mathcal{Q}(A)$, let $\Phi(x) \sim \Phi(y)$ denote the fact that $\Phi(x), \Phi(y)$ are neighbours, *i.e.*, points $x, y \in A$ have matching descriptions.

Example Let (X, δ_Φ) be a descriptive proximity space. Then let $\{\Phi(x)\}$ denote an equivalence class represented by the feature vector $\Phi(x)$ that describes $x \in X$. Then $\Phi(y) \in \{\Phi(x)\}$, provided $\Phi(y) = \Phi(x)$, *i.e.*, $x, y \in X$ have matching descriptions. For example, define the descriptive groupoid $A(\circ_\Phi)$ such that

$$A = \{\Phi(x) \in \mathcal{Q}(X) : \Phi(x) \in \{\Phi(x)\}\} \quad (6.8)$$

, and

$$\circ_\Phi(\Phi(x), \Phi(y)) = \Phi(x). \quad (6.9)$$

Then $\Phi(x), \Phi(y) \in \mathcal{Q}(A)$ are neighbourly in groupoid A , provided $\Phi(x)$ and $\Phi(y)$ belong to the same equivalence class, *i.e.*, $\Phi(x) \in \{\Phi(y)\}$. ■

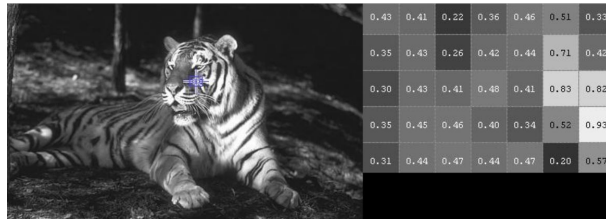


Figure 6.4: Image to groupoid space transformation

The notion of neighbourliness of elements in a groupoid extends to neighbourliness between disjoint groupoids. Let X, Y be disjoint descriptive proximity spaces and let $A(\circ_{\Phi}), B(\bullet_{\Phi})$ be descriptive proximal groupoids such that $A \subset X, B \subset Y$. Then groupoids $A(\circ_{\Phi})$ and $B(\bullet_{\Phi})$ are neighbourly, provided $a \sim b$ for some $a \in A, b \in B$. For examples of neighbourly mesh cells see Fig. 6.2(a) and Fig. 6.2(b). This leads to the following result.

Theorem 6.3.1. *Let $(X, \delta_{\Phi}), (Y, \delta_{\Phi})$ be descriptive proximity spaces, $A \subset X, B \subset Y$. If groupoids $A(\circ_{\Phi}), B(\bullet_{\Phi})$ are neighbourly, then $A \delta_{\Phi} B$.*

Proof. Immediate from the definition of descriptive near sets [126]. □

Neighbourly groupoid elements can be identified by for example the colour of patches in Fig. 6.3 and Fig. 6.4. Neighbourly elements have matching patches whilst ε -tolerant groupoids have matching patches defined by tolerance parameter $\varepsilon > 0$.

6.3.2 Digital Groupoid Set Pattern Generators

A *pattern generator* is derived from some form of regular structure [172]. In geometry, a regular polygon is a polygon with n sides that have the same length and are symmetrically placed around a common center (see Fig. 5.33 for an example). A geometric pattern contains a repetition of a regular polygon. An element in a groupoid

$A(\circ)$ is regular, provided $a \in aAa$, *i.e.*, $a \circ y \circ a = a$ for some $y \in A$ [173]. A groupoid is regular, provided every element is regular.

Example From Fig. 5.33, let $\Phi(x), \Phi(y) \in \mathcal{Q}(A)$ be neighbourly elements of groupoid A . Then

$$\Phi(x) \circ \Phi(y) \circ \Phi(x) = \Phi(y) \circ \Phi(x) = \Phi(x), \text{ since, } \Phi(x) = \Phi(x) \quad (6.10)$$

. Hence, $\Phi(x)$ is a regular element.

An algebraic pattern contains a repetition of regular structures such as a regular element or a regular groupoid. For example, an algebraic pattern contains a repetition of neighbourly elements from groupoids. In this subsection, the focus is on proximal algebraic patterns. A *proximal algebraic pattern* in a descriptive proximity space (X, δ_{Φ}) (denoted by $\mathfrak{P}(A)$) is derived from a repetition of structures such as groupoids A that contain a mixture of neighbourly (regular) and non-neighbourly (non-regular) elements, *i.e.*,

$$\mathfrak{P}_{\Phi}(\mathcal{Q}(A)) = \{\mathcal{Q}(B) \in 2^{\mathcal{Q}(X)} : \Phi(a) \delta_{\Phi} \Phi(b) = \Phi(a), \quad (6.11)$$

$$\text{for some, } \Phi(a) \in \mathcal{Q}(A), \Phi(b) \in \mathcal{Q}(B)\} \quad (6.12)$$

Example From the digital images in Fig. 6.3 and Fig. 6.4, we can identify groupoids containing neighbourly elements. A proximal groupoid derived from the digital image in Fig. 6.3 has a number of neighbourly elements such as those with feature values 0.36, 0.44, 0.59. Similarly, a proximal groupoid from Fig. 6.4 includes 0.36, 0.60, 0.63 as members. Then, from Theorem 6.3.1 and the definition of a proximal algebraic pattern, we obtain

$$\mathfrak{P}_{\Phi}(A) = \{0.36, 0.44, 0.59\} \quad (6.13)$$

Similarly, we obtain a second proximal algebraic pattern, namely,

$$\mathfrak{P}_\Phi(B) = \{0.36, 0.60, 0.63\} \quad (6.14)$$

. Patterns $\mathfrak{P}_\Phi(A), \mathfrak{P}_\Phi(B)$ are examples of neighbourly patterns. ■

Theorem 6.3.2. *In a descriptive proximity space, a proximal groupoid containing regular elements generates a proximal groupoid pattern.*

Proof. Assume A in a descriptive proximity space X is the only proximal groupoid containing neighbourly elements. Then $\mathfrak{P}(A) = \{A\}$ is a proximal groupoid pattern containing only the groupoid A . Let A, B be a pair of neighbourly proximal groupoids in X . Then, from Theorem 6.3.1, $A \delta\Phi B$ and either A or B is a generator of a proximal groupoid pattern. □

Theorem 6.3.3. *In a descriptive proximity space, a proximal groupoid pattern is a collection of neighbourly groupoids.*

Proof. Immediate from Theorem 6.4.3 and the definition of a proximal algebraic pattern. □

The likelihood of finding proximal algebraic patterns in nature is fairly significant although patterns in natural scenes such as mountains, horses etc. seldom, if ever, contain regular structures such as regular polygons or regular algebraic structures (see Fig. 5.35-Fig. 5.46). Proximal algebraic patterns are commonly found in digital images, hence proximal algebraic structures may be useful in classifying digital images.

6.4 General Pattern Generation

This section introduces an approach to pattern recognition that facilitates stable image-based pattern generation. This approach complements the I.B. Gurevich descriptive approach to analyzing and understanding images by the introduction of descriptive-based set pattern generation that could be useful in classifying digital images. Set patterns are viewed in the context of a descriptive proximity space, which results from an extension of the V.A. Efremovič axioms [170], elucidated by Yu.M. Smirnov [124]. The Gurevich Descriptive Approach to Image Analysis and Image Understanding (DAIA) and Descriptive Analysis (DA) image formalization space in which one analyzes image forms is complemented with a proximity space in which variations of Grenander pattern generators could be used to generate test image and query image set patterns that are either near or far from each other. This is a pattern-based approach in which the nearness or remoteness of patterns serve as an indicator that a test image either belongs or does not belong to a class of images represented by a query image. Coupled with the descriptive approach to proximal pattern generation, we also consider pattern stability. Stable pattern generation enforces rules that inhibit the sets in a pattern from drifting or wandering away from the pattern generator [174] that could ensure reliable pattern-based classification of images.

A form of set patterns [172, 174, §17.5] of particular interest in pattern recognition is given in terms of what are known as descriptive motif patterns. A *descriptive motif pattern* is a collection of sets such that each member of the collection is descriptively close to a motif. A *motif* is a set with members that are near one or more members of other sets. Motifs are a particular form of set pattern

generators [174]. Visual motif patterns are found in scenes, geometric structures and digital images. A *visual motif pattern* is a form of descriptive motif pattern that is a collection of sets such that each member of the collection is visually close to a motif. Visual motif patterns have a number of important applications [147,159,174].

Sets become endowed with descriptions and structures when we introduce feature vectors that describe members of the sets, for example sets of features in digital images and regions of Voronoï diagrams. These descriptions and structures lead to a form of topology of the sets with potential considerable practical applications in solving image analysis and classification problems. A visual pattern is considered *stable*, provided the members of the pattern do not wander or drift away from the pattern generator, neither spatially nor descriptively. In other words a pattern is stable if it does not contain bad elements. We introduce stability criteria for the generation of set patterns that are tightly coupled with a pattern generator.

Observe the Voronoï tessellation in Fig. 5.33. Let the motif generator set be any cell of the tessellation. From this, it is clear that since every other cell is the same, the cells do not wander or drift away from the motif pattern generator and hence it's a stable pattern collection. It is however not an interesting pattern since every element of the motif collection has the same information as any other.

Let X be a nonempty set of non-abstract point patterns in a proximity space (X, \mathcal{R}_δ) and let $\Phi = \{\phi_1, \dots, \phi_n\}$ be a set of probe functions that represent features of each $x \in X$. This leads to a proximal view of sets of points in tessellated digital images [126]. A *probe function* $\Phi : X \rightarrow \mathbb{R}$ represents a feature of a sample point in a tessellated image plane. Let $\Phi(x) = (\phi_1(x), \dots, \phi_n(x))$ denote a feature vector

for x , which provides a description of each $x \in X$. To obtain a descriptive proximity relation (denoted by δ_Φ), one first chooses a set of probe functions. Let $A, B \in 2^X$ and $\mathcal{Q}(A), \mathcal{Q}(B)$ denote sets of descriptions of points in A, B , respectively. For example, $\mathcal{Q}(A) = \{\Phi(a) : a \in A\}$. The expression $A \delta_\Phi B$ reads *A is descriptively near B*. Similarly, $A \underline{\delta}_\Phi B$ reads *A is descriptively far from B*. The descriptive proximity of A and B is defined by

$$A \delta_\Phi B \Leftrightarrow \mathcal{Q}(A) \cap \mathcal{Q}(B) \neq \emptyset \quad (6.15)$$

. Similarly, the EF-proximity of $A, B \subset X$ (denoted $A \delta B$) is defined by

$$A \delta B \Leftrightarrow A \cap B \neq \emptyset \quad (6.16)$$

.

In an ordinary metric closure space [164, §14A.1] X , the closure of $A \subset X$ (denoted by $\text{cl}(A)$) is defined by

$$\text{cl}(A) = \{x \in X : D(x, A) = 0\}, \text{ where} \quad (6.17)$$

$$D(x, A) = \inf \{d(x, a) : a \in A\} \quad (6.18)$$

, *i.e.*, $\text{cl}(A)$ is the set of all points x in X that are close to A . $D(x, A)$ is the Hausdorff distance [175, §22, p. 128] between x and the set A and $d(x, a) = |x - a|$ (standard distance). Subsets $A, B \in 2^X$ are spatially near (denoted by $A \delta B$), provided the intersection of closure of A and the closure of B is nonempty, *i.e.*, $\text{cl}(A) \cap \text{cl}(B) \neq \emptyset$. That is, nonempty sets are spatially near, provided the sets have at least one point in common.

The Efremovič nearness relation δ (called a *discrete* proximity [170]) is defined by

$$\delta = \{(A, B) \in 2^X \times 2^X : \text{cl}(A) \cap \text{cl}(B) \neq \emptyset\} \quad (6.19)$$

. The pair (X, δ) is called an EF-proximity space. In a proximity space X , the closure of A in X coincides with the intersection of all closed sets that contain A .

Let X be a nonempty set of points, $\mathcal{P}(X)$ the power set of X , $\mathcal{P}^2(X)$ the set of all collections of subsets of X . A single point $x \in X$ is denoted by a lowercase letter, a subset $A \in \mathcal{P}(X)$ by an uppercase letter, collection of subsets in $\mathcal{P}^2(X)$ by a round letter such as $\mathcal{B} \in \mathcal{P}^2(X)$. The *closure* of a subset $A \in \mathcal{P}(X)$ (denoted by $\text{cl}A$) is defined by

$$\text{cl}A = \{x \in X : x \delta A\},$$

i.e., $\text{cl}A$ is the set of all points x in X that are near A . Let δ on a nonempty set X denote a spatial nearness (proximity) relation. For $A, B \in \mathcal{P}(X)$, $A \delta B$ (reads A is spatially near B), provided $A \cap B \neq \emptyset$, *i.e.*, the intersection of A and B is not empty ($\text{cl}A$ and $\text{cl}B$ have at least one point in common).

Definition δ -space (Proximity Space).

Let X be a space endowed with a relation δ satisfying axioms so that for any two sets $A, B \in X$, it is determinable whether A and B are close or not. Then the relation δ is defined by

$$\delta = \{(A, B) \in \mathcal{P}(X) \times \mathcal{P}(X) : \text{cl}A \cap \text{cl}B \neq \emptyset\} \quad (6.20)$$

. Sets A and B are close if their closures intersect. A δ -space is a spatial proximity space. $\delta(A, B) = 0$ if sets A, B are close in a δ -space. Otherwise, put $\delta(A, B) = 1$, if sets A, B are far from each other in a δ -space. ■

We call a set X a proximity space (or, briefly, δ -space) if for any two subsets A and B in X they relate in such a way that the following axioms are satisfied;

P.1 If set A is close to B , then B is close to A .

P.2 $A \cup B$ is close to C , if and only if, at least one of the sets A or B is close to C .

P.3 Two points are close, if and only if, they are the same point.

P.4 All nonempty sets are far from the empty set \emptyset .

P.5 For any two sets A and B which are far from each other, there exists C and D , $C \cup D = X$, such that A is far from C and B is far from D (**Efremovič axiom**).

Remark Efremovič's Axioms. The proximity space axioms P.1-P.5 were given by Yu. M. Smirnov [124] based on what V. Efremovič introduced during the first half of the 1930s [170]. ■

6.4.1 Descriptive EF-Proximity Pattern Generation Spaces

In the study of patterns, a descriptive form of EF-proximity is useful [167]. Before we elucidate more on descriptive EF-proximity spaces for pattern generation, we briefly introduce some necessary notation and concepts underlying descriptive proximity. Let X be a nonempty set endowed with a descriptive proximity relation δ_Φ , $x \in X$, $A, B \in \mathcal{P}(X)$, and let $\Phi = \{\phi_1, \dots, \phi_i, \dots, \phi_n\}$, be a set of probe functions $\phi_i : X \rightarrow \mathbb{R}$ that represent features of each point x , where $\phi_i(x)$ equals a feature value of x . Let $\Phi(x)$ denote a feature vector for the object x , *i.e.*, a vector of feature values that describe x , where

$$\Phi(x) = (\phi_1(x), \dots, \phi_i(x), \dots, \phi_n(x)).$$

A feature vector provides a description of an object. Let $A, B \in \mathcal{P}(X)$. Let $\mathcal{Q}(A), \mathcal{Q}(B)$ denote sets of descriptions of points in A, B , respectively. For exam-

ple,

$$\mathcal{Q}(A) = \{\Phi(a) : a \in A\} \quad (6.21)$$

The expression $A \delta_{\Phi} B$ reads *A is descriptively near B*. The descriptive proximity of A and B is defined by

$$A \delta_{\Phi} B \Leftrightarrow \mathcal{Q}(\text{cl}A) \cap \mathcal{Q}(\text{cl}B) \neq \emptyset \quad (6.22)$$

. *Descriptive remoteness* of A and B (denoted by $A \underline{\delta}_{\Phi} B$) is defined by

$$A \underline{\delta}_{\Phi} B \Leftrightarrow \mathcal{Q}(\text{cl}A) \cap \mathcal{Q}(\text{cl}B) = \emptyset \quad (6.23)$$

The *descriptive intersection* $\underset{\Phi}{\cap}$ of A and B is defined by

$$A \underset{\Phi}{\cap} B = \{x \in A \cup B : \Phi(x) \in \mathcal{Q}(\text{cl}A) \text{ and } \Phi(x) \in \mathcal{Q}(\text{cl}B)\} \quad (6.24)$$

The descriptive intersection will be nonempty, provided there is at least one element of $\text{cl}A$ with a description that matches the description of at least one element of $\text{cl}B$. That is, a nonempty descriptive intersection of generated patterns or sets A and B is a set containing $a \in \text{cl}A$ and $b \in \text{cl}B$ such that $\Phi(a) = \Phi(b)$. Observe that A and B can be disjoint and yet $A \underset{\Phi}{\cap} B$ could be nonempty. In finding subsets $A, B \in \mathcal{P}(X)$ that are descriptively near, one considers the descriptive intersection of the closure of A and the closure of B . That is, $\text{cl}A \underset{\Phi}{\cap} \text{cl}B \neq \emptyset$ implies $A \delta_{\Phi} B$. The descriptive

proximity (nearness) relation δ_Φ is defined by

$$\delta_\Phi = \left\{ (A, B) \in \mathcal{P}(X) \times \mathcal{P}(X) : \text{cl}A \underset{\Phi}{\cap} \text{cl}B \neq \emptyset \right\} \quad (6.25)$$

$A \underline{\delta} B$ (reads A is far (remote) from B), provided $\text{cl}A$ and $\text{cl}B$ have no points in common such that $\underline{\delta} = \mathcal{P}(X) \times \mathcal{P}(X) \setminus \delta$. Sets that are far from each other relative to the locations of the points in the sets (the points in one set are not among the points of the other set) are called *spatially remote* sets. The complement of a set $C \in \mathcal{P}(X)$ is denoted by C^c .

Definition δ_Φ -space (Descriptive Proximity Pattern Space).

Let Φ be a set of probe functions that represent features of points in a set. Let X be a space endowed with a relation δ_Φ satisfying descriptive EF-axioms $P_\Phi.1 - P_\Phi.5$ similar to $P.1 - P.5$ so that, for any two sets $A, B \in X$, it is determinable whether A and B are descriptively close or not. That is, A and B are descriptively close, provided there are points $a \in A, b \in B$ with matching descriptions. With a metric d defined on X , it can be determined whether sets are infinitesimally close or not, with δ_Φ defined by

$$\delta_\Phi = \{(A, B) \in \mathcal{P}(X) \times \mathcal{P}(X) : D(\mathcal{Q}(A), \mathcal{Q}(B)) = 0\} \quad (6.26)$$

, where

$$D(\mathcal{Q}(A), \mathcal{Q}(B)) = \inf \{d(\Phi(a), \Phi(b)) : a \in A, b \in B\}, \text{ where} \quad (6.27)$$

$$d(\Phi(x), \Phi(y)) = \sum_{i=1}^n |\phi_i(x) - \phi_i(y)| : \phi_i \in \Phi \quad (6.28)$$

. We call a pattern or set X a descriptive EF proximity space (or, briefly, δ_Φ -space), provided, for any two subsets A, B in X , it is determinable whether A and B are close *descriptively* in such a way that the following axioms are satisfied;

P $_\Phi$.1 If set A is descriptively close to B , then B is descriptively close to A .

P $_\Phi$.2 $A \cup B$ is descriptively close to C , if and only if, at least one of the sets A or B is descriptively close to C .

P $_\Phi$.3 Two points $x, y \in X$ are descriptively close, if and only if, the description of x matches the description of y .

P $_\Phi$.4 All nonempty sets are descriptively far from the empty set \emptyset .

P $_\Phi$.5 For any two sets A and B which are descriptively far from each other, there exists C and D , $C \cup D = X$, such that A is descriptively far from C and B is descriptively far from D (**Descriptive Efremovič axiom**). ■

Theorem 6.4.1. *Let (X, δ) , (X, δ_Φ) be spatial and descriptive EF-spaces, respectively, with nonempty sets $A, B \in \mathcal{P}(X)$, $A \cap B \neq \emptyset$. Then $A \cap B \subseteq A \underset{\Phi}{\cap} B$.*

Proof. Let $A, B \in \mathcal{P}(X)$ and assume $A \cap B \neq \emptyset$, i.e., $\delta(A, B) = 0$. If $x \in A \cap B$, then, by definition, $\Phi(x) \in \mathcal{Q}(A)$ and $\Phi(x) \in \mathcal{Q}(B)$. By assumption $x \in A \cap B \subseteq A \cup B$. Then, $x \in A \underset{\Phi}{\cap} B$ and $\delta_\Phi(A, B) = 0$. Hence, $A \cap B \subseteq A \underset{\Phi}{\cap} B$. □

Recall that a set A has a cover that is a collection of subsets \mathcal{C} , provided $A \subset \mathcal{C}$. To obtain the following result for descriptive proximity spaces, we introduce the descriptive closure of a set A (denoted by $\text{cl}_\Phi A$), which is defined by

$$\text{cl}_\Phi A = \bigcup \{ \{y\} \in \mathcal{P}(X) : y \delta_\Phi a \text{ for some } a \in A \} \quad (6.29)$$

Lemma 6.4.1. *Every subset of a descriptive proximity space has a cover.*

Proof. Let A be a subset in a descriptive proximity space X . Each $a \in A$ is descriptively near itself. Hence, $a \in \text{cl}_\Phi A$, since, by definition, $y \in X$ belongs to $\text{cl}_\Phi A$, provided $y \delta_\Phi a$ for some $a \in A$. Then $\text{cl}_\Phi A \supset A$. Hence, $\text{cl}_\Phi A$ is a cover of A . \square

To obtain the following result for digital images, define the descriptive complement of a set C (denoted C_Φ^c) by

$$C_\Phi^c = \{y \in X : \Phi(y) \notin \mathcal{Q}(C)\} \quad (6.30)$$

.

Lemma 6.4.2. *Choose Φ to be a set of probe functions that represent pixel features. Let X be a set of picture points endowed with the descriptive proximity δ_Φ . Then, for any two sets A, B descriptively far from each other in X , we have*

$$\mathbf{A} \underline{\delta}_\Phi \mathbf{B} \Rightarrow \mathbf{A} \underline{\delta}_\Phi \mathbf{C} \text{ and } \mathbf{B} \underline{\delta}_\Phi \mathbf{C}^c, \text{ for some } C \text{ in } X.$$

Proof. From Lemma 6.4.1, let C be a descriptive cover of B , i.e., $B \subset C$. Then

observe the following:

$$\begin{aligned}
 & A \underline{\delta}_\Phi B \text{ in } X, \text{ and,} \\
 & \text{exists } C : B \subset C, \\
 & \text{exists } D : D = C_\Phi^c, \text{ then} \\
 & X = D \cup C, \\
 & B \underline{\delta}_\Phi D, \\
 & A \subset C_\Phi^c, \text{ hence,} \\
 & A \underline{\delta}_\Phi C, \text{ hence, we can write} \\
 & \mathbf{A} \underline{\delta}_\Phi \mathbf{B} \Rightarrow \mathbf{A} \underline{\delta}_\Phi \mathbf{C} \text{ and } \mathbf{B} \underline{\delta}_\Phi \mathbf{C}^c, \text{ for some } C \text{ in } X
 \end{aligned}$$

□

This leads to the following result for pictures (digital images).

Theorem 6.4.2. *Choose Φ to be a set of probe functions representing pixel features. Let X be a set of picture points endowed with the descriptive proximity δ_Φ . Then X is a descriptive EF-space.*

Proof. In X , A is descriptively close to B , provided $D(\mathcal{Q}(A), \mathcal{Q}(B)) = 0$, i.e., $A \underset{\Phi}{\cap} B \neq \emptyset$. A is far from B , provided $D(\mathcal{Q}(A), \mathcal{Q}(B)) > 0$, i.e., $A \underset{\Phi}{\cap} B = \emptyset$. From Lemma 6.4.1, $\text{cl}_\Phi A, \text{cl}_\Phi B$ are covers of A, B , respectively. $\text{cl}_\Phi A$ is close to $\text{cl}_\Phi B$, provided $D(\text{cl}_\Phi A, \text{cl}_\Phi B) = 0$, i.e., $\text{cl}A \cap \text{cl}B \neq \emptyset$.

P.1: A is descriptively close to $B \Rightarrow D(\mathcal{Q}(A), \mathcal{Q}(B)) = 0 \Rightarrow D(\mathcal{Q}(B), \mathcal{Q}(A)) = 0 \Rightarrow B$ is close to A .

P.2: Let A, E be any two sets in X . $\text{cl}_\Phi A \cup \text{cl}_\Phi E$ is far from $\text{cl}_\Phi C$, if and only if,

$\text{cl}_\Phi A$ is far from $\text{cl}_\Phi C$ and $\text{cl}_\Phi E$ is far from $\text{cl}_\Phi C$. Since $A \cap E \subset \text{cl}_\Phi(A \cup E)$, then $(A \cap E) \cap C = \emptyset$. Put another way, $D(A \cup E, C) = 0$. Since $A, E \subset \text{cl}_\Phi(A \cup E)$, if and only if, $D(\mathcal{Q}(A), \mathcal{Q}(C)) = 0$ or $D(\mathcal{Q}(E), \mathcal{Q}(C)) = 0$.

P.3: Points $x, y \in X$ are descriptively close $\Leftrightarrow D(\Phi(\{x\}), \Phi(\{y\})) = 0 \Leftrightarrow \Phi(x) = \Phi(y)$.

P.4: Let $A \subset \mathcal{P}(X)$, then $A \underset{\Phi}{\cap} \emptyset = \emptyset$, i.e., A is descriptively far from the empty set.

P.5: Immediate from Lemma 6.4.2. □

6.4.2 Motif Pattern Generators

The study of set patterns became prominent due to pioneering works by T. Pavlidis [176] and U. Grenander [172, §17.5]. This foundation inspired recent works on the study of visual set patterns in digital images [147, 177] and [159, §14.5]. The focus here is on pattern generators that are a set of points called motifs and what are known as motif set patterns. A motif set is an *indivisible and small atomic region called a cell*. A *pattern generator* M defines a collection of sets that are near M . Let G be a set of all pattern generators on a set X and let $M \in G$. That is, a pattern generator M defines a class $[M]_{\sim_{\delta_G}}$ such that

$$[M]_{\sim_{\delta}} = \{A \in \mathcal{P}(X) : A \sim_{\delta} M \Leftrightarrow A \delta M\} \quad (6.31)$$

. In other words, every member of class $[M]_{\sim_{\delta}}$ is near the pattern generator M . This ensures motif pattern set stability. In effect, $[M]_{\sim_{\delta}}$ is a motif set pattern (denoted by $\mathfrak{P}_M(X)$) on space X . This can lead to a partition of X denoted by $X_{/\sim_{\delta}}$ provided

$$[M]_{\sim_{\delta}} \cap [M']_{\sim_{\delta}} = \emptyset, \text{ for } M, M' \in G \quad (6.32)$$

. Set patterns usually overlap. So in general, the collection of patterns on X may not partition X . The relation \sim_{δ_G} is not an equivalence relation because, in general, it will not be transitive and an individual pattern on the space will instead be a tolerance class.

In a given proximity space, motifs can be found to serve as set pattern generators. Let M, M_1, M_2 be motifs. From this, we obtain the following result.

Theorem 6.4.3.

- (1) M generates a spatial set pattern $\mathfrak{P}(M)$.
- (2) M generates a spatial set pattern $\underline{\mathfrak{P}}(M)$ (collection of sets remote from M).
- (3) The pair M, Φ generates a descriptive set pattern $\mathfrak{P}_\Phi(M)$.
- (4) The pair M, Φ generates a descriptive set pattern $\underline{\mathfrak{P}}_\Phi(M)$ (collection of sets descriptively remote from M).
- (5) $M_1 \cup M_2$ (union of motifs) generates a spatial set pattern $\mathfrak{P}(M_1 \cup M_2)$ (collection of sets spatially near $M_1 \cup M_2$).
- (6) $M_1 \cup M_2$ generates a spatial set pattern $\underline{\mathfrak{P}}_\Phi(M_1 \cup M_2)$ (collection of sets remote from $M_1 \cup M_2$).
- (7) $M_1 \cup M_2, \Phi$ (union of motifs, Φ) generates a set pattern $\mathfrak{P}(M_1 \cup M_2)$ (collection of sets descriptively near $M_1 \cup M_2$).
- (8) $M_1 \cup M_2, \Phi$ (union of motifs, Φ) generates a set pattern $\underline{\mathfrak{P}}(M_1 \cup M_2)$ (collection of sets descriptively remote from $M_1 \cup M_2$).
- (9) $M_1 \cap M_2$ (intersection of motifs) generates a set pattern $\mathfrak{P}(M_1 \cap M_2)$ (collection of sets near $M_1 \cap M_2$).
- (10) $M_1 \cap M_2$ (intersection of motifs) generates a set pattern $\underline{\mathfrak{P}}(M_1 \cap M_2)$ (collection of sets descriptively remote from $M_1 \cap M_2$).
- (11) $M_1 \cap M_2, \Phi$ (intersection of motifs plus Φ) generates a descriptive set pattern

$\mathfrak{P}_\Phi(M_1 \cap M_2)$ (collection of sets descriptively near $M_1 \cap M_2$).

(12) $M_1 \cap M_2, \Phi$ (intersection of motifs plus Φ) generates a descriptive set pattern

$\underline{\mathfrak{P}}_\Phi(M_1 \cap M_2)$ (collection of sets descriptively remote from $M_1 \cap M_2$).

Proof. Let $(X, \delta), (X, \delta_\Phi)$ be spatial and descriptive EF-proximity spaces, respectively, and let M, M' be subsets in X . Assume that the base space is a Hausdorff space, *i.e.*, distinct points belong to disjoint neighbourhoods. We prove only (1) and (3).

(1)**Spatial case:** Let M be a neighbourhood of a point x in X . Since M is near itself, $\mathfrak{P}(M)$ is nonempty. Find $A \subset X$ such that $A \delta M$, *i.e.*, there is at least one $a \in A$ so that $a \delta M$ (the point a is spatially near M , *i.e.*, $D(\{a\}, M) = 0$). Then $A \in \mathfrak{P}(M)$. Continuing this process, motif M generates the spatial motif pattern $\mathfrak{P}(M)$. Let B, C be disjoint neighbourhoods of distinct points $b, c \in X$, then B and C serve as generators of spatial motif patterns $\mathfrak{P}(B), \mathfrak{P}(C)$.

(3)**Descriptive case:** Choose Φ to be a set of probe functions that represent features of each x in X . Since M is descriptively near itself, $\mathfrak{P}_\Phi(M)$ is nonempty. Find $A \subset X$ such that $A \delta_\Phi M$, *i.e.*, there is at least one $a \in A$ and at least one $m \in M$ so that $a \delta_\Phi m$. In effect, $A \underset{\Phi}{\cap} M$ is nonempty. Then $A \in \mathfrak{P}_\Phi(M)$. Continuing this process, motif M generates the descriptive motif pattern $\mathfrak{P}_\Phi(M)$. Let B, C be disjoint bounded neighbourhoods of descriptively distinct points $b, c \in X$ (*i.e.*, $\Phi(b) \neq \Phi(c)$), then B and C serve as generators of descriptive motif patterns $\mathfrak{P}_\Phi(B), \mathfrak{P}_\Phi(C)$. \square

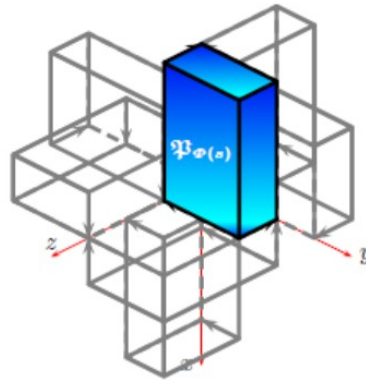


Figure 6.5: Shaded Box Point Set Pattern

Let X be a set of points with a distinguished point $x \in X$. An example of an elementary set pattern $\mathfrak{P}_{\Phi(x)}$ is a *descriptive point set pattern*, which is a set of points that satisfy the descriptive nearness property.

Descriptive Nearness Principle.

Points belong to a descriptive point set pattern, provided the points are descriptively near a distinguished point (sometimes called the pattern *focal point*) [174, p. 123].

The descriptive nearness property provides a basis for determining which points are members of a point set pattern. In general, point set patterns are characterized by distinguished points called *landmarks* by U. Grenander [172, §17.3].

Example Box Point Set Pattern.

Let S be a set of box surface points represented by Fig. 6.5 and let $s \in S$ be a pattern generator. Further, let Φ be a set of probe functions representing pixel colours. For $\phi \in \Phi$, assume that $\phi(s)$ equals a colour intensity in the interval $[0, 0, 255]$. Then

$\mathfrak{P}_\Phi(s)$ is an example of a box point set pattern, which is the set of all box surface points x descriptively near s .

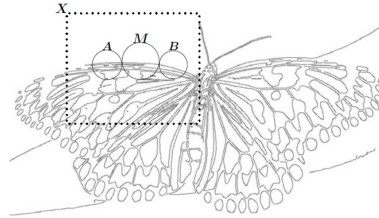


Figure 6.6: Spatial Edge Set Pattern $\mathfrak{P}(M) = \{M, A, B\}$

6.4.3 Spatial Proximity Pattern Generation Method

There are four basic steps in the spatial proximity pattern generation method.

- (Spat.1) Choose a digital image (see step Spat.1 in Fig. 6.7). Let \mathcal{J} be a set of points in the chosen digital image endowed with a spatial proximity relation δ .
- (Spat.2) Choose a region-of-interest X in image \mathcal{J} (see step Spat.2 in Fig. 6.7). The remaining two steps in this pattern generation method are also shown in Fig. 6.7.
- (Spat.3) Let $M \doteq N_x$ be a neighbourhood of a point $x \in X$ (M is called a motif).
- (Spat.4) Determine all sets $A \in \mathcal{P}(X)$ that are near M , *i.e.*, find A such that the closure of A has nonempty intersection with the closure of M , *i.e.*, $\text{cl}A \cap \text{cl}M \neq \emptyset$. The resulting spatial pattern is a collection $\mathfrak{P}(M)$ defined by

$$\mathfrak{P}(M) = \{A \in \mathcal{P}(X) : \text{cl}A \cap \text{cl}M \neq \emptyset\} \quad (6.33)$$

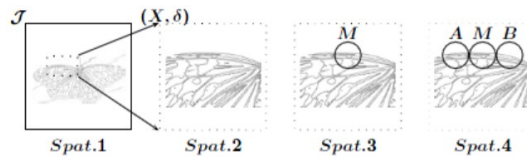


Figure 6.7: Local Spatial Pattern Generation Method

Example Sample Spatial Pattern Generation.

Let X be a set of edge pixels in a region of interest in an image \mathcal{J} shown Fig. 6.6 and assume that X is endowed with a spatial proximity relation δ . The steps in generating a spatial motif set pattern are shown in Fig. 6.7. A region-of-interest X is selected in \mathcal{J} . Then select a motif M to be represented by the spherical neighbourhood of a point $x \in X$ in Fig. 6.7. Next determine those sets A, B that are close to M . Assume that $\text{cl}A \delta \text{cl}M$ and $\text{cl}B \delta \text{cl}M$. Since $M \delta M$, consequently $M \in \mathfrak{P}(M)$. Hence, the edge set pattern $\mathfrak{P}(M) = \{M, A, B\}$ is an example of a spatial motif set pattern.

■

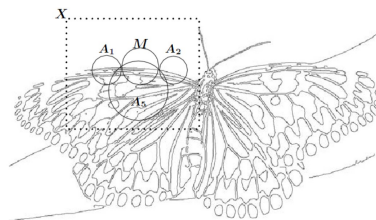


Figure 6.8: $\mathfrak{P}_\Phi(M) = \{M, A_1, A_2, A_5\}$

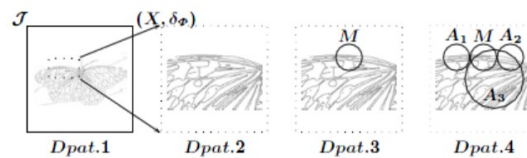


Figure 6.9: Local Descriptive Pattern Generation Method

6.4.4 Descriptive Proximity Pattern Generation Method

The steps in the descriptive proximity pattern generation model are symmetric with the steps in the spatial proximity generation method. The descriptive proximity pattern we have in mind is a descriptive proximity motif pattern $\mathfrak{P}_\Phi(M)$, identified as a distinguished set M . There are a number of nuances in this second pattern generation method, namely, (1) the possibility of a larger region-of-interest, since the sets descriptively near a motif need not be spatially near the motif, (2) choice of a set Φ , a set of probe functions used to extract features of pixels in a digital image, (3) replacing a spatial proximity with a descriptive proximity relation δ_Φ . See Fig. 6.8 for a sample descriptive motif set pattern and see Fig. 6.9 for an illustration of the descriptive motif set generation method, where $\mathfrak{P}_\Phi(M) = \{M, A_1, A_2, A_3\}$. The steps specifying the descriptive proximity pattern generation method are given next.

- (Dpat.1) Choose a digital image \mathcal{J} and a set of probe functions Φ representing features of pixels in \mathcal{J} . Let \mathcal{J} be endowed with a descriptive proximity relation δ_Φ .
- (Dpat.2) Choose a region-of-interest X in image \mathcal{J} (see step Dpat.2 in Fig. 6.9). The remaining two steps in this pattern generation method are also shown in Fig. 6.9.
- (Dpat.3) Choose a subset M in X to serve as a motif. The points in M can be found relative to the choice of a single, distinguished point of interest x in X . That is, let $M \doteq N_{\Phi(x)}$ be a descriptive neighbourhood of a point $x \in X$ (M is called a descriptive motif). M is defined by

$$M \doteq N_{\Phi(x)} : \tag{6.34}$$

$$N_{\Phi(x)} = \{y \in X : \Phi(y) = \Phi(x)\} \tag{6.35}$$

(**Dpat.4**) Determine all sets $A \in \mathcal{P}(X)$ that are descriptively near M , *i.e.*, find $\text{cl}A \underset{\Phi}{\cap} \text{cl}M \neq \emptyset$. The resulting spatial pattern is a collection $\mathfrak{P}_{\Phi}(M)$ defined by

$$\mathfrak{P}_{\Phi}(M) = \left\{ A \in \mathcal{P}(X) : \text{cl}A \underset{\Phi}{\cap} \text{cl}M \right\} \quad (6.36)$$

6.5 Assessing Pattern Stability

In the study of descriptive patterns in a pair of digital images A, B , it is necessary to propagate a pattern in image B with some assurance that each new set added to a pattern is not far from the pattern generator [178]. That is, given a pattern generator M , each new set A added to pattern $\mathfrak{P}_{\Phi}(M)$ must be sufficiently near M , *spatially*.

P.E. Forsseén and D. Lowe observed that shape descriptors are reliable in detecting maximally stable extremal regions in digital images [179]. Descriptive motif set pattern growth is stable, provided the shape-based description of each set added to the pattern matches the shape-based description of the pattern motif. This interpretation of pattern stability is comparable to U. Grenander's notion of configuration transformation stability [172, §4.1.1]. To arrive at a formal definition of pattern stability, we introduce the descriptive distance between collections in terms of the Čech distance between sets.

Let $A, B \in \mathcal{C}$ be nonempty sets in a space \mathcal{C} and let

$$D(A, B) = \inf \{|a - b| : a \in A, b \in B\} \quad (6.37)$$

be the Čech distance between A and B . That is, a configuration transformation T on a configuration space \mathcal{C} is stable, if, for any $\varepsilon > 0$, there exists a δ such that

$$D(A, B) \leq \delta \Rightarrow D(T(A), T(B)) \leq \varepsilon \quad (6.38)$$

. Let (X, δ_Φ) be a descriptive proximity Hausdorff space and let $A, B \in \mathcal{P}, \mathcal{A}, \mathcal{B} \in \mathcal{P}^2(X)$. Next, consider a descriptive form of a Grenander configuration transformation, namely, T_Φ . That is, the transformation $T_\Phi \doteq \mathfrak{P}_\Phi : \mathcal{P}(X) \rightarrow \mathcal{P}^2(X)$ is defined by

$$\mathfrak{P}_\Phi(M) = \mathcal{A} : M \delta_\Phi B \text{ for } B \in \mathcal{A}, \text{ and } D(M, B) \leq \varepsilon.$$

Definition Pattern Stability Sufficiently Near Criterion.

Let $\mathfrak{P}_\Phi(M)$ be a descriptive motif pattern constructed on a nonempty set X , $\varepsilon > 0$ and let $A \in \mathfrak{P}_\Phi(M)$. The pattern $\mathfrak{P}_\Phi(M)$ is stable, provided the distance requirement $D(M, A) < \varepsilon$ is satisfied. That is, $\mathfrak{P}_\Phi(M)$ is stable, provided A is *sufficiently near* M for each A added to $\mathfrak{P}_\Phi(M)$. ■

Let $B \ll A$ denote the fact that B is a *proximal neighbourhood* of A , provided $A \subset B$. From Def. 6.5, we obtain the following result.

Lemma 6.5.1. *Let $M \subset X$, a T_2^Φ space and let $\mathfrak{P}_\Phi(M)$ be a descriptive motif pattern. Let $A, B \in \mathfrak{P}_\Phi(M)$. $\mathfrak{P}_\Phi(M)$ is stable, if and only if, $D(M, A) < \varepsilon$ and $B \ll A$ implies $D(M, B) < \varepsilon$.*

Let $B \ll A$ denote that B is a proximal neighbourhood of A , i.e., $A \subset B$ in a proximity space and B is far from A^c . ■

From Def. 6.5 and Lemma 6.5.1, we obtain the following result.

Theorem 6.5.1. Descriptive Pattern Stability.

Let \mathfrak{P}_Φ be a pattern configuration transformation used to construct collections of

patterns on X endowed with a descriptive proximity δ_Φ such that Φ is a set of probe functions representing shape descriptors and let $M \in \mathcal{P}(X)$, $\varepsilon > 0$. Then the following are equivalent.

- (1) $\mathfrak{P}_\Phi(M)$ is stable.
- (2) $D(M, A) < \varepsilon$ for each $A \in \mathfrak{P}_\Phi(M)$.
- (3) $D(M, A) < \varepsilon$ and $B \ll A$ implies $D(M, B) < \varepsilon$.

Proof.

(1) \Leftrightarrow (2): $\mathfrak{P}_\Phi(M)$ is stable, if and only if, from Def. 6.5, $D(M, A) < \varepsilon$ for each $A \in \mathfrak{P}_\Phi(M)$.

(1) \Leftrightarrow (3): $\mathfrak{P}_\Phi(M)$ is stable, if and only if, from Lemma 6.5.1, $D(M, A) < \varepsilon$ and $B \ll A$ implies $D(M, B) < \varepsilon$.

(2) \Leftrightarrow (3): $D(M, A) < \varepsilon$ for each $A \in \mathfrak{P}_\Phi(M)$, if and only if, $B \in \mathfrak{P}_\Phi(M)$, provided $B \ll A$. □

Here, the aim is to construct multiple patterns across disjoint regions of digital images that resemble each other, so we introduce a stability criterion for the generation of multiple patterns. Let $\mathcal{A}, \mathcal{B} \in \mathcal{P}^2(X)$ be collections containing sets $A, B \in \mathcal{P}(X)$, respectively. To complete the definition of pattern stability, we introduce the descriptive distance D_Φ , which is a descriptive form of the distance between sets introduced by E. Čech [164, §18.A.2]. The distance D_Φ is used to define the descriptive distance \mathbb{D}_Φ between collections of sets. The descriptive distance $\mathbb{D}_\Phi : \mathcal{P}^2(X) \times \mathcal{P}^2(X) \rightarrow \mathbb{R}$ between collections \mathcal{A}, \mathcal{B} is defined by

$$\mathbb{D}_\Phi(\mathcal{A}, \mathcal{B}) = \inf \{D_\Phi(A, B) : A \in \mathcal{A}, B \in \mathcal{B}\}, \text{ where,} \quad (6.39)$$

$$D_\Phi(A, B) = \inf \{d(\Phi(a), \Phi(b)) : a \in A, b \in B\} \quad (6.40)$$

. The descriptive distance \mathbb{D}_Φ can be used to measure the distance between descriptive motif set patterns, since such patterns are collections of nonempty sets that are descriptively near each other. Let $\{A\}, \{B\}$ denote collections, each containing one set. Then \mathfrak{P}_Φ is a *stable descriptive pattern*, if, for any $\varepsilon > 0$, there exists a $\delta > 0$ such that

$$\mathbb{D}_\Phi(\{A\}, \{B\}) \leq \delta \Rightarrow \mathbb{D}_\Phi(\mathfrak{P}_\Phi(A), \mathfrak{P}_\Phi(B)) < \varepsilon \quad (6.41)$$

. That is, whenever sets A and B are descriptively near, then the corresponding patterns $\mathfrak{P}_\Phi(A), \mathfrak{P}_\Phi(B)$ are descriptively near. This form of set pattern stability works well in comparing regions of pairs of digital images, where we need to guarantee that the transformation that produces the descriptive set patterns in separate image regions is stable.

Definition Multiple Pattern Stability.

Let \mathfrak{P}_Φ be a pattern configuration transformation used to construct collections of patterns on X endowed with a descriptive proximity δ_Φ and let $\varepsilon > 0, \delta > 0$. Let $x, y \in X$ be distinct points and let M_1, M_2 be disjoint neighbourhoods of x, y , respectively. Further, let $\mathcal{A}, \mathcal{B} \in \mathcal{P}^2(X)$ with $M_1 \in \mathcal{A}, M_2 \in \mathcal{B}$. Patterns $\mathfrak{P}_\Phi(M_1) \in \mathcal{A}, \mathfrak{P}_\Phi(M_2) \in \mathcal{B}$ are stable, provided

$$\mathbb{D}_\Phi(\mathcal{A}, \mathcal{B}) \leq \delta \Rightarrow \mathbb{D}_\Phi(\mathfrak{P}_\Phi(M_1), \mathfrak{P}_\Phi(M_2)) < \varepsilon.$$

That is, descriptively near collections of sets lead to descriptively near motif set patterns. ■

In order to ensure stability in comparing image regions in the same digital image regions in pairs of images, it is necessary to consider pixel features that can be reliably matched, regardless of the appearance of the surroundings of a region. In this

section, the focus is on constructing motif set patterns containing neighbourhoods of points defined by connected point sets that are straight edges. Neighbourhood selection is determined by the gradient orientation of the focal point of a pattern motif neighbourhood. The construction of a pattern motif (a descriptive neighbourhood of point) reduces to finding a connected set of points along an edge such that the edge points have matching gradient orientation. Hence, a gradient orientation-based motif set pattern results from finding neighbourhoods of points containing straight edges with pixel gradient orientations that match the gradient orientation of the points in the motif neighbourhood of the pattern.

Keeping in mind the underlying descriptive uniform topology in a Hausdorff T_2^Φ space X endowed with descriptive proximity δ_Φ , an image pixel y belongs to a neighbourhood of point x , provided the gradient orientation of y matches the gradient orientation of x . Let Φ be a set of shape descriptors that includes pixel gradient orientation. In addition, let the descriptive neighbourhood $N_{\Phi(x)}$ be a pattern motif M that is a connected set of points belonging to a straight edge, *i.e.*, $y \in N_{\Phi(x)}$, provided $\Phi(y) = \Phi(x)$. Then the pattern $\mathfrak{P}_\Phi(M)$ is a collection of straight edges defined by

$$\mathfrak{P}_\Phi(M) = \{N_{\Phi(y)} \in \mathcal{P}(X) : N_{\Phi(y)} \delta_\Phi M\} \quad (6.42)$$

. Pattern stability is achieved by guaranteeing that only matching straight edges belong to the pattern $\mathfrak{P}_\Phi(M)$. In comparing regions across pairs of digital images, stability is achieved by comparing straight edge patterns. Let $x, y \in X, Y$ be pixels in a pair of digital images X, Y , respectively. Further, let $\mathfrak{P}_\Phi(M_1), \mathfrak{P}_\Phi(M_2)$ be straight edge shape patterns in images X, Y , respectively, such that $M_1 = N_{\Phi(x)}, M_2 = N_{\Phi(y)}$. Pattern $\mathfrak{P}_\Phi(M_x)$ is close to pattern $\mathfrak{P}_\Phi(M_y)$, provided the straight edges represented

by neighbourhoods in the patterns have matching edge-neighbourhood motifs, *i.e.*,

$\mathfrak{P}_\Phi(M_1) \delta_\Phi \mathfrak{P}_\Phi(M_2)$, if and only if,

$N_{\Phi(x)} \delta_\Phi N_{\Phi(y)}$, if and only if,

$\Phi(x) = \Phi(y)$. ■

From Def. 6.5 and Theorem 6.5.1, we obtain the following result.

Theorem 6.5.2. *Let \mathfrak{P}_Φ be a pattern configuration transformation used to construct collections of patterns on X , a T_2^Φ space endowed with a descriptive proximity δ_Φ such that Φ is a set of probe functions representing shape descriptors. Let $M_1, M_2 \in \mathcal{P}(X)$, and let $\varepsilon > 0$. Further, let $\mathcal{A}, \mathcal{B} \in \mathcal{P}^2(X)$. Then the following are equivalent.*

(1) $\mathfrak{P}_\Phi(M_1) \in \mathcal{A}, \mathfrak{P}_\Phi(M_2) \in \mathcal{B}$ are stable.

(2) $D(M_1, A) < \varepsilon, D(M_2, B) < \varepsilon$ for each $A \in \mathfrak{P}_\Phi(M_1)$ and for each $B \in \mathfrak{P}_\Phi(M_2)$.

Definition Pattern Stability.

Let $th > 0$ denote an expectation threshold and let $E[\cdot]$ denote the expected value of \cdot . Further, let $\mathfrak{P}_\Phi(M, X)$ be a pattern generated by M in X and $\mathfrak{P}_\Phi(M, Y)$, pattern generated by M in Y . The *stability of any description-based pattern* $\mathfrak{P}_\Phi(M)$ (denoted by $Stab(\mathfrak{P}_\Phi(M))$) is defined by

$$Stab(\mathfrak{P}_\Phi(M)) = \begin{cases} 1, & \text{if } E[\mathbb{D}_\Phi(\mathfrak{P}_\Phi(M, X), \mathfrak{P}_\Phi(M, Y))] \leq th, \\ 0, & \text{otherwise } \mathfrak{P}_\Phi(M) \text{ is unstable} \end{cases} \quad (6.43)$$

. where X and Y are two independent samples from some unknown distribution.

Pattern $\mathfrak{P}_\Phi(M)$ is stable, provided $Stab(\mathfrak{P}_\Phi(M)) = 1$. ■

Furthermore, given two patterns $\mathfrak{P}_\Phi(M_1)$ and $\mathfrak{P}_\Phi(M_2)$, pattern generation will be

stable, provided $M_1 \underline{\delta}_\phi M_2$ and $Stab(\mathfrak{P}_\Phi(M_1)) = Stab(\mathfrak{P}_\Phi(M_2)) = 1$. In addition, for any set A , $A \delta_\Phi M_1$ and $A \underline{\delta}_\phi M_2$ will ensure that set A will always be added to pattern $\mathfrak{P}_\Phi(M_1)$. This is advantageous in achieving pattern stability for the method proposed here compared to the traditional clustering methods such as k-means clustering, since pattern stability, in our case, derives its strength from the fact that each set A added to a pattern has *descriptive proximity* to the pattern generator M in a descriptive proximity space.

Remark Resulting Image Understanding.

A result of a digital image or its tessellation endowed with an EF-proximity relation (either spatial or descriptive) is image understanding. That is, the nearness and remoteness of subsets in an image are highlighted thanks to the EF-proximity relation. In effect, comparisons and contrasts between image parts are facilitated by endowing an image (as a set of points) with an EF-proximity relation. The contrasts between sets of points become apparent when one considers axiom P.5 ($P_\Phi.5$), which provides a natural separation of some image subsets in terms of their remoteness from others, either spatially or descriptively. That is, for any two sets in a δ -space that are not close, there exists a δ -function that separates them [124]. What Smirnov has observed about δ -spaces carries over into description-based δ_Φ -spaces in the study of images. This is apparent from Theorem 6.4.2. ■

An EF-space defines a topological space [124, Chapter 1, p. 9]. Hence, the set of points in a digital image endowed with an EF-proximity relation defines a topology on the image. The descriptive counterpart of Smirnov's work on EF-spaces leads to the following result for descriptive EF-spaces.

Theorem 6.5.3. *A descriptive EF-space defines a topological space.*

Proof.

Let the set X be endowed with descriptive EF-proximity δ_Φ . Define the descriptive remoteness proximity relation $\underline{\delta}_\Phi$ as follows:

$$\underline{\delta}_\Phi = \left\{ (A, B) \in \mathcal{P}(X) \times \mathcal{P}(X) : A \underset{\Phi}{\cap} B = \emptyset \right\} \quad (6.44)$$

. Then define

$$\tau = \delta_\Phi \cup X \setminus \underline{\delta}_\Phi \quad (6.45)$$

. We need to show that τ is a topology. Let $A, B \in \mathcal{P}(X)$.

\cap : case 1: $A \underset{\Phi}{\cap} B \neq \emptyset \Rightarrow A \delta_\Phi B \Rightarrow A \underset{\Phi}{\cap} B \in \tau$.

case 2: $A \underset{\Phi}{\cap} B = \emptyset \Rightarrow A \underline{\delta}_\Phi B \Rightarrow A \underset{\Phi}{\cap} B \in \tau$.

\cap : $(A \cup B) \delta_\Phi (A \cup B) \Rightarrow (A \cup B) \in \tau$.

$X \delta_\Phi X \Rightarrow X \in \tau$.

$\emptyset \underset{\Phi}{\cap} \emptyset = \emptyset \Rightarrow (\emptyset, \emptyset) \in \underline{\delta}_\Phi \Rightarrow \emptyset \in \tau$. Hence, τ is a topology. \square

Remark Descriptive Image Analysis Approach Revisited.

From what has been observed, it is now possible to revisit Part (3) of the Gurevich Descriptive Approach to Image Analysis *and understanding* (DAIA) given by I.B. Gurevich and V.V. Yashina [180], which we designate as (3*) with an added part given in italics:

(3*) Use *EF-proximity* and an algebraic language to describe image models and procedures to construct and transform them. ■

Also, from Theorem 6.4.2, it is now possible to refine Descriptive Analysis (DA) property (4) given by I.B. Gurevich and V.V. Yashina [181, §1.2], which we designate as (4*) with an added part given in italics:

(4*) The set of points *endowed with a descriptive EF-proximity* is a topological space that consists of objects, called “points,” and topology which determines the closeness of two points; the connectability of a subset of the set of points; the neighbourhood of points; the presence of the point boundaries, curves, and arcs.

■

Property (4.*) represents a description-based extension of a result in Smirnov [124, Chapter 1, p. 9]; a topology is naturally defined in a descriptive δ_Φ -space.

Descriptive EF-proximity is useful in describing, analyzing and classifying the parts within a single digital image or the parts in either near or remote sets in separate digital images [147, 174]. The basic approach to the study of set patterns introduced here reflects recent work on descriptively near sets (see, *e.g.*, [167, 182]). Applications of descriptive EF-proximity are many (see, *e.g.*, [159, 177]).

6.6 Descriptive Pattern-Based Approach to Classification

This section introduces a basic approach in pattern-based classification of digital images (or equivalent transformations). This approach hinges on the introduction of continuous descriptive proximity maps between pairs of images and the adherence of each implementation to a set of pattern nearness axioms.

Let M be a pattern generator in a digital image X that represents a class of images. Let $\mathfrak{P}(M'), \mathfrak{P}_\Phi(M')$ be spatial and descriptive motif patterns in Y . Then we have the following pattern nearness axioms.

P.1^o Let f be a map between descriptive proximity spaces X and Y . $A \delta_\Phi B$ in X implies $f(A) \delta_\Phi f(B)$.

P.2^o Define a continuous map $f : X \rightarrow Y$ such that, for each $x \in X$ that is an adherence

point of M , $f(x)$ is an adherence point of $M' \doteq f(M)$. Due to the mapping f , $D_{\Phi}(M, M') < \varepsilon'$, descriptive nearness of pattern motifs, *i.e.*, M is descriptively near M' .

P.3^o Descriptive nearness of pattern motif and pattern cells:

$$D_{\Phi}(M', A_i) < \varepsilon', \text{ for each } A_i \in \mathfrak{P}_{\Phi}(M').$$

P.4^o Spatial nearness of pattern motif and pattern cells:

$$D(M', A_i) < \varepsilon, \text{ for each } A_i \in \mathfrak{P}(M'). \quad \blacksquare.$$

To achieve practical realisation of Axiom P.2^o, we introduce the notion of descriptive points of adherence in a set. Recall that an *adherence point* of a set in a proximity space is any isolated point in the set [183, §28, p. 57]. For example, 2 is an adherent point that is not in the subinterval $(2, 8]$.

Definition A *descriptive adherence point of a set* is any descriptively isolated point in the set. That is, a point is descriptively isolated in a set, provided there is no other point with the same description in the set.

Since proximity space defines a topology on the space, we define a continuous map in terms of proximity spaces.

Definition A map f of one proximity space P into another proximity space Q is a *continuous map*, provided the image $f(a)$ of every point of adherence $a \in A$ is a point of adherence of the set $f(A)$ in Q . A map f of one descriptive proximity space P into descriptive proximity space Q is a *continuous map*, provided the image $f(a)$ of

every point of descriptive adherence point $a \in A$ is a descriptive point of adherence of the set $f(A)$ in Q .

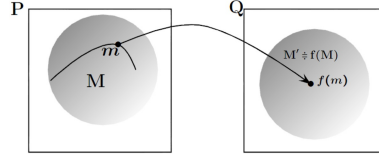


Figure 6.10: Continuous map $f : P \rightarrow Q$: $D_{\Phi}(M, M') = 0$

Example Continuous Map between Descriptive Proximity Spaces.

Let P, Q be a pair of digital images that are descriptive proximity spaces and assume that M is a set of points in P . Choose Φ to be a set of probe functions that represent the features of points in P, Q . Let M be a pattern motif in P and let $f : P \rightarrow Q$ be a continuous mapping of P into Q such that the image $f(a)$ is the center of a descriptive neighbourhood $N_{\Phi(f(a))}$ of $f(a)$. From the fact that f is a continuous map from P into Q , and $m \in M$ is a descriptive adherence point of M , then $f(m)$ is a descriptive adherence point of $M' \doteq f(M)$. See, *e.g.*, Fig. 6.10. ■

The distance D_{Φ} defines the descriptive distance \mathbb{D}_{Φ} between motif set patterns in a pair of images X, Y . The descriptive distance $\mathbb{D}_{\Phi} : \mathcal{P}^2(X) \times \mathcal{P}^2(Y) \rightarrow \mathbb{R}$ between patterns $\mathcal{A} \doteq \mathcal{P}_{\Phi}(M), \mathcal{B} \doteq \mathcal{P}_{\Phi}(M')$ is defined by

$$\mathbb{D}_{\Phi}(\mathcal{A}, \mathcal{B}) = \inf \{D_{\Phi}(A, B) : A \in \mathcal{A}, B \in \mathcal{B}\}, \text{ where,}$$

$$D_{\Phi}(A, B) = \inf \{d(\Phi(a), \Phi(b)) : a \in A, b \in B\}.$$

Let $X_{/\delta_{\Phi}}$ be a collection of image classes determined by the descriptive EF-proximity δ_{Φ} on a set X .

Algorithm 3: Pattern-Based Class Membership Test Method

Input : Descriptive EF-space P , Descriptive EF-space Q , Φ , continuous function $f : P \rightarrow Q$

Output: Test image decision

Choose ROI $X \subset P$;

Choose ROI $Y \subset Q$;

$NM_{st} \doteq 1$;

if (descriptive adherence point $x \in X$ exists) **then**

$M \doteq N_{\Phi(x)}$;

 Enforce conditions $P.2^o - P.4^o$;

 Find $\mathfrak{P}_{\Phi}(M)$;

else if (no adherent point exists in X) **then**

$NM_{st} \doteq 0$;

return NM_{st} ;

if ($NM_{st} = 1$ & $\exists f(x) \in Y$ exists) **then**

$M' \doteq N_{\Phi(f(x))}$;

 Enforce conditions $P.2^o - P.4^o$ and Find $\mathfrak{P}_{\Phi}(M')$;

else if (no adherent point exists in Y) **then**

$NM_{st} \doteq 0$;

return NM_{st} ;

if $NM_{st} = 1$ **then**

 compute $d \doteq NM_{st}(\mathfrak{P}_{\Phi}(M), \mathfrak{P}_{\Phi}(M'))$;

if $d = 1$ **then**

return d ;

else if $d = 0$ **then**

return d ;

Algorithm 4: Pattern-Based Classification Method

Input : Descriptive EF-space P , EF-space Classes $P_{/\delta_\Phi}$, Collection of EF-spaces \mathcal{Q} ,

Output: Classified Test Images in Collection \mathcal{T}

count $\doteq |\mathcal{Q}|$;

while (count > 0) **do**

 select $Q \in \mathcal{Q}$;

 select $P \in P_{/\delta_\Phi}$;

 run Algorithm 3 with P, Q ;

if (Algorithm 3 returns 1) **then**

$\mathcal{T} \doteq \mathcal{T} \cup Q$;

 count \doteq count - 1;

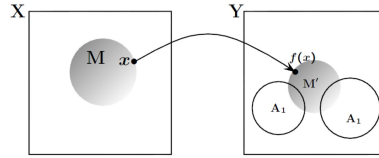


Figure 6.11: $\delta_\Phi(M, M') = 0$, and $\delta_\Phi(A_i, M') = 0$.

Remark Practical Realisation of Axiom P.2^o.

Axiom P.2^o is pivotal in the pattern-based classification of digital images. Let a query image be a set of points X and let the set of points Y be a test image. Choose Φ , a set of probe functions that represent features of points in X and let $\varepsilon > 0$. Let x be a point in a query image X and let $N_{\Phi(x)}$ be a descriptive neighbourhood of the form

$$N_{\Phi(x)} \doteq \{a \in X : d(\Phi(x), \Phi(a)) < \varepsilon\} \quad (6.46)$$

. Let the query image pattern generator (motif) be $M \doteq N_{\Phi(x)}$. Then find $y \in Y$ such that $d(\Phi(x), \Phi(a)) < \varepsilon$, *i.e.*, attempt to find a test image point y that is descriptively close to the point x in the query image. Let $f : X \rightarrow Y$ be a continuous mapping between proximity spaces X, Y . Let $m \in M, f(m) \in Q$. If a point $y \in Y$ is found in

the test image such that

$$f(x) \delta_{\Phi} y,$$

then construct a bounded descriptive neighbourhood $N_{\Phi(y)} \doteq N_{\Phi(f(m))}$ in the test image. That is, find all points in Y that are both spatially and descriptively near $f(m)$.

Then let the test image pattern generator (motif) be $M' \doteq N_{\Phi(f(m))}$. Let $\varepsilon' > 0$. Here, we depart from Smirnov's approach. That is, after the pattern generator M' has been found in Y using $f(m)$ as the center of a bounded descriptive neighbourhood $N_{\Phi(f(m))}$, then check if Axiom P.2^o holds true such that $D_{\Phi}(M, M') < \varepsilon'$. It is important that M' in Y is descriptively close to M in X , since we will then have some assurance that a descriptive pattern $\mathfrak{P}_{\Phi}(M')$ in Y will be comparable to the descriptive pattern $\mathfrak{P}_{\Phi}(M)$ in X .

After that, make sure Axioms P.3^o and P.4^o are also enforced. In that case, $\delta_{\Phi}(A_i, M') = 0$ for each A_i in the descriptive motif pattern $\mathfrak{P}_{\Phi}(M')$.

If δ_{Φ} -space Y is a member of the class of images represented by $\mathfrak{P}_{\Phi}(M)$ in X , then

$$\delta_{\Phi}(\mathfrak{P}_{\Phi}(M), \mathfrak{P}_{\Phi}(M')) = 0 \tag{6.47}$$

, *i.e.*, the pattern generated in Y will be descriptively close to the pattern generated in X . ■

6.7 Conclusion

Chapter 6 is an introductory chapter in that it lays the foundations for the applications of near sets in pattern studies and classification. The mathematical theory and background necessary for the foundation is provided in terms of relevant theorems,

lemmas, near set construction etc. Algorithms are also provided for facilitation of future works. The summary, conclusions and directions of future works are provided in Chapter 7.

Chapter 7

Summary, Conclusion and Future Work

In this work, a general domain partitioning algorithm is presented. The partitioning allows us to characterize structures in feature-endowed spaces by constructing tessellations based on important features in the domain. This is complementary to other space partitions including random space tessellations.

The Voronoï diagram of a point set is characteristic of the underlying pattern and the interaction of the units of the pattern. This means that a tessellation of a non-random pattern constructed on random sets would not bear fundamental and true information of the underlying image pattern. This realization makes it necessary to seek out models for identifying point patterns in a space representative of the space so that the tessellations can be constructed on those feature-informed point pattern sets. This work presented models for extracting point pattern sets based on features and information of a digital image domain.

In the literature, mesh cell quality guarantees are well established for triangular

mesh cells as well as for random and other forms of tessellations. Despite the ease of quality guarantees in these scenarios, the refined meshes still lack representative and reliable information present in the underlying non-random pattern and signal spaces modeled on random or fixed process assumptions. This work in addition to formulation of feature-driven models for point pattern set extraction also verifies a technique that guarantees improved mesh cell qualities of general element shapes.

The information content of Voronoï tessellations has been quantified using information theoretic methods. It is revealed that there is a range of the information parameter for which maximum information exposure is probable per the general information measure. This range of the parameter also corresponds with the range for which there is greater discrimination in information content within the classes of the signal categories. In addition to this, a global solution index is introduced. It is noteworthy that within a signal category, the global quality measure exhibits convergence properties. The potential of an information theoretic technique in processing Voronoï regions in images has also been explored. It has been demonstrated that this can reveal fundamental pattern organization information for understanding patterns. Theoretical results pertaining to Voronoï diagrams and their features have been identified and proved. These form a mathematical background for subsequent applications and analysis.

The global quality index and the information content of the Voronoï signature of a pattern speaks to the underlying nature of the signal or representative summary pattern. The information present in each Voronoï region can be exploited for signal analysis. This has been demonstrated in the processing and enhancement of medical

images, with the aim of aiding decision making. For example, a Voronoï signature composed of a repeated unit indicates a simple underlying pattern. This connotes with the interestingness and complexity of the pattern. In this particular case, every Voronoï cell contains the same information as any other cell, hence the simplicity and uninterestingness of the pattern. As seen in the analysis of facial patterns, the underlying patterns are hardly simple and hence the interestingness of the patterns. This corresponds with global quality indices that are not identical with unity indices in the case of repeated cells in simple patterns. Also, the relationship between the quality of cells and their information content exhibits discriminatory behaviour across the signal categories despite the general convergence behaviour of quality. These observations are identified to inform future work. It is thought that the ease of pattern perception and identification is related to the interaction of pattern units and their overall influence on symmetry. We therefore think that future work should focus in the direction of the relation between pattern symmetry and pattern perception by the Human Visual System (HVS). Our future work should also focus on exploiting the full potential of the our method in image recognition and classification.

The HVS is highly efficient in its adaptability and pattern recognition ability. It is thought that our success in artificial intelligence, computer vision and pattern recognition would be proportional in measure to the extent to which we can understand its operation and model it accordingly. Given signal outputs of HVS, our hope is to identify models in computational geometry that sufficiently model HVS.

Given the richness of Voronoï signatures of various sources of signals, future work

will focus on exploiting their potential for pattern classification based on features obtained from those spaces. As already outlined in some algorithms in the work, further pattern analysis would be based on extracted sets such as near sets, groupoid elements etc. It is expected to yield a pathway to practical image classification using those extracted features. This is feasible given the ability of the approach to characterize underlying patterns and interactions between the units of the pattern.

Bibliography

- [1] E. A-iyeh and J. Peters, “Measure of tessellation quality of voronoï meshes,” *Theory and Applications of Mathematics & Computer Science*, vol. 5, no. 2, pp. 158–185, 2015.
- [2] —, “Rényi entropy in measuring information levels in voronoï tessellation cells with application in digital image analysis,” *Theory and Applications of Mathematics & Computer Science*, vol. 6, no. 1, 2016.
- [3] E. A-iyeh and J. F. Peters, “Gini index-based digital image complementing in the study of medical images,” *Intelligent Decision Technologies*, vol. 9, no. 2, pp. 209–218, 2015.
- [4] E. A-iyeh and J. F. Peters, “Proximal groupoid patterns in digital images,” *CoRR*, vol. abs/1603.01842, 2016. [Online]. Available: <http://arxiv.org/abs/1603.01842>
- [5] T. Seacrest, “Mathematical models of image processing,” Ph.D. dissertation, Harvey Mudd College, 2006, supervisor: Professor Weiqing Gu. [Online]. Available: <https://www.math.hmc.edu/seniorthesis/archives/2006/tseacres/tseacres-2006-thesis.pdf>
- [6] C. Sorzano, M. Pérez-Gandía, and A. Otero-Quintana, “Mathematical models in image processing.” Intl. Congress of Mathematics in Engineering and Architecture, invited speaker, 2007.

- [7] A. K. Jain, “Advances in mathematical models for image processing,” *Proceedings of the IEEE*, vol. 69, no. 5, pp. 502–528, 1981.
- [8] A. Okabe, B. Boots, K. Sugihara, and S. N. Chiu, *Spatial tessellations: concepts and applications of Voronoi diagrams*. John Wiley & Sons, 2009, vol. 501.
- [9] F. Aurenhammer, “Voronoi diagrams—a survey of a fundamental geometric data structure,” *ACM Computing Surveys (CSUR)*, vol. 23, no. 3, pp. 345–405, 1991.
- [10] J. Liu and S. Liu, “A survey on applications of voronoi diagrams,” *Journal of Engineering Graphics*, vol. 22, no. 2, pp. 125–132, 2004.
- [11] H. Edelsbrunner, *Geometry and topology for mesh generation*. Cambridge University Press, 2001.
- [12] H. Edelsbrunner and R. Seidel, “Voronoi diagrams and arrangements,” *Discrete & Computational Geometry*, vol. 1, no. 1, pp. 25–44, 1986.
- [13] H. Edelsbrunner, *Algorithms in combinatorial geometry*. Springer, 1987, vol. 10.
- [14] M. Melkemi and D. Vandorpe, “Voronoi diagrams and applications,” in *Eighth Canadian Conference on Image Processing and Pattern Recognition*, vol. 88, 1994, p. 95.
- [15] P. A. Arbeláez and L. D. Cohen, “A metric approach to vector-valued image segmentation,” *International Journal of Computer Vision*, vol. 69, no. 1, pp. 119–126, 2006.
- [16] A. Cheddad, D. Mohamad, and A. A. Manaf, “Exploiting voronoi diagram properties in face segmentation and feature extraction,” *Pattern Recognition*, vol. 41, no. 12, pp. 3842–3859, 2008.
- [17] K. Kise, A. Sato, and M. Iwata, “Segmentation of page images using the area voronoi diagram,” *Computer Vision and Image Understanding*, vol. 70, no. 3, pp. 370–382, 1998.

- [18] M. Ramella, M. Nonino, W. Boschin, and D. Fadda, “Cluster identification via voronoi tessellation,” *arXiv preprint astro-ph/9810124*, 1998.
- [19] R. van de Weygaert, “Fragmenting the universe. 4^{iv}. the clustering properties of voronoi foams.”
- [20] R. van de Weygaert and V. Icke, “Voronoi vertices as abell clusters,” *Astronomy and Astrophysics*, vol. 213, pp. 1–9, 1989.
- [21] Q. Du, V. Faber, and M. Gunzburger, “Centroidal voronoi tessellations: applications and algorithms,” *SIAM review*, vol. 41, no. 4, pp. 637–676, 1999.
- [22] P.-O. Persson and G. Strang, “A simple mesh generator in matlab,” *SIAM review*, vol. 46, no. 2, pp. 329–345, 2004.
- [23] P.-O. Persson, “Mesh generation for implicit geometries,” Ph.D. dissertation, Citeseer, 2004.
- [24] M. J. Dry, “Using relational structure to detect symmetry: A voronoi tessellation based model of symmetry perception,” *Acta Psychologica*, vol. 128, no. 1, pp. 75–90, 2008.
- [25] F. Meutzner, W. Münchgesang, N. A. Kabanova, M. Zschornak, T. Leisegang, V. A. Blatov, and D. C. Meyer, “On the way to new possible na-ion conductors: The voronoi–dirichlet approach, data mining and symmetry considerations in ternary na oxides,” *Chemistry–A European Journal*, vol. 21, no. 46, pp. 16 601–16 608, 2015.
- [26] U. Lorz, “Cell-area distributions of planar sections of spatial voronoi mosaics,” *Materials characterization*, vol. 25, no. 3, pp. 297–309, 1990.
- [27] H. Hermann, H. Wendrock, and D. Stoyan, “Cell-area distributions of planar voronoi mosaics,” *Metallography*, vol. 23, no. 3, pp. 189–200, 1989.

- [28] M. Ferraro and L. Zaninetti, “Statistics of cross sections of voronoi tessellations,” *Physical Review E*, vol. 84, no. 4, p. 041107, 2011.
- [29] H. Hilhorsta, “Statistical properties of planar voronoi tessellations,” *The European Physical Journal B-Condensed Matter and Complex Systems*, vol. 64, no. 3, pp. 437–441, 2008.
- [30] C. D. Barr, “Applications of voronoi tessellations in point pattern analysis,” Ph.D. dissertation, University of California, Los Angeles, 2008.
- [31] C. Duyckaerts, G. Godefroy, and J.-J. Hauw, “Evaluation of neuronal numerical density by dirichlet tessellation,” *Journal of neuroscience methods*, vol. 51, no. 1, pp. 47–69, 1994.
- [32] M. Browne, “Regularized tessellation density estimation with bootstrap aggregation and complexity penalization,” *Pattern Recognition*, vol. 45, no. 4, pp. 1531–1539, 2012.
- [33] C. Duyckaerts and G. Godefroy, “Voronoi tessellation to study the numerical density and the spatial distribution of neurones,” *Journal of chemical neuroanatomy*, vol. 20, no. 1, pp. 83–92, 2000.
- [34] S. Chiu, “Spatial point pattern analysis by using voronoi diagrams and delaunay tessellations—a comparative study,” *Biometrical journal*, vol. 45, no. 3, pp. 367–376, 2003.
- [35] B. E. Shapiro, H. Jonsson, P. Sahlin, M. Heisler, A. Roeder, M. Burl, E. M. Meyerowitz, and E. D. Mjolsness, “Tessellations and pattern formation in plant growth and development,” *arXiv preprint arXiv:1209.2937*, 2012.
- [36] T. J. Taylor and I. I. Vaisman, “Statistical geometry and topology of real and model protein structures,” in *Voronoi Diagrams in Science and Engineering, 2006. ISVD’06. 3rd International Symposium on.* IEEE, 2006, pp. 196–207.

- [37] T. Bourquard, J. Bernauer, J. Azé, and A. Poupon, “Comparing voronoi and laguerre tessellations in the protein-protein docking context,” in *Voronoi Diagrams, 2009. ISVD’09. Sixth International Symposium on*. IEEE, 2009, pp. 225–232.
- [38] M. A. Mostafavi, L. H. Beni, and K. Hins-Mallet, “Representing dynamic spatial processes using voronoi diagrams: Recent developments,” in *Voronoi Diagrams, 2009. ISVD’09. Sixth International Symposium on*. IEEE, 2009, pp. 109–117.
- [39] N. Fu, H. Imai, and S. Moriyama, “Voronoi diagrams on periodic graphs,” in *Voronoi Diagrams in Science and Engineering (ISVD), 2010 International Symposium on*. IEEE, 2010, pp. 189–198.
- [40] D.-M. Yan, K. Wang, B. Lévy, and L. Alonso, “Computing 2d periodic centroidal voronoi tessellation,” in *Voronoi Diagrams in Science and Engineering (ISVD), 2011 Eighth International Symposium on*. IEEE, 2011, pp. 177–184.
- [41] A. Idrissi, K. Polok, W. Gadomski, I. Vyalov, A. Agapov, M. Kiselev, M. Barj, and P. Jedlovszky, “Detailed insight into the hydrogen bonding interactions in acetone–methanol mixtures. a molecular dynamics simulation and voronoi polyhedra analysis study,” *Physical Chemistry Chemical Physics*, vol. 14, no. 17, pp. 5979–5987, 2012.
- [42] J. Zhang, M. Emelianenko, and Q. Du, “Periodic centroidal voronoi tessellations,” *International Journal of Numerical Analysis and Modeling*, vol. 9, no. 4, pp. 950–969, 2012.
- [43] S. N. Chakraborty, E. M. Grzelak, B. C. Barnes, D. T. Wu, and A. K. Sum, “Voronoi tessellation analysis of clathrate hydrates,” *The Journal of Physical Chemistry C*, vol. 116, no. 37, pp. 20 040–20 046, 2012.
- [44] M. Goberna, M. Rodríguez, and V. V. de Serio, “Voronoi cells via linear inequality systems,” *Linear Algebra and Its Applications*, vol. 436, no. 7, pp. 2169–2186, 2012.

- [45] V. Dvořák and J. Novosad, “Influence of mesh quality and density on numerical calculation of heat exchanger with undulation in herringbone pattern,” in *19th International Conference on Circuits, Systems, Communications and Computers, Zakynthos, Greece*, 2015.
- [46] D. L. González and T. Einstein, “Voronoi cell patterns: Theoretical model and applications,” *Physical Review E*, vol. 84, no. 5, p. 051135, 2011.
- [47] N. Ahuja, “Dot pattern processing using voronoi neighborhoods,” *Pattern Analysis and Machine Intelligence, IEEE Transactions on*, no. 3, pp. 336–343, 1982.
- [48] M. Reitzner, E. Spodarev, and D. Zaporozhets, “Set reconstruction by voronoi cells,” *Advances in Applied Probability*, vol. 44, no. 04, pp. 938–953, 2012.
- [49] M. Sambridge, J. Braun, and H. McQueen, “Geophysical parametrization and interpolation of irregular data using natural neighbours,” *Geophysical Journal International*, vol. 122, no. 3, pp. 837–857, 1995.
- [50] I. Hödl, J. Hödl, A. Wörman, G. Singer, K. Besemer, and T. J. Battin, “Voronoi tessellation captures very early clustering of single primary cells as induced by interactions in nascent biofilms,” *PloS one*, vol. 6, no. 10, p. e26368, 2011.
- [51] K. Sugihara, “Approximation of generalized voronoi diagrams by ordinary voronoi diagrams,” *CVGIP: Graphical Models and Image Processing*, vol. 55, no. 6, pp. 522–531, 1993.
- [52] N. Mayya and V. Rajan, “Voronoi diagrams of polygons: A framework for shape representation,” *Journal of Mathematical Imaging and Vision*, vol. 6, no. 4, pp. 355–378, 1996.
- [53] R. Ogniewicz and M. Ilg, “Voronoi skeletons: Theory and applications,” in *Computer Vision and Pattern Recognition, 1992. Proceedings CVPR’92., 1992 IEEE Computer Society Conference on*. IEEE, 1992, pp. 63–69.

- [54] N. Ahuja, B. An, and B. Schachter, “Image representation using voronoi tessellation,” *Computer vision, graphics, and image processing*, vol. 29, no. 3, pp. 286–295, 1985.
- [55] N. Amenta and M. Bern, “Surface reconstruction by voronoi filtering,” *Discrete & Computational Geometry*, vol. 22, no. 4, pp. 481–504, 1999.
- [56] P. L. George, “Adaptive mesh generation in 3 dimensions by means of a delaunay based method. applications to mechanical problems.” in *III European Conference on Computational Mechanics*. Springer, 2006, pp. 18–18.
- [57] P. R. Eiseman, “Adaptive grid generation,” *Computer Methods in Applied Mechanics and Engineering*, vol. 64, no. 1, pp. 321–376, 1987.
- [58] V. Rajan, “Optimality of the delaunay triangulation in d ,” *Discrete & Computational Geometry*, vol. 12, no. 1, pp. 189–202, 1994.
- [59] J. Peraire, M. Vahdati, K. Morgan, and O. C. Zienkiewicz, “Adaptive remeshing for compressible flow computations,” *Journal of computational physics*, vol. 72, no. 2, pp. 449–466, 1987.
- [60] M.-C. Rivara, “Mesh refinement processes based on the generalized bisection of simplices,” *SIAM Journal on Numerical Analysis*, vol. 21, no. 3, pp. 604–613, 1984.
- [61] J. Ruppert, “A delaunay refinement algorithm for quality 2-dimensional mesh generation,” *Journal of algorithms*, vol. 18, no. 3, pp. 548–585, 1995.
- [62] G. Voronoï, “Sur un problème du calcul des fonctions asymptotiques,” *J. für die reine und angewandte Math.*, vol. 126, pp. 241–282, 1903, jFM 38.0261.01.
- [63] ———, “Nouvelles applications des paramètres continus à la théorie des formes quadratiques. premier mémoire,” *J. für die reine und angewandte Math.*, vol. 133, pp. 97–178, 1907.

- [64] —, “Sur un problème du calcul des fonctions asymptotiques,” *J. für die reine und angewandte Math.*, vol. 134, pp. 198–287, 1908, jFM 39.0274.01.
- [65] P. Coles, “Voronoi cosmology,” 1991.
- [66] G. Chapman, “The application of information theory to the analysis of population distributions in space,” *Economic Geography*, pp. 317–331, 1970.
- [67] A. McLean, “Voronoi diagrams of music,” URL [http://doc. gold. ac. uk/~ma503am/essays/voronoi/voronoi-diagrams-of-music. pdf](http://doc.gold.ac.uk/~ma503am/essays/voronoi/voronoi-diagrams-of-music.pdf). Accessed, vol. 8, 2007.
- [68] M. Hamanaka and K. Hirata, “Applying voronoi diagrams in the automatic grouping of polyphony,” *Information Technology Letters*, vol. 1, no. 1, pp. 101–102, 2002.
- [69] J. Møller and Ø. Skare, “Coloured voronoi tessellations for bayesian image analysis and reservoir modelling,” *Statistical modelling*, vol. 1, no. 3, pp. 213–232, 2001.
- [70] C. Demir and B. Yener, “Automated cancer diagnosis based on histopathological images: a systematic survey,” *Rensselaer Polytechnic Institute, Tech. Rep*, 2005.
- [71] E. Agrell, “Voronoi regions for binary linear block codes,” *Information Theory, IEEE Transactions on*, vol. 42, no. 1, pp. 310–316, 1996.
- [72] J. Peters, “Proximal Voronoi regions, convex polygons, & Leader uniform topology,” *Advances in Math.*, vol. 4, no. 1, pp. 1–5, 2015.
- [73] —, “Visibility in proximal Delaunay meshes,” *Advances in Math.*, vol. 4, no. 1, 2015, *to appear*.
- [74] —, “Proximal delaunay triangulation regions,” *PJMS [Proc. of the Korean Math. Soc.]*, 2015, *to appear*.
- [75] B. Shrestha, “Classification of plants using images of their leaves,” *Submitted to the Graduate School. Appalachian State University. in partial fulfillment of the requirements for the degree of MASTER OF SCIENCE*, 2010.

- [76] M. M. Deza and E. Deza, *Encyclopedia of distances*. Springer, 2009.
- [77] M. S. Ebeida and S. A. Mitchell, “Uniform random voronoi meshes,” in *Proceedings of the 20th International Meshing Roundtable*. Springer, 2012, pp. 273–290.
- [78] M. Bern and P. Plassmann, “Mesh generation,” *Handbook of Computational Geometry*, vol. 6, 1999.
- [79] R. Brauwerman, S. J. Zoll, C. L. Farmer, and M. Gunzburger, “Centroidal voronoi tessellations are not good jigsaw puzzles,” <http://www.math.iastate.edu/reu/1999/cvt.pdf>, 1999.
- [80] M. Ferraro and L. Zaninetti, “On the statistics of area size in two-dimensional thick voronoi diagrams,” *Physica A: Statistical Mechanics and its Applications*, vol. 391, no. 20, pp. 4575–4582, 2012.
- [81] N. Ahuja and B. J. Schachter, “Pattern models,” 1982.
- [82] R. Bhatia and K. Lawrence, “Two-dimensional finite element mesh generation based on stripwise automatic triangulation,” *Computers & Structures*, vol. 36, no. 2, pp. 309–319, 1990.
- [83] J. Shewchuk, “What is a good linear finite element? interpolation, conditioning, anisotropy, and quality measures (preprint),” *University of California at Berkeley*, vol. 73, 2002.
- [84] Y. Liu, W. Wang, B. Lévy, F. Sun, D.-M. Yan, L. Lu, and C. Yang, “On centroidal voronoi tessellation energy smoothness and fast computation,” *ACM Transactions on Graphics (ToG)*, vol. 28, no. 4, p. 101, 2009.
- [85] J. Burns, “Centroidal voronoi tessellations,” 2009.
- [86] M. Gunzburger, “Centroidal voronoi tessellations.” CCS-2/CNLS Seminar, Los Alamos National Laboratory, 2003.

- [87] B. Boots and D. Murdoch, “The spatial arrangement of random voronoi polygons,” *Computers & Geosciences*, vol. 9, no. 3, pp. 351–365, 1983.
- [88] Z. Fan, Y. Wu, X. Zhao, and Y. Lu, “Simulation of polycrystalline structure with voronoi diagram in laguerre geometry based on random closed packing of spheres,” *Computational materials science*, vol. 29, no. 3, pp. 301–308, 2004.
- [89] J.-S. Ferenc and Z. Nédá, “On the size distribution of poisson voronoi cells,” *Physica A: Statistical Mechanics and its Applications*, vol. 385, no. 2, pp. 518–526, 2007.
- [90] S. Kumar and S. K. Kurtz, “Properties of a two-dimensional poisson-voronoi tessellation: a monte-carlo study,” *Materials Characterization*, vol. 31, no. 1, pp. 55–68, 1993.
- [91] F. Jarai-Szabo and Z. Neda, “On the size-distribution of poisson voronoi cells,” *arXiv preprint cond-mat/0406116*, 2004.
- [92] P. Calka *et al.*, “Precise formulae for the distributions of the principal geometric characteristics of the typical cells of a two-dimensional poisson-voronoi tessellation and a poisson line process,” *Advances in Applied Probability*, vol. 35, no. 3, pp. 551–562, 2003.
- [93] Á. Plaza, J. P. Suárez, M. A. Padrón, S. Falcón, and D. Amieiro, “Mesh quality improvement and other properties in the four-triangles longest-edge partition,” *Computer Aided Geometric Design*, vol. 21, no. 4, pp. 353–369, 2004.
- [94] J. Park and S. M. Shontz, “Two derivative-free optimization algorithms for mesh quality improvement,” *Procedia Computer Science*, vol. 1, no. 1, pp. 387–396, 2010.
- [95] S. P. Sastry, S. M. Shontz, and S. A. Vavasis, “A log-barrier method for mesh quality improvement and untangling,” *Engineering with Computers*, vol. 30, no. 3, pp. 315–329, 2014.

- [96] P. Knupp, “Mesh quality improvement for scidac applications,” in *Journal of Physics: Conference Series*, vol. 46, no. 1. IOP Publishing, 2006, p. 458.
- [97] P. W. de Bruin, F. Vos, F. H. Post, S. Frisken-Gibson, and A. M. Vossepoel, “Improving triangle mesh quality with surfacenet,” in *Medical Image Computing and Computer-Assisted Intervention—MICCAI 2000*. Springer, 2000, pp. 804–813.
- [98] M. S. Ebeida, S. A. Mitchell, A. A. Davidson, A. Patney, P. M. Knupp, and J. D. Owens, “Efficient and good delaunay meshes from random points,” *Computer-Aided Design*, vol. 43, no. 11, pp. 1506–1515, 2011.
- [99] H. P. Moravec, “Obstacle avoidance and navigation in the real world by a seeing robot rover.” DTIC Document, Tech. Rep., 1980.
- [100] C. Harris and M. Stephens, “A combined corner and edge detector.” in *Alvey vision conference*, vol. 15. Manchester, UK, 1988, p. 50.
- [101] W. Förstner and E. Gülch, “A fast operator for detection and precise location of distinct points, corners and centres of circular features,” in *Proc. ISPRS intercommission conference on fast processing of photogrammetric data*, 1987, pp. 281–305.
- [102] L. Kitchen and A. Rosenfeld, “Gray-level corner detection,” DTIC Document, Tech. Rep., 1980.
- [103] J. J. Koenderink and W. Richards, “Two-dimensional curvature operators,” *JOSA A*, vol. 5, no. 7, pp. 1136–1141, 1988.
- [104] D. G. Lowe, “Distinctive image features from scale-invariant keypoints,” *International journal of computer vision*, vol. 60, no. 2, pp. 91–110, 2004.
- [105] T. Lindeberg, “Feature detection with automatic scale selection,” *International journal of computer vision*, vol. 30, no. 2, pp. 79–116, 1998.
- [106] ———, *Scale-Space*. Wiley Online Library, 2008.

- [107] ———, *Scale-space theory in computer vision*. Springer Science & Business Media, 1993.
- [108] K. Mikolajczyk and C. Schmid, “Scale & affine invariant interest point detectors,” *International journal of computer vision*, vol. 60, no. 1, pp. 63–86, 2004.
- [109] H. Wang and M. Brady, “Real-time corner detection algorithm for motion estimation,” *Image and Vision Computing*, vol. 13, no. 9, pp. 695–703, 1995.
- [110] S. M. Smith and J. M. Brady, “Susana new approach to low level image processing,” *International journal of computer vision*, vol. 23, no. 1, pp. 45–78, 1997.
- [111] E. Rosten and T. Drummond, “Machine learning for high-speed corner detection,” in *Computer Vision–ECCV 2006*. Springer, 2006, pp. 430–443.
- [112] D. Guru and R. Dinesh, “Non-parametric adaptive region of support useful for corner detection: a novel approach,” *Pattern Recognition*, vol. 37, no. 1, pp. 165–168, 2004.
- [113] S. K. Kang, Y. C. Choung, and J. A. Park, “Image corner detection using hough transform,” in *Pattern Recognition and Image Analysis*. Springer, 2005, pp. 279–286.
- [114] S. J. Park, M. B. Ahmad, R. Seung-Hak, S. J. Han, and J. A. Park, “Image corner detection using radon transform,” in *Computational Science and Its Applications–ICCSA 2004*. Springer, 2004, pp. 948–955.
- [115] H. Pan, Y. Zhang, C. Li, and H. Wang, “An adaptive harris corner detection algorithm for image mosaic,” in *Pattern Recognition*. Springer, 2014, pp. 53–62.
- [116] B. Kim, J. Choi, Y. Park, and K. Sohn, “Robust corner detection based on image structure,” *Circuits, Systems, and Signal Processing*, vol. 31, no. 4, pp. 1443–1457, 2012.

- [117] J. Canny, “A computational approach to edge detection,” *Pattern Analysis and Machine Intelligence, IEEE Transactions on*, no. 6, pp. 679–698, 1986.
- [118] D. G. Lowe, “Object recognition from local scale-invariant features,” in *Computer vision, 1999. The proceedings of the seventh IEEE international conference on*, vol. 2. Ieee, 1999, pp. 1150–1157.
- [119] H. Mitchell, “Image key points,” in *Image Fusion*. Springer, 2010, pp. 163–166.
- [120] X. Feng, Y. Lai, X. Mao, J. Peng, X. Jiang, and A. Hadid, “Extracting local binary patterns from image key points: Application to automatic facial expression recognition,” in *Image Analysis*. Springer, 2013, pp. 339–348.
- [121] M. Woźniak and Z. Marszałek, “An idea to apply firefly algorithm in 2d image key-points search,” in *Information and Software Technologies*. Springer, 2014, pp. 312–323.
- [122] M. Brown and D. G. Lowe, “Invariant features from interest point groups.” in *BMVC*, no. s 1, 2002.
- [123] A. Teterin, “A geometric approach to classification: a new model of the operation of a neuron,” *Computational mathematics and mathematical physics*, vol. 32, no. 12, pp. 1797–1805, 1992.
- [124] J. M. Smirnov, “On proximity spaces,” *Math. Sb. (N.S.)*, vol. 31, no. 73, pp. 543–574, 1952, english translation: Amer. Math. Soc. Trans. Ser. 2, 38, 1964, 5-35.
- [125] J. Peters, *Topology of Digital Images. Visual Pattern Discovery in Proximity Spaces*, ser. Intelligent Systems Reference Library. Springer, 2014, vol. 63, ISBN 978-3-642-53844-5, pp. 1-342.
- [126] —, “Near sets: An introduction,” *Math. in Comp. Sci.*, vol. 7, no. 1, pp. 3–9, 2013, DOI 10.1007/s11786-013-0149-6.

- [127] “Psychological image collection at stirling database, pain expression subset,” June 2009.
- [128] D. A. Field, “Laplacian smoothing and delaunay triangulations,” *Communications in applied numerical methods*, vol. 4, no. 6, pp. 709–712, 1988.
- [129] M. Bern and D. Eppstein, “Mesh generation and optimal triangulation,” *Computing in Euclidean geometry*, vol. 4, pp. 47–123, 1995.
- [130] W. Buell and B. Bush, “Mesh generationa survey,” *Journal of Engineering for Industry*, vol. 95, no. 1, pp. 332–338, 1973.
- [131] L. A. Freitag and C. Ollivier-Gooch, “A comparison of tetrahedral mesh improvement techniques,” 1996.
- [132] N. Amenta, M. Bern, and D. Eppstein, “Optimal point placement for mesh smoothing,” *Journal of Algorithms*, vol. 30, no. 2, pp. 302–322, 1999.
- [133] Z. Wang, A. C. Bovik, H. R. Sheikh, and E. P. Simoncelli, “Image quality assessment: From error visibility to structural similarity,” *Image Processing, IEEE Transactions on*, vol. 13, no. 4, pp. 600–612, 2004.
- [134] R. T. Jantzen and K. Volpert, “On the mathematics of income inequality: Splitting the gini index in two,” *The American Mathematical Monthly*, vol. 119, no. 10, pp. 824–837, 2012.
- [135] F. Farris, “The gini index and measures of inequality,” *The Amer. Math. Monthly*, vol. 117, no. 10, pp. 851–864, 2010.
- [136] C. Gini, “On the measurement of concentration and variability of characters,” *Metron - International Journal of Statistics*, vol. LXIII, no. 1, pp. 1–38, 2005.
[Online]. Available: <http://EconPapers.repec.org/RePEc:mtn:ancoec:0501>

- [137] —, “Variabilità e mutabilità (Variability and mutability),” *Memorie di Metodologica Statistica, Libreria Eredi Virgilio Veschi, Rome*, pp. 1–156, 1955.
- [138] —, “Measurement of inequality of income,” *Economic Journal*, vol. 31, pp. 22–43, 1921.
- [139] J. Portilla, V. Strela, M. Wainwright, and E. Simoncelli, “Image denoising using scale mixtures of Gaussians in the wavelet domain,” *IEEE Trans. on Image Processing*, vol. 12, no. 11, pp. 1338–1351, 2003.
- [140] P. Nazil, G. Shubhrata, and V. Kesari, “Facial expression recognition using facial characteristic point snad gini index,” *Engineering and Systems, IEEE Conference on*, pp. 1–6, 2012.
- [141] N. Hurley and S. Rickard, “Comparing measures of sparsity,” *Information Theory, IEEE Transactions on*, vol. 55, no. 10, pp. 4723–4741, 2009.
- [142] Q.-N. Tran, “Mining medical databases with modified gini index classification,” in *Information Technology: New Generations, 2008. ITNG 2008. Fifth International Conference on*. IEEE, 2008, pp. 195–200.
- [143] D. Zonoobi, A. A. Kassim, and Y. V. Venkatesh, “Gini index as sparsity measure for signal reconstruction from compressive samples,” *IEEE Journal of Selected Topics In Signal Processing*, vol. 5, no. 5, pp. 927–932, 2011.
- [144] C. Akujuobi, O. Odejide, A. Annamalai, and G. Fudge, “Sparseness measures of signals for compressive sampling,” in *Signal Processing and Information Technology, 2007 IEEE International Symposium on*. IEEE, 2007, pp. 1042–1047.
- [145] E. Test, V. Kecman, R. Strack, Q. Li, and R. Salman, “Feature ranking for pattern recognition: A comparison of filter methods,” in *Southeastcon, 2012 Proceedings of IEEE*. IEEE, 2012, pp. 1–5.

- [146] J. Peters, *Topology of Digital Images. Visual Pattern Discovery in Proximity Spaces*. Berlin: Springer Intelligent Systems Reference Library, 2013.
- [147] ———, “Local near sets. Pattern discovery in proximity spaces,” *Math. in Comp. Sci.*, 2013.
- [148] W. E. Snyder, “Nc state university image analysis laboratory database,” 2002. [Online]. Available: <http://www.ece.ncsu.edu/imaging/Archives/ImageDatabase/index.html>
- [149] A. Rényi *et al.*, “On measures of entropy and information,” in *Proceedings of the Fourth Berkeley Symposium on Mathematical Statistics and Probability, Volume 1: Contributions to the Theory of Statistics*. The Regents of the University of California, 1961.
- [150] R. Hartley, “Transmission of information,” *Bell Systems Technical Journal*, p. 535, 1928.
- [151] H. Nyquist, “Certain factors affecting telegraph speed,” *Bell Systems Technical Journal*, p. 324, 1924.
- [152] P. Bromiley, N. Thacker, and E. Bouhova-Thacker, “Shannon entropy, Rényi’s entropy, and information,” The University of Manchester, U.K., Tech. Rep., 2010, <http://www.tina-vision.net/docs/memos/2004-004.pdf>.
- [153] G. Leibon and D. Letscher, “Delaunay triangulations and voronoi diagrams for riemannian manifolds,” in *Proceedings of the sixteenth annual symposium on Computational geometry*. ACM, 2000, pp. 341–349.
- [154] S. J. Owen, “A survey of unstructured mesh generation technology,” in *IMR*, 1998, pp. 239–267.

- [155] J. Z. Wang, J. Li, and G. Wiederhold, “Simplicity: Semantics-sensitive integrated matching for picture libraries,” *Pattern Analysis and Machine Intelligence, IEEE Transactions on*, vol. 23, no. 9, pp. 947–963, 2001.
- [156] S. Naimpally, *Proximity Spaces*. Cambridge, UK: Cambridge University Press, 1970, x+128 pp., ISBN 978-0-521-09183-1.
- [157] A. Di Concilio, “Proximity: A powerful tool in extension theory, functions spaces, hyperspaces, boolean algebras and point-free geometry,” in *Beyond Topology, AMS Contemporary Mathematics 486*, F. Mynard and E. Pearl, Eds. Amer. Math. Soc., 2009, pp. 89–114.
- [158] R. Engelking, *General Topology, Revised & completed edition*. Berlin: Heldermann Verlag, 1989.
- [159] S. Naimpally and J. Peters, *Topology with Applications. Topological Spaces via Near and Far*. Singapore: World Scientific, 2013.
- [160] F. Riesz, “Stetigkeitsbegriff und abstrakte mengenlehre,” *m IV Congresso Internazionale dei Matematici*, vol. II, pp. 18–24, 1908.
- [161] S. Naimpally, “Near and far. A centennial tribute to Frigyes Riesz,” *Siberian Electronic Mathematical Reports*, vol. 2, pp. 144–153, 2009.
- [162] A. DiConcilio and S. Naimpally, “Proximal set-open topologies,” *Boll. Unione Mat. Italy*, vol. 8, no. 1-B, pp. 178–191, 2000.
- [163] A. DiConcilio, “Topologizing homeomorphism groups of rim-compact spaces,” vol. 153, no. 11, pp. 1867–1885, 2006.
- [164] E. Čech, *Topological Spaces*. London: John Wiley & Sons Ltd., 1966, fr seminar, Brno, 1936-1939; rev. ed. Z. Frolik, M. Katětov.

- [165] V. Efremovič, “The geometry of proximity I,” *Mat. Sb.*, vol. 31, pp. 189–200 (in Russian), 1951, mR 14, 1106.
- [166] J. Peters and S. Ramanna, “Pattern discovery with local near sets,” in *Proc. Jornadas Chilenas de Computación 2012 workshop on pattern recognition*, R. Alarcón and P. Barceló, Eds. Valparaiso: The Chilean Computing Society, 2012, pp. 1–4.
- [167] J. Peters and S. Naimpally, “Applications of near sets,” *Amer. Math. Soc. Notices*, vol. 59, no. 4, pp. 536–542, 2012, DOI: <http://dx.doi.org/10.1090/noti817>.
- [168] W. Thron, *Topological Structures*. Oxford, UK: Holt, Rinehart and Winston, 1966.
- [169] J. Peters, E. İnan, and M. Öztürk, “Spatial and descriptive isometries in proximity spaces,” *General Mathematics Notes*, vol. 21, no. 2, pp. 1–10, 2014.
- [170] V. Efremovič, “The geometry of proximity I (in Russian),” *Mat. Sb. (N.S.)*, vol. 31(73), no. 1, pp. 189–200, 1952.
- [171] J. Peters and S. Naimpally, “Applications of near sets,” *Notices of the Amer. Math. Soc.*, vol. 59, no. 4, pp. 536–542, 2012, DOI: <http://dx.doi.org/10.1090/noti817>.
- [172] U. Grenander, *General Pattern Theory. A Mathematical Study of Regular Structures*. Oxford, UK: Oxford Univ. Press, 1993, xxi + 883 pp.
- [173] A. Clifford and G. Preston, *The Algebraic Theory of Semigroups*. American Mathematical Society, Providence, R.I., 1964, xv+224pp.
- [174] J. F. Peters, “Topology of digital images,” *Visual Pattern Discovery in Proximity Spaces*, vol. 63, 2014.
- [175] F. Hausdorff, *Grundzüge der Mengenlehre*. Leipzig: Veit and Company, 1914, viii + 476 pp.
- [176] T. Pavlidis, “Analysis of set patterns,” *Pattern Recog.*, vol. 1, pp. 165–178, 1968.

- [177] J. Peters, “Nearness of local admissible covers. Theory and application in micropalaeontology,” *Fund. Inform.*, pp. 1–12, 2013.
- [178] G. Dee and J. Langer, “Propagating pattern selection,” *Physical Review Letters*, vol. 50, no. 6, p. 383, 1983.
- [179] P. Forsseén and D. Lowe, “Shape descriptors for maximally stable external regions,” in *Proc. IEEE Conf. on Computer Vision*. IEEE, 2007, 1-8.
- [180] I. Gurevich and V. Yashina, “Descriptive approach to image analysis: Image formalization space,” *Pat. Recog. and Im. Anal.*, vol. 18, no. 4, pp. 518–541, 2008.
- [181] —, “Descriptive approach to image analysis: Image formalization space,” *Pat. Recog. and Im. Anal.*, vol. 22, no. 4, pp. 495–518, 2012.
- [182] J. Peters, S. Tiwari, and R. Singh, “Approach merotopies and associated near sets,” *Theory and Applications of Mathematics & Computer Science*, vol. 3, no. 1, pp. 1–12, 2013.
- [183] W. Young and G. Young, *The Theory of Sets of Points*, 2nd Ed. Bronx, N.Y.: Chelsea Pub. Co., 1972, xvi+326pp.